MECHANICS OF HIERARCHICAL, FILAMENTOUS TISSUES

A Dissertation
Presented to
The Academic Faculty

By

Jonathan Andrew Michel

In Partial Fulfillment
of the Requirements for the Degree
Doctor of Philosophy in the
School of Physics

Georgia Institute of Technology

December 2019

MECHANICS OF HIERARCHICAL, FILAMENTOUS TISSUES

Approved by:

Professor Peter J. Yunker, Advisor
School of Physics
Georgia Institute of Technology

Professor Phillip N. First
School of Physics
Georgia Institute of Technology

Professor Harold Kim
School of Physics
Georgia Institute of Technology

Professor D. Zeb Rocklin
School of Physics
Georgia Institute of Technology

Professor Saad Bahmla
School of Biomedical Engineering
Georgia Institute of Technology

Date Approved: October 31, 2019

There is something fascinating about science. One gets such wholesale returns of conjecture out of such a trifling investment of fact.

Mark Twain

For my parents, who always encouraged my interest in science, and my sister, who has always politely humored me when I ramble about it.

ACKNOWLEDGEMENTS

I wish to thank my family, who provided critical support and tolerated extended periods of aloofness as I struggled to produce a thesis. I also wish to acknowledge my advisor, Professor Peter Yunker, whose vision and optimism were invaluable sustaining forces. I also must acknowledge my office mates, who have provided me with valuable feedback and sustaining comradery, and who have consistently endured my penchant for puns with grace. I am also grateful to my colleagues within the broader Soft Matter community at Georgia Tech, who have provided useful outside perspectives on my work. I have also enjoyed the friendship and moral support provided to me by many members of the Physics community at large. They have alternatively been there to commiserate, rejoice, and give me a nudge when I needed one to see this thesis through.

TABLE OF CONTENTS

LIST OF TABLES

LIST OF FIGURES

SUMMARY

Structural hierarchy, the property of possessing spatial organization on multiple, distinct length scales, is omnipresent in biological tissues, and is increasingly popular as a means of pursuing designer properties of human-made materials. Hierarchy can offer economy of material, resilience against fracture, and novel mechanical response; however, the apparent opportunity for errors in assembly at multiple stages naïvely seems to present an imposing obstacle to the evolution of hierarchical tissue. Nonetheless, many organisms, from many evolutionary lineages, exhibit structural hierarchy.

In this work, we build upon previous efforts to model tissue as spring networks. We create networks with a nested, self-similar structure, whose geometrical attributes can be independently varied at each scale. Following previous researchers, we focus upon the mean coordination number, which gives the typical number of nearest neighbors to which a vertex in a network is connected, as a parameter for controlling the elastic properties of structures. We extend this idea, defining separate coordination numbers for the network architecture, and find a simple scaling law relating a material's stiffness to its structural attributes at each length scale. We validate this scaling law with simulations, and find it to hold for structures derived from crystalline lattices and triangulations of random point sets. From this scaling law, we predict that the variability in the stiffness of a network resulting from variability in its structural attributes at each length scale diminishes with increasing levels of hierarchy, up to some threshold. Our results suggest that robustness to errors in assembly may be a generic benefit of a modular assembly process.

Finally, we elucidate the role of large-scale and small-scale structural attributes. We find the small scale structure sets the vibrational density of states of our model systems at large frequency, while the large-scale structure is important in coordinating a system-wide, percolating force network to stiffen the material.

CHAPTER 1
INTRODUCTION

1.1 Defining the Problem

Structural hierarchy, the property of possessing spatial organization on multiple, distinct length scales, is omnipresent in the natural world, [1, 2, 3, 4] and has long been of interest in technical mechanics [5]. In nature, such diverse tissues as the stems of plants, mammalian bones, the shells of crustaceans and the exoskeletons of sea sponges exhibit structure on scales from the molecular to the macroscale. Structural hierarchy has also become a topic of increasing interest in the design of man-made materials, and has been shown to provide a means of achieving greater toughness, economy of material and novel mechanical response [6, 7, 8, 9, 10, 11]. In spite of the apparent advantages of hierarchy, the number of hierarchical levels of human-made materials has been constrained by the difficulty and expense of building and maintaining such structures.

We therefore find it natural to pose the following question: *Why is structural hierarchy so prevelant and successful in biological tissues?* I motivate this inquiry with the following general observation: The more levels of assembly there are, the more distinct opportunities there appear to be to make an error. With ever more stages of assembly, then, it may naïvely seem that, as errors in assembly accumulate, a material's properties will become so variable as to render it useless. In fact, organisms routinely assemble tissues with robust and predictable properties suited to their function. This leads to the conjecture that the geometry of hierarchical structures confers an innate mechanical advantage.

In pursuing hunch, one must contend with a number of challenges. Tissues perform a diverse array of tasks, and accordingly possess diverse material properties. They may also be made of diverse constituents, and the mechanical characteristics of many tissues

stem from the fact that they are composites; bone, for instance, consists of a protein scaffold dressed with the mineral hydroxyapatite [12]. To constrain the study, we note that a common structural motif is an interlinked network of fibers. Over the past few decades, researchers have made strides in understanding such structures by modeling them as networks of elastic beams, which are capable of resisting bending and flexion [13, 14, 15, 16]. In this work, we seek to extend these modeling efforts to consider networks in which each bond is endowed with a fine-scale structure of bonds. Each bond in this fine-scale structure may then be replaced with a still finer structure. At the lowest level, bonds will be considered for modeling purposes to be made of elastic continua.

In this work, the material properties of interest will be the elastic moduli of the model systems under consideration. Following previous researchers, I vary these materials' elastic moduli by alternating the connectivity of the networks of beams from which they are constructed.

1.2 Theory of Elastic Frames

1.2.1 Maxwell Counting

A seminal advance in the systematic, quantitative theory of the rigidity of networks of beams was contributed by James Clerk Maxwell, in his 1864 article "On the Calculation of the Equilibrium and Stiffness of Frames" [17]. Maxwell presented an ingenious counting rule, according to which, in order to be rigid, a frame with N nodes, embedded in a d-dimensional space must have a number B bonds given by

$$B = N \cdot d - d - \binom{d}{2} \tag{1.1}$$

A heuristic argument for 1.1 is as follows: absent any constraints, the N points initially have $d \cdot N$ spatial degrees of freedom. Adding a bond capable of resisting stretching and compression then fixes the distance between a pair of points, thus reducing the number of

degrees in the system by one. Rigidity requires that the number of degrees of freedom be reduced to the number of rigid body translations, which is simply d, plus the number of rigid rotations in d dimensions, given by $\binom{d}{2}$. The result given in Eq. 1.1 is commonly referred to as Maxwell counting.

In the limit that the number of sites, N, in a frame is large, the number of bonds per joint in the frame must be approximately equal to the dimension, d, of the space in which the frame is embedded. As each bond is shared by two joints in the frame, each joint should have, on average, approximately $2d$ neighbors for the frame to be stiff. This mean number of neighbors is commonly referred to as the mean coordination number of the frame. An excellent modern review of these ideas may be found in, for instance, Ref. [18].

1.2.2 States of Self Stress and Rigidity of Generic Lattices

A frame is said to have linear rigidity if, to leading order, any relative displacement of its vertices costs a non-zero amount of energy. While equation 1.1 has proven to be of enduring value in anticipating linear stability, some caveats bear mentioning. First, the Maxwell criterion above is arrived at under the assumption that nodes in the network interact only through attractive and repulsive central forces. Moreover, even with the presumption of pure central force interactions, the Maxwell counting criterion is not strictly necessary or sufficient. As noted by Calladine [19], the Maxwell criterion is not strictly necessary because some networks support states of self stress, in which some bonds bear non-zero tensile or compressive forces without there being a net force on any joint in the network, and such pre-stresses confer linear stability.

The condition for mechanical equilibrium when some bonds bear non-zero loads may be expressed in matrix form, by means of a linear operator mapping the tensions in each of B bonds to the net forces on each of N nodes. Suppose bond b_i, which connects nodes j and k, bears a tension τ_i. If, in the reference state, nodes j and k have positions $\vec{r}_j$ and $\vec{r}_k$, there will be a restoring force $\vec{F}_{jk}$ on node j given by

$$\vec{F}_{jk} = -\tau_i \hat{r}_{kj}, \tag{1.2}$$

where $\hat{r}_{jk}$ is the unit vector pointing from $\vec{r}_k$ to $\vec{r}_j$. Now let $\mathbf{T}$ be a mapping from the B-dimensional vector of tensions, $\vec{\tau}$, to the $d \cdot N$-dimensional vector of forces, $\vec{F}$, with $d \cdot N$ rows and B columns. The ith elements of rows $d(j-1)$ to $d \cdot j - 1$ of $\mathbf{T}$ are then the negative of the d components of $\hat{r}_{jk}$. Likewise, the ith elements of rows $d(k-1)$ to $d \cdot k - 1$ are the negative of the components of $\hat{r}_{jk} = \hat{r}_{kj}$. States of self-stress are then defined by requiring

$$\mathbf{T}\vec{\tau} = 0, \tag{1.3}$$

and the number of states of self stress is then the dimension of the nullspace of $\mathbf{T}$. Introducing a set of pre-tensions to the bonds of an elastic network can stiffen modes that are nominally soft, a fact famously exploited by Buckminster Fuller to create so-called "tensegrity" structures [20].

Frames that nominally have enough bars to satisfy the Maxwell condition may also have redundant bonds, such that each bond does not provide a constraint on the motion of the joints that is linearly independent from the constraints provided by all other bonds. This problem may be formulated in graph theoretic terms, with the frame specified as a graph $\mathcal{G}$ containing the vertex set $\mathbf{V}$, joined by a set $\mathbf{E}$ of undirected edges, with positive weights, where vertices correspond to joints in a frame, and edges correspond to bars connecting pairs of joints. Such a graph represents a rigid frame if, once enough external constraints are imposed to prevent body rotations and translations, there exists a unique way to assign each vertex in the graph a Cartesian point, such that the Euclidean distance between any two points to which adjacent vertices are assigned equals the weight of the edge between those vertices. Laman [21] has demonstrated that, for a two-dimensional frame, with no special symmetries, there will be no redundant bonds if, and only if, for any subset of n

vertices and b bonds,

$$b \leq 2 \cdot n - 3. \tag{1.4}$$

Hendrickson [22] has identified an equivalent statement to Eq. 1.4 which, while stated in dense, graph theoretic terms, has proven to enable a much more computationally efficient manner of searching for redundant bonds, via the celebrated Pebble Game algorithm due to Jacobs and Thorpe [23].

1.3 Dilute Lattices

In modeling biological tissues, a core theoretical tool is the dilute elastic lattice, generally formed by first arranging network sites in a Bravais lattice, or a lattice with a basis, adding a bond between every pair of nearest neighbors, and then randomly removing bonds with probability $1 - p$, where p is referred to as the bond portion. In a seminal work by Feng, et al. [24], the authors predict the elastic constants of a dilute, triangular lattice with central force interactions between sites by treating the dilute lattice as an effective medium, in which no bonds are removed, but bonds are softer than those in the original lattice. This approach leads to the prediction of a first-order transition of elastic moduli to zero at a bond portion of $\frac{2}{3}$. As each site in an undiluted triangular lattice with nearest neighbor bonds is connected to six neighbors, this corresponds to a coordination number of 4, the minimum dictated by Maxwell counting. Above the threshold bond portion, stiffness is found to scale linearly with bond portion. Similar results are obtained for the three-dimensional face-centered cubic lattice, whose sites have a coordination number of 12 before dilution, and which therefore must retain at least half its bonds to remain rigid, as Maxwell counting demands a coordination number of 6 in three dimensions. Additional effective medium theory (EMT) treatments of the dilute triangular lattice have taken into account bending stiffness due to flexion of bonds [25] and a harmonic bending stiffness at joints between

neighbor bonds [26]. Both approaches predict an avoidance of the abrupt transition to zero of the elastic moduli at $p = \frac{2}{3}$, with scaling depending upon the sort of bending stiffness assumed, and the relative cost of bending and stretching of bonds.

1.4 Present Task

While there have been many remarkable advancements in our understanding of filamentous materials over the past half century, we perceive a lingering need for new guiding principles to explain how structural attributes on distinct length scales influence the overall properties of hierarchical materials. In the following chapters, we seek to build on previous studies of dilute lattices by simulating hierarchical structures in which the bonds on the largest scale are made of a network of small bonds. We will the proceed to develop an extended scaling law to capture the dependence of stiffness on the portion of bonds retained at each length scale. Hierarchical networks are attracting interest as a means of creating materials with designer properties [27, 28]. For our part, we wish to know how the use of bond portion as a control parameter may extend to hierarchical systems, and to understand the interplay of large-scale and small-scale structure in setting the overall mechanical attributes of a material. We now introduce a model system to explore these concepts.

CHAPTER 2
CREATING HIERARCHICAL NETWORKS

Investigating the properties of heirarchical, filamentous structures that allow them to possess robustly realized mechanical properties demands a tractable model system. We present such a system below, in which a self-similar, crystalline structure is produced, from which material is removed in a quasi-random manner. In developing a protocol for removing material, We seek to build upon the notion of bond portion, the fraction of bonds retained in a mechanical network possessing a single characteristic length scale, to establish an independent control parameter for each level of a hierarchical structure with an arbitrary number of distinct levels of spatial organisation.

2.1 Choice of Starting Structure

We begin with the well-studied triangular lattice in two dimensions. This lattice may be specified in terms of the primitive lattice vectors

$$\vec{a}_1 = \Big(1, 0\Big), \tag{2.1}$$

$$\vec{a}_2 = \Big(\frac{1}{2}, \frac{\sqrt{3}}{2}\Big). \tag{2.2}$$

We next suppose each bond in this lattice is made of a lattice of smaller bonds. The small-scale lattice will once more be chosen to be the triangular lattice, with one of its six-fold rotational symmetry axes aligned with the long axis of the large-scale bond, and an equal amount of material to either side of the center line of the large-scale bond. The transition to the two-level structure is illustrated in Fig. 2.1.

This process may in principle be iterated ad infinitum: at each iteration, the bonds at

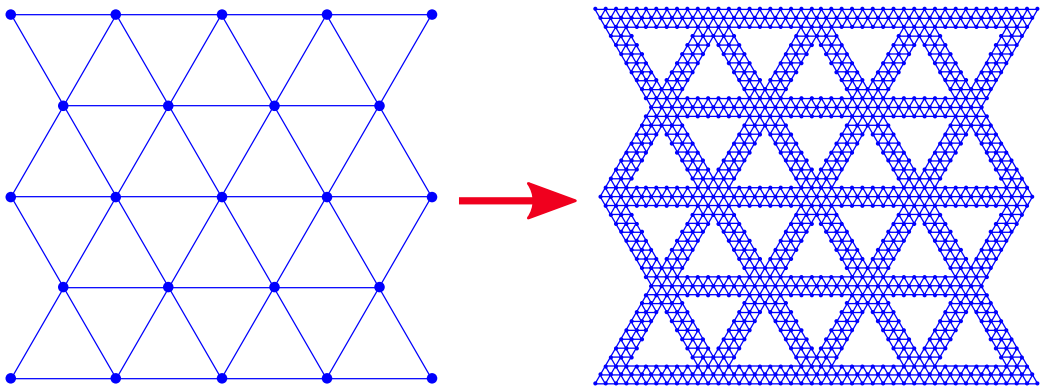

Figure 2.1: A two-level structure is formed by replacing each bond with a lattice structure made of smaller bonds.

the smallest length scale may themselves be replaced by a lattice of even smaller bonds. In this work, we have directly simulated networks with up to three levels of structural hierarchy (shown in Fig. 2.2). In a following chapter, I propose a means of extrapolating from simulation data to speculate about the properties of networks with greater numbers of hierarchical length scales.

2.2 Commensuration of Large and Small Scale

For the self-similar, crystalline structure considered here, we consistently ensure that an edge of a large-scale bond corresponds with a row of bonds on the smaller length scale, and that each large-scale vertex corresponds to a small-scale vertex. Denoting the large and small bond lengths by l_l and l_s, respectively, we then require $l_s = l_l/n$, where n is an integer, and require the large-scale bonds to have a width w that is an integral multiple of $\sqrt{3}l_s$. This final requirement is due to the fact that, for a triangular lattice with lattice spacing l, parallel rows of bonds are separated by $\frac{l\sqrt{3}}{2}$. The requirement that there be an equal number of small-scale bonds to either side of the center line of a large-scale bond demands that there be an odd number r rows, with $r-1$ spacings and overall width $\frac{(r-1)l_s}{\sqrt{3}}$.

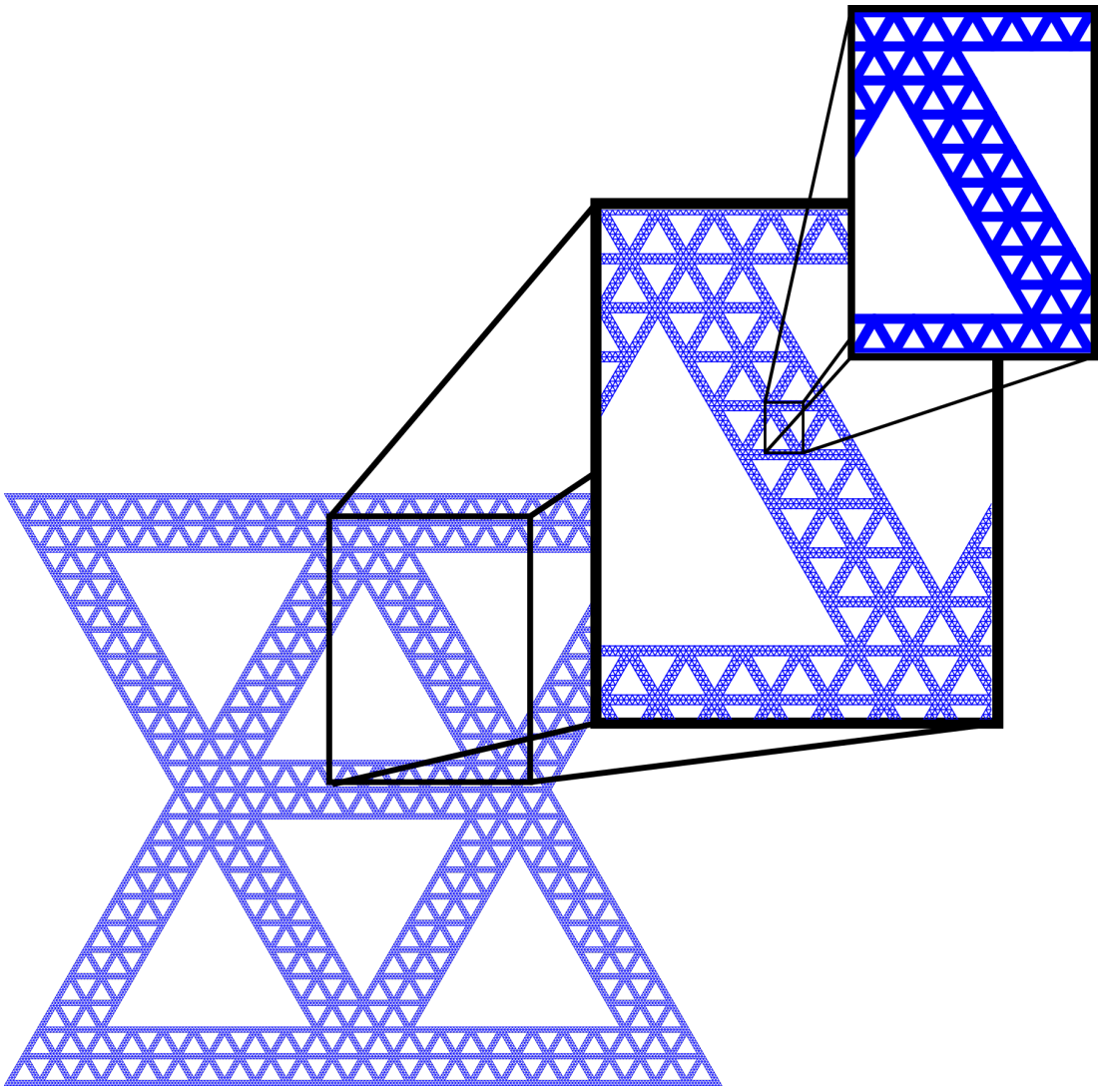

Figure 2.2: A structure is shown in which the procedure introduced above is iterated one step further.

2.3 Multiscale Dilution

We now seek to generalize the notion of bond dilution. It is common practice to remove bonds entirely at random, allowing for the possibility of isolated portions of the network that do not mechanically participate, and even the absence of a system-spanning cluster, such that there can be no linear resistance to an applied stress. We regard this as unrealistic for tissue, and antagonistic to our objective of precisely specifying the bond portion at each scale. This second concern is due to the fact that entirely random removal of small-scale bonds may cleave a large-scale bond, or rupture a junction between two large-scale bonds.

We start by specifying each length scale to be created. The large-scale structure is created and diluted first. Dilution is performed by connecting all points using a randomly generated spanning tree. The spanning tree is created by randomly shuffling all edges, then adding edges to the spanning tree provided that they do not create a cycle, as determined by the union-find algorithm, until all vertices are included in the spanning tree. Following creation of a random spanning tree, we randomly add edges that have not yet been selected until the desired number of bonds have been retained. This process creates a "skeleton", from which an envelope is created, with large-scale bonds endowed with some non-zero width, w, obeying the criterion stated above.

We next produce the network structure at the next-smallest length scale, and retain those small-scale bonds which fit within this large-scale envelope. We initially partition the small-scale structure sub-networks contained within individual large-scale bonds, and additionally note those segments that straddle adjacent pairs of large-scale bonds. We then connect the small-scale vertices within each large-scale bonds in a randomly generated minimum spanning tree, in the manner described above, and additionally ensure each adjacent pair of large-scale bonds is connected by at least one small-scale tether. After this, unused small-scale bonds are added at random, until the desired overall fraction has been retained. If another structure is to be defined at an even finer length scale, the bonds mak-

ing up the current smallest length scale may themselves be endowed with some non-zero width, and serve as the new envelope. This procedure is illustrated schematically in Fig. 2.3.

Networks with varying levels of structural hierarchy may be regarded as increasingly sparse assemblies made from the same fundamental building block — a short fiber of given length and stretching modulus. Networks with just a single characteristic length scale are the result of directly assembling such building blocks to produce the final structure. Networks with two levels of hierarchy are the result of first assembling individual fibers into a lattice to produce large-scale bonds, and stitching these large scale bonds together. As more intermediate stages of assembly are added, the final structure becomes progressively less dense, and thus it is to be expected that the maximum attainable stiffness (that which is observed when all bonds are retained on all scales) will decrease. In the following chapter, We will present a confirmation of this decrease in maximum possible stiffness by direct calculation. This is not necessarily a liability for a tissue, as an increase in stiffness may not necessary or even desirable, and any benefit conferred by extra material may be not be worth the added expense of construction and additional weight. Crucially, we will demonstrate that, for a given target stiffness and an error-prone assembly process, the most hierarchical structure capable of attaining the desired stiffness will offer the least variability in its mechanical properties.

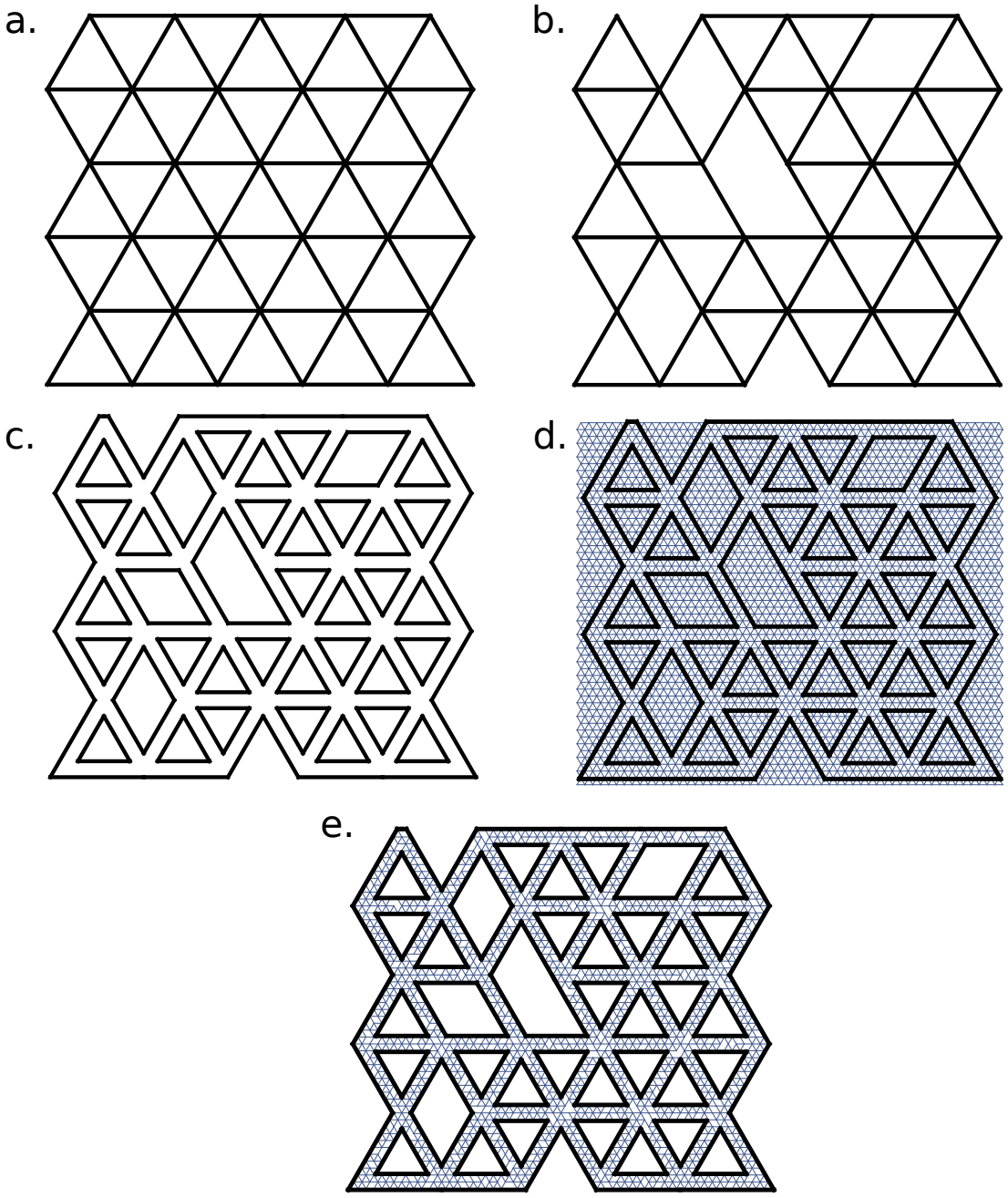

Figure 2.3: We begin with a triangular lattice (**a**), pare away a certain portion of bonds (**b**), endow the bonds with some non-zero stiffness (**c**), lay the resultant envelope over a small-scale structure to determine which small-scale (**d**) bonds to keep, and finally dilute the small-scale structure (**e**).

CHAPTER 3

SIMULATION PROCEDURE

In this chapter we discuss the manner in which physical properties of the structures to be investigated were determined. Here, we are principally concerned with the tensile stiffness of the networks, to be obtained by a simulated tensile strain. Below, we detail the process of imposing boundary conditions and performing a structural relaxation of the network, as well as the means by which simulation data are analyzed and values for the tensile stiffness are computed. Finally, we present a comparison of simulation data with model predictions.

3.1 Structural Relaxation Procedure

We begin with the constraint that the y coordinates of the bottom nodes of the network remain fixed, while constraining the top nodes to have some displacement d in the y direction. The x coordinates of the top and bottom, and both the x and y coordinates of all other vertices, are relaxed, such that the residual strain energy is minimized for the given constraints. Connections are modeled as linear springs, such that when two vertices i and j, with rest positions $\vec{r}_{i,0}$ and $\vec{r}_{j,0}$ are displaced by the vectors $\vec{u}_i$ and $\vec{u}_j$, vertex i is subject to the force

$$\vec{F}_{j\,\mathrm{on}\,i} = -k_{ij}(|\vec{r}_i + \vec{u}_i - \vec{r}_j - \vec{u}_j| - |\vec{r}_i - \vec{r}_j|)\frac{\vec{r}_i + \vec{u}_i - \vec{r} - \vec{u}_j}{|\vec{r}_i + \vec{u}_i - \vec{r}_j - \vec{u}_j|}, \tag{3.1}$$

where $k_{i,j}$ denotes the spring stiffness of the bond connecting the two nodes. We suppose each bond to be a fiber with the same stretching modulus, μ, so that if the rest separation between nodes i and j is l_{ij}, the bond between these nodes has stiffness

$$k_{ij} = \frac{\mu}{l_{ij}} \tag{3.2}$$

As we are interested in the fluctuation of stiffness in response to variation in certain structural attributes, the precise value of μ is not of essential importance, and we set it to 1 for convenience.

Relaxation is carried out using the Fast Inertial Relaxation Engine (FIRE) algorithm [29]. This technique employs a modified molecular dynamics, in which each degree of freedom in the optimization is given a velocity and inertial mass. This inertial mass helps the search avoid becoming trapped in a false minimum. The force on each degree of freedom is calculated by taking the gradient of the energy with respect to that degree of freedom and adding additional terms to damp and steer the motion, to keep the search moving downhill in the energy landscape. If the search begins moving in a direction of increasing energy, the search is momentarily halted, and the process is resumed with the parameters to be relaxed beginning from "rest". As the relaxation process is carried out, the RMS value of all force components on all vertices in the network is recorded, and the search is terminated when this value descends below a given threshold. Once the network has been relaxed, the interaction energies between all pairs of connected nodes are computed and summed to determine the residual strain energy in the network. Strains of several different magnitudes are imposed on the network, to produce a curve of energy vs. displacement.

As noted above, we presume each bond to be a fiber with unit stretching modulus. As this stretching modulus has units of energy per unit length, this sets a natural characteristic force scale. For one and two-scale networks, we relaxed nodes until the residual RMS force descended below 10^{-11}, in units of stretching modulus. Calculations for three-level networks, which had as many as a million bonds, proved much more demanding, and relaxed until the RMS force reached 10^{-9}, in units of stretching modulus.

3.2 Determination of Stiffness

After determining the energy for five values of strain, we fit a power law to the data, and compute the stiffness of the network by taking the second derivative of the power law with

respect to the displacement of the top nodes. In cases in which a power law fit could not yield a correlation coefficient, r, of at least $.9$, we found that the residual strain energy was negligibly small — often, after one of the bond portions descended below a critical value, the strain energy would drop by eight orders of magnitude. In Fig. 3.1, we provide characteristic examples of a strong fit, a marginal fit, and a poor fit.

For one and two-level networks, we produced three network realizations for each combination of parameters considered, and calculated the final stiffness as the mean of the stiffness values obtained for these realizations. As an initial check on our technique, we performed calculations for one-level dilute lattice, with bond portions varying from .6 to 1, in steps of .05. we considered square samples measuring 50 by 50, in units of the lattice spacing. When simulating two-level networks, we varied both the large and small-scale bond portions from .6 to 1, in steps of .05. In this case, samples were once again square, and measured 10 by 10, in units of the large-scale bond length. Small-scale bonds were one tenth the length of large-scale bonds, and large-scale bonds contained three rows of small-scale bonds, giving them a width of $\sqrt{3}$ times the small-scale bond length. Owing to the greater expense of simulating three-level networks, we varied the bond portion at each scale from .8 to 1, in steps of .1, and considered one realization for each case. Once more, networks were square and measured 10 by 10, in units of large-scale bond length. The bonds on the intermediate scale were one-tenth the length of the bonds on the largest scale, and the bonds at the smallest scale were one-tenth the length of the bonds on the intermediate scale. In keeping with the two-level case, large-scale bonds contained three rows of intermediate-scale bonds, and intermediate-scale bonds contained three rows of small-scale bonds.

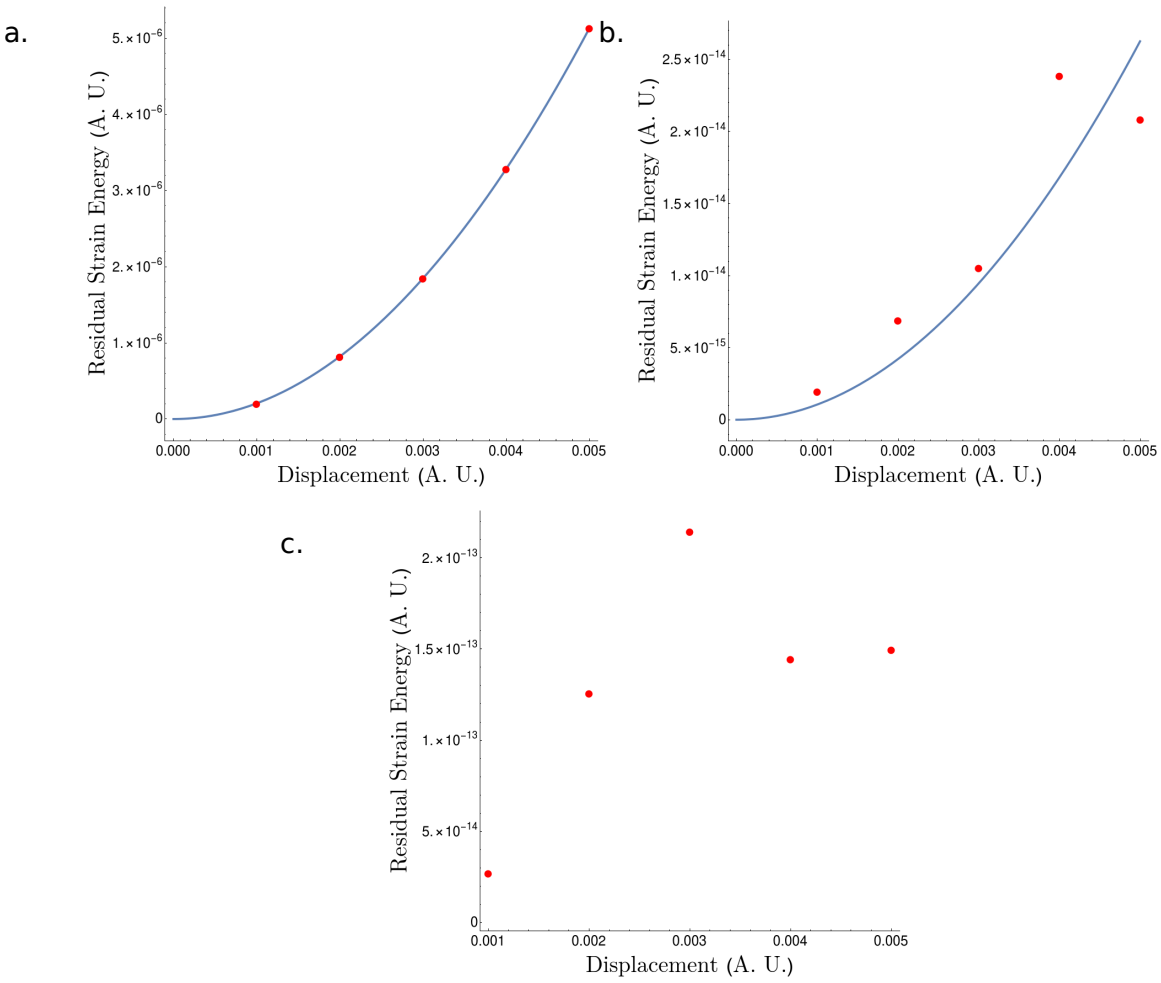

Figure 3.1: We show plots of energy vs. tensile stretch, in arbitrary simulation units, for cases in which **a.** a strong fit to a parabola could be obtained, **b.** a marginal fit was obtained and **c.** a case in which the data appear erratic. Crucially, the residual strain energies shown in **c.** are much lower than those in **a.**, and we regard networks that yield plots such as **c.** as having zero stiffness.

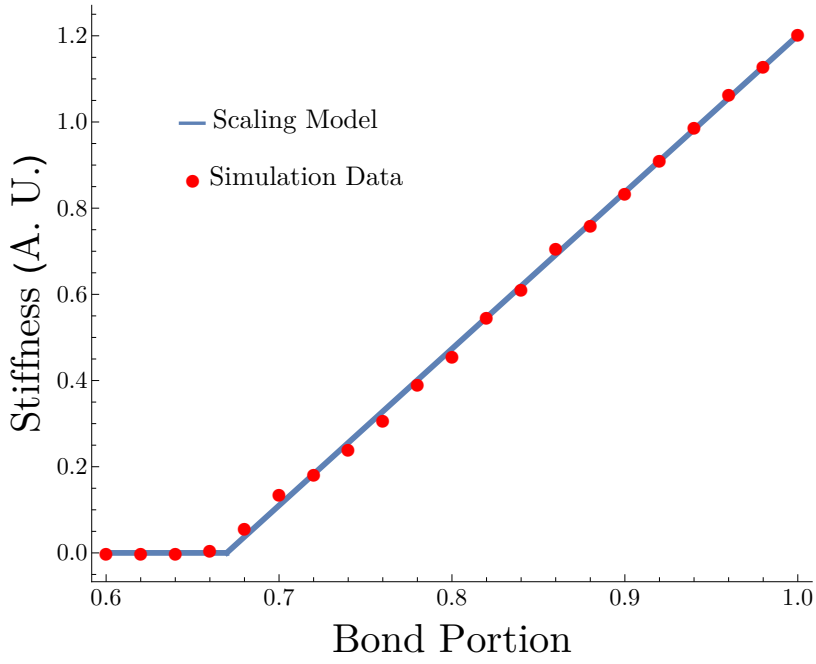

Figure 3.2: Data are shown confirming good agreement between the scaling model for the simple dilute triangular lattice and simulation data.

3.3 Simulation Results

3.3.1 Single Length Scale Structures

Our simulations of one-level networks exhibited good agreement with previous investigations. Recall that, for the single-scale triangular lattice, Feng, et al. [24] predict that elastic moduli should scale with the bond portion, p, as

$$K(p) = \begin{cases} K_{max}\frac{(p-p_c)}{1-p_c}, & p \geq p_c \\ 0, & p < p_c, \end{cases} \tag{3.3}$$

where, from Maxwell counting, the critical bond portion p_c is expected to be $\frac{2}{3}$. In practice, we find a marginally higher critical bond portion, $p_c = .670$, with excellent agreement between simulation data and Eq. 3.3 ($r^2 = .983$). We show a comparison between our model fit and simulation data for a single-level structure in Fig. 3.2.

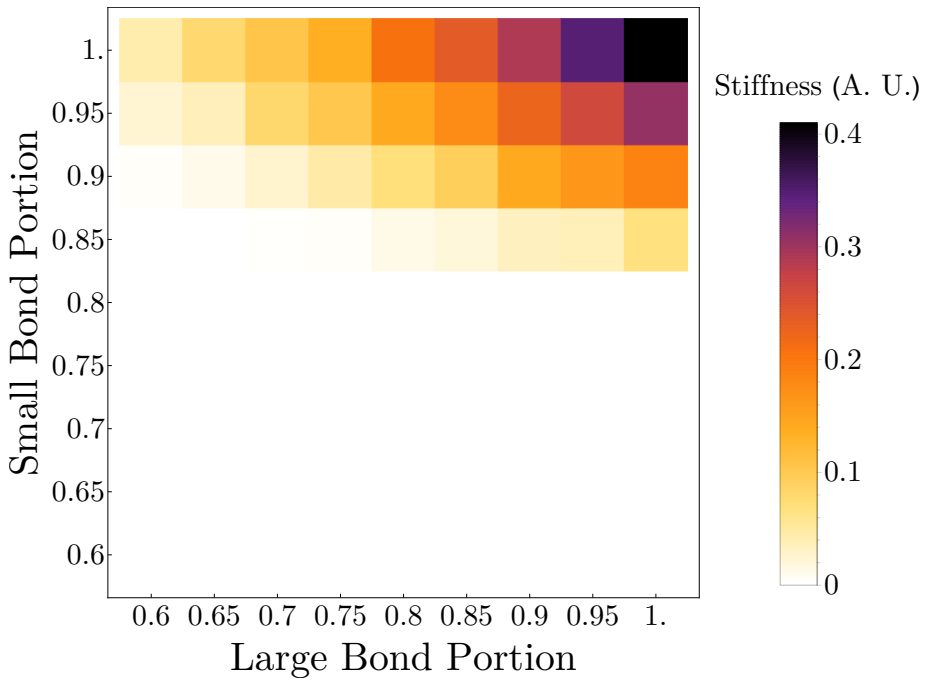

Figure 3.3: Data are shown for the tensile stiffness, in simulation units, of filamentous networks with two levels of structural hierarchy, in which the large and small-scale bond portions are varied from .6 to 1. Note the much more abrupt softening as the small-scale bond portion is decreased.

3.3.2 Two-Level Networks

We now discuss simulation results for networks formed by replacing each bond in a possibly dilute triangular lattice with a lattice of smaller bonds, as described earlier. We systematically varied the small and large-scale bond portions in the range $[.6, 1]$ to map out the stiffness in two-dimensional parameter space, as shown in Fig. 3.3. Two striking aspects of the stiffness data for two-level networks are the markedly lower maximum stiffness than that of single-level networks, and the much more rapid decrease in stiffness resulting from small-scale dilution as opposed to large-scale dilution.

The lower maximum attainable stiffness, as noted in Chapter 2, may be ascribed to the lower density of a two-level structure. Our choice of large-scale bonds that are 10 times the length of small-scale bonds, and which contain three rows of small-scale bonds, is equivalent to carving a regular array of equilateral triangules from a single-scale triangular

lattice, with each hole possessing a side length 7 times the length of a small-scale bond. A primitive cell for this hierarchical structure is then a parallelogram spanned by the vectors:

$$\vec{v}_1 = (10l_s, 0)\,, \tag{3.4}$$

and

$$\vec{v}_2 = \left(5l_s, 5\sqrt{3}l_s\right), \tag{3.5}$$

and total area

$$A_{cell} = 50\sqrt{3}l_s^2, \tag{3.6}$$

where l_s denotes the length of a small-scale bond.

Each primitive cell contains two triangular holes, each with area

$$A_{hole} = \frac{49\sqrt{3}l_s^2}{4} \tag{3.7}$$

Summing the areas for the two holes, we find that approximately half the area of the small-scale network is removed to create the large-scale structure, and so the decrease in stiffness is sensible.

We now address the markedly more abrupt softening associated with the dilution of small-scale bonds as opposed to large-scale bonds. A key observation is that, due to the finite width of large-scale bonds, hierarchical structures gain a great deal of surface. Small-scale bonds at the edges of large-scale bonds have only four neighbors, rather than the six neighbors possessed by small-scale bonds in the interior. Removal of small-scale bonds therefore immediately presents the liability of introducing soft modes of deformation into the network. Most large-scale bonds, on the other hand, are in the bulk, and a far greater fraction of them must be removed before the network becomes under-constrained. In fact,

two-level networks can remain rigid even when the large-scale bond portion is markedly less than the value of $\frac{2}{3}$ expected from naïve Maxwell counting. We attribute this to an effective bending stiffness at the junctions between large-scale bonds, as the angles between large-scale bonds cannot in general be varied without changing the lengths of small-scale bonds. We quantify this bending stiffness in Appendix A.

We now attempt to capture the behavior shown in Fig. 3.3 by expanding Eq. 3.3. We take the bond portion in Eq. 3.3 to be the large-scale bond portion, and assume that the stiffness of each large-scale bond is inherited from its small-scale structure, and can thus be related to some excess bond portion at the small scale. Defining p_l as the portion of large-scale bonds retained, and p_s as the portion of small-scale bonds retained, we then propose the following ansatz for the stiffness, K:

$$K = \begin{cases} K_{max}\frac{(p_l - p_{l,c})(p_s - p_{s,c})}{(1-p_l)(1-p_s)}, & p_l > p_{l,c} \quad \& \quad p_s > p_{s,c} \\ 0, & p_l < p_{l,c} \quad \text{or} \quad p_s < p_{s,c} \end{cases} \tag{3.8}$$

where K_{max} is the maximum attainable stiffness, and $p_{l,c}$ and $p_{s,c}$ are the large and small-scale critical bond portions, respectively.

We seek a fit of our simulation data to Eq. 3.8 by setting K_{max} equal to the stiffness of the fully connected, two-level triangular lattice, and using an extrapolation procedure to determine values for $p_{l,c}$ and $p_{l,s}$. To obtain $p_{l,c}$, we consider stiffness values for networks with full small-scale bond portion and varying large-scale bond portion. We consider just those networks with non-negligible stiffness, fit a line to stiffness vs. bond portion data, and determine the critical large-scale bond portion by finding the x intercept of this fit. Further information on this procedure may be found in Appendix B. We applied a similar procedure to find the small-scale bond portion. We summarize our findings in Table 3.1.

We find this fitted model aptly captures the simulation data, as shown in Fig. 3.4. A plot of the stiffness given by the model vs. the simulation value for a given pair of large and small-scale bond portions yields a linear trend with a slope of 1.01, and an r^2 value of

Table 3.1: Data are shown for the fit of the expanded scaling ansatz to simulation data for two-level networks. We note a markedly more abrupt softening of the network with decreasing small-scale bond portion.

Parameter	Value
K_{max} (A. U.)	.411
$p_{l,c}$	.58
$p_{s,c}$	.83

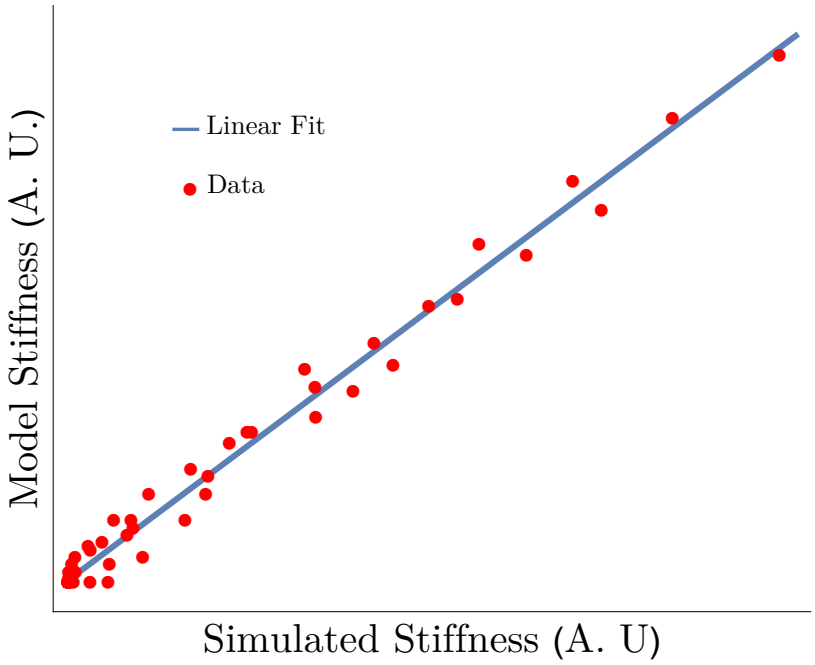

Figure 3.4: Data are shown comparing the fitted scaling model to simulation data for the tensile stiffness for networks with two levels of structural hierarchy. We find the model aptly captures the dependence of the tensile stiffness on the small and large-scale bond portions.

.989. We therefore conclude our scaling model works well for two levels.

3.3.3 Three-Level Networks

We sought to further test our scheme for expanding Eq. 3.3 to networks with three levels of structural hierarchy. We were somewhat more parsimonious with our simulations of three-levels networks, due to the vastly greater number of bonds we needed to simulate to have a statistically significant number of bonds at the large, intermediate, and smallest length scales. A network that was fully connected on each scale, and that measured 10

large bonds by 10 large bonds, had $\sim 10^6$ small-scale bonds. We focused on the cube in three-level bond portion space spanning .8 to 1 for small-scale, intermediate-scale and large-scale bond portion, although a small-scale bond portion of .8 proved to be below the threshold for marginal stiffness. We varied each bond portion in steps of .1. In Fig 3.5, we show stiffness vs. large-scale and intermediate bond portion, with the small-scale bond portion fixed at .9 and 1.

We now seek to build upon Eq. 3.8, by adding an intermediate bond portion and accompanying critical bond portion, to obtain

$$K = K_{max}\frac{(p_l - p_{l,c})(p_{im} - p_{im,c})(p_s - p_{s,c})}{(1 - p_{l,c})(1 - p_{im,c})(1 - p_{s,c})}, \tag{3.9}$$

where as before, K_{max} indicates the maximum attainable stiffness, p_l, p_{im} and p_s denote the large, intermediate, and small-scale bond stiffnesses, respectively, and the addtion of a c in a subscript denotes the critical bond portion. To find the three critical bond portions, we used a similar procedure to that employed for the two-level case. Because the critical bond portions for the large and intermediate scales appeared to be lower than $.8$, We fit a line to a plot of stiffness vs. either large or intermediate-scale bond portion, with the other two bond portions fixed, and extrapolated to estimate the crtical bond portion. For the small-scale bond portion, because only bond portions 1 and .9 yield non-zero stiffness values, we also considered the combination of bond portions $p_l = 1$, $p_{im} = 1$, and $p_s = .85$, so our fit of stiffness vs. small-scale bond portion with fixed large-scale and intermediate-scale bond portion would have at least three non-zero values of stiffness. Further details may be found in Appendix B. Parameters for the three-level model are reported in Table 3.2.

We find that the large and small-scale critical bond portions are very similar to those obtained for two-level lattices, while the intermediate critical bond portion lies between these two. While the intermediate bond portion is somewhat larger than the central force threshold, it is much lower than the small-scale critical bond portion. We attribute this to the fact that, while large-scale bonds each contain three rows of intermediate-scale bonds, such that

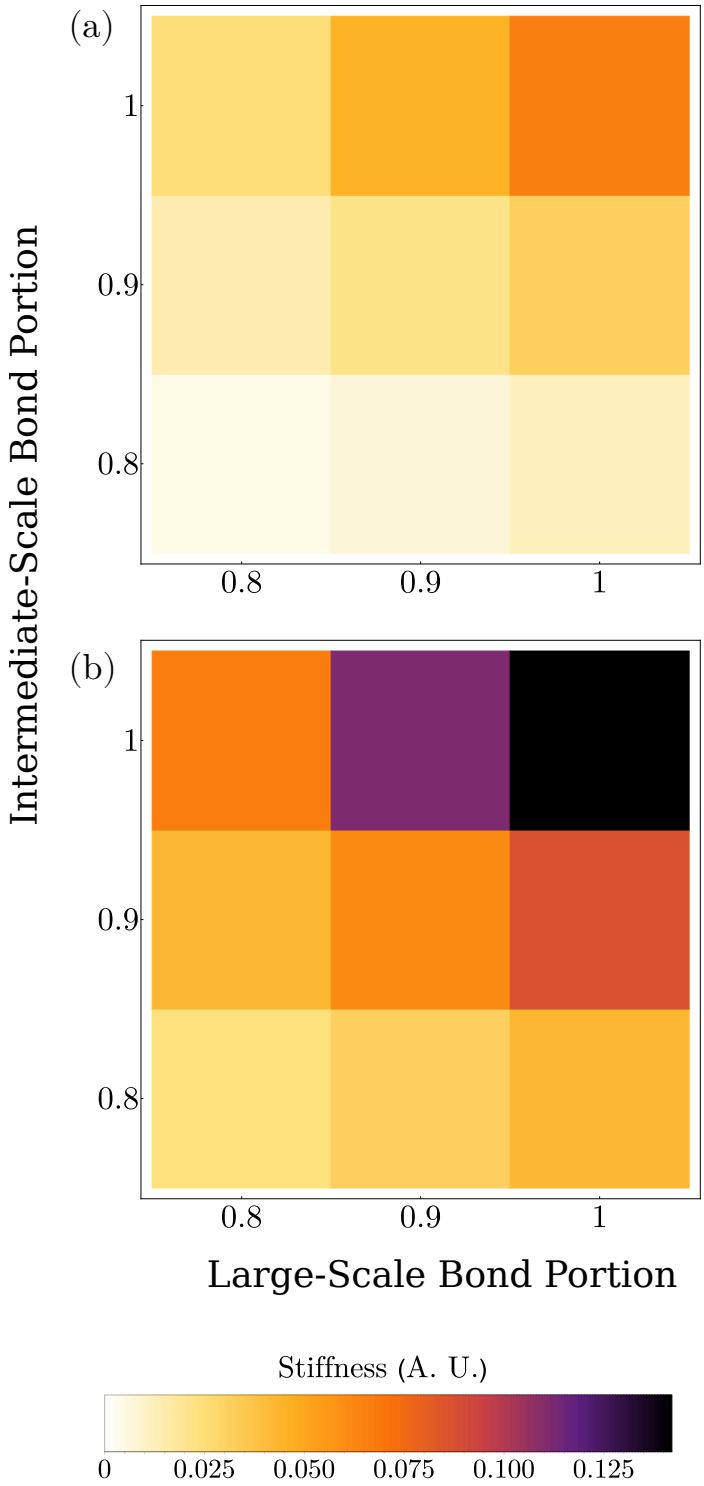

Figure 3.5: We compare the scaling of stiffness with varying large-scale and intermediate-scale bond portions, while the small-scale bond portion is fixed at **(a)** .9 and **(b)** 1.

Table 3.2: Data are shown for the fit of our expanded scaling ansatz to simulation data for three-level networks. The network is still most permissive of low large-scale coordination number, but the critical intermediate-scale bond portion is markedly lower than that of the small scale.

Parameter	Value
K_{max} (A. U.)	.142
$p_{l,c}$	.62
$p_{im,c}$	.72
$p_{s,c}$	.83

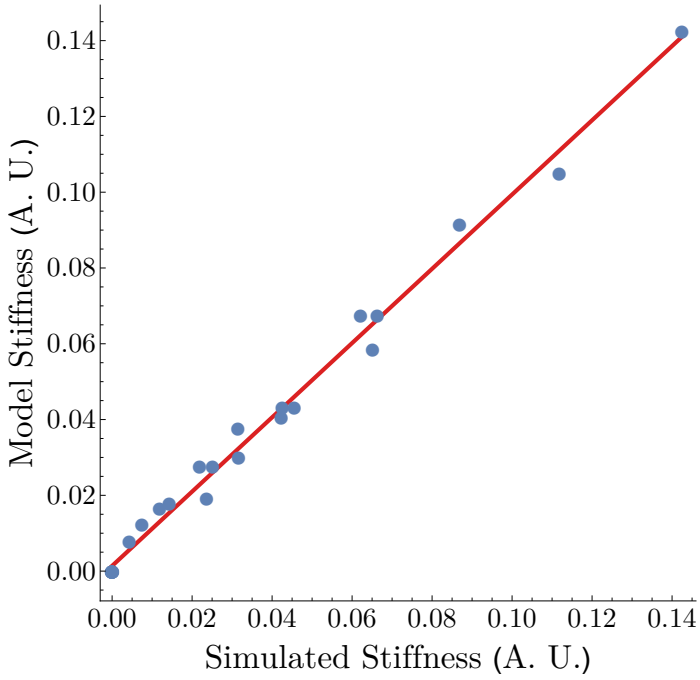

Figure 3.6: We show a comparison between the fitted model and simulation data for ordered triples in bond portion space, with bond portions varied from .8 to 1, in steps of .1.

under-coordinated edge vertices will immediately result from removal of intermediate-scale bonds, bonds on the intermediate scale also have an emergent bending stiffness, inherited from the small-scale structure. We expect this to somewhat mitigate the effect of edge vertices with low coordination number, thus delaying the loss of rigidity. In comparing our data to the model, we once more find good agreement. A plot of our fitted model value vs. our simulation value for each triple of bond portions considered yields a slope of .98 with an r^2 value of .99, as exhibited in Fig. 3.6.

3.4 Discussion

The success of the model for one, two and three-level networks encourages me to postulate a general model for networks with an arbitrary number N levels of structural hierarchy. While We have specifically considered the case in which the ratio of bonds on one scale to those on the next-smallest scale is $10:1$, and large-scale bonds contain three rows of small-scale bonds, we have found by direct calculation that our model works for a two-level structure in which large-scale bonds are twenty times the length of small-scale bonds, and contain five rows of small-scale bonds. We have also established general constraints on the aspect ratio of large-scale bonds. Details of these calculations are provided in Appendix C. For now, we note two extremes that may become an issue. Large-scale bonds may be too slender, such that, as the network contracts in the direction transverse to an applied tensile strain, bonds oriented transverse to the direction of applied strain immediately buckle. On the other hand, large-scale bonds may be so broad that the gaps between adjacent large-scale bonds shrink to tiny apertures, such that the resulting structure is better modeled as a lattice with one characteristic length scale and an array of small perforations. To avoid these concerns, we find that lattices should obey

$$l/w \gtrsim 2 + 3/w, \tag{3.10}$$

and

$$\frac{l}{w} \lesssim \varepsilon^{-1/2}, \tag{3.11}$$

where l and w are the length and width of large-scale bonds. We have found that the networks considered here comfortably obey these bounds. We have also repeated our analysis of two-level structures for networks in which the small-scale bond length is kept the same, but the width and length of large-scale bonds are doubled, and have once more found Eq. 3.8 to apply to such networks. Details of the calculation are given in Appendix E.

Provided a hierarchical network obeys the above constraints, we then propose that a network with N levels of structural hierarchy will have a stiffness

$$K = K_{max} \prod_{i=1}^{N} \begin{cases} \frac{p_i - p_{i,c}}{1 - p_{i,c}}, & p_i > p_{i,c} \\ 0, & p_i \leq p_{i,c} \end{cases} \tag{3.12}$$

where p_i and $p_{i,c}$ denote the bond portion and critical bond portion for the ith scale.

An expression such as Eq. 3.12 can offer valuable insight into the mechanics of complex, filamentous structures. Such materials can be difficult to simulate, and even when simulations are available, analyzing the results to gain physical insight can be a formidable task. Our model puts us in a position to discuss possible liabilities and advantages organisms may have encountered while evolving larger, more hierarchical tissues.

CHAPTER 4
ERROR TOLERANCE

Having developed a useful scaling model for capturing the stiffness of hierarchical, filamentous networks, we now investigate the implications for the robustness of such structures against errors in assembly. We consider the result of random errors in the portion of bonds retained at each stage of assembly on the final stiffness of a network. Using a combination of computation and analytical work, we find that increasing the number of levels of hierarchy generally diminishes the relative variation in stiffness of the finished product. We show that this result persists for multiple types of statistical distributions of assembly errors. Findings discussed herein are now in publicaiton in *PNAS* [30].

4.1 Simulating Random Errors

To develop a notion of error tolerance, we must first give a quantitative definition of error. We suppose that a material with N levels of structural hierarchy has some optimal stiffness, K, achieved by a certain combination of bond portions $\vec{p}^* = (p_1^*, \cdots, p_N^*)$. We now suppose that, in practice, the actual set of bond portions varies from this target point in bond portion space by some vector $\vec{\delta}$, with some probability distribution function in N-dimensional bond portion space $\mathcal{P}(\vec{\delta})$. For some network realization with the set of bond portions $\vec{p}+\vec{\delta}$, we then define error as the difference $K(\vec{p}+\vec{\delta})-K(\vec{p})$ between the optimal and actual stiffness.

We first consider a case in which the target point in bond portion space is near the threshold of vanishing stiffness. Here, we numerically compute the probability distribution function of the stiffness, given a desired point in bond portion space. We suppose for the time being that the bond portion on each hierarchical scale is independently and identically distributed, such that the total PDF for the distribution of errors for an N-level structure,

$\mathcal{P}(\vec{\delta})$, may be written

$$\mathcal{P}(\vec{\delta}) = \prod_{i=1}^{N} \mathcal{P}(\delta_i) \tag{4.1}$$

To produce PDFs for network stiffness, we start with a target point and add a pseudorandom number to the bond portion at each hierarchical level. We then calculate the stiffness corresponding to this modified point in bond portion space, as illustrated schematically in Fig. 4.1. For networks with one and two levels of structure, we use interpolation, while for networks with three levels, we use a fit function of the form Eq. 3.12. For each level, we have assumed a Gaussian distribution of errors on each scale with a uniform variance σ^2. In each case, we perform $50,000$ trials, and numerically estimate a PDF from a histogram of our data.

We show a PDF resulting from our procedure in Fig. 4.2, and note a striking feature – PDFs become markedly narrower with increasing numbers of hierarchical levels, and the PDF for the single-level structure has a peak at zero stiffness. For one level structures, there is the liability that a random walk in bond portion space about the target value will veer beyond the cusp at which stiffness vanishes. We note that, for a one-level structure, every step in bond portion space corresponds to a change in stiffness. For a two-level structure, however, a deviation from the target point in bond portion space can be parallel to a contour of constant stiffness, perpendicular to this contour, or some combination of the two. With increasing numbers of structural hierarchy, the space of paths that, to leading order, leave the stiffness unchanged, grows. Therefore, provided the variability of a material's structural attributes is not too great, a modular assembly process may actually offer a built in resilience to large fluctuations in its final material properties.

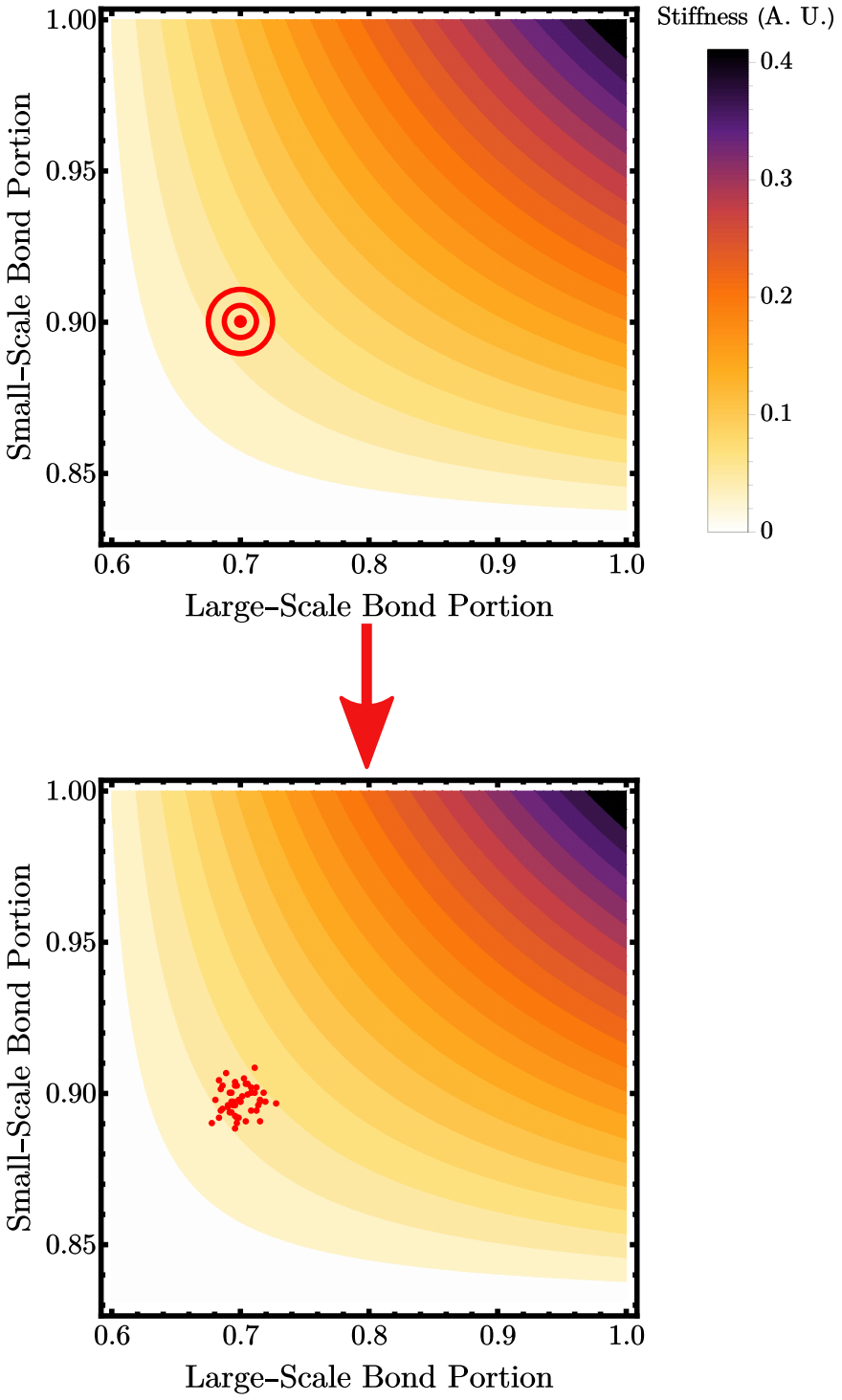

Figure 4.1: We show in **(a)** a target point in bond portion space, marked with a bull's eye, superimposed on a contour plot showing stiffness vs. large and small- scale bond portion. In **(b)**, we show a collection of random points, uniformly distributed about the target point, at which stiffness is to be evaluated to determine the distribution of mechanical properties that would result from a slightly error-prone assembly process.

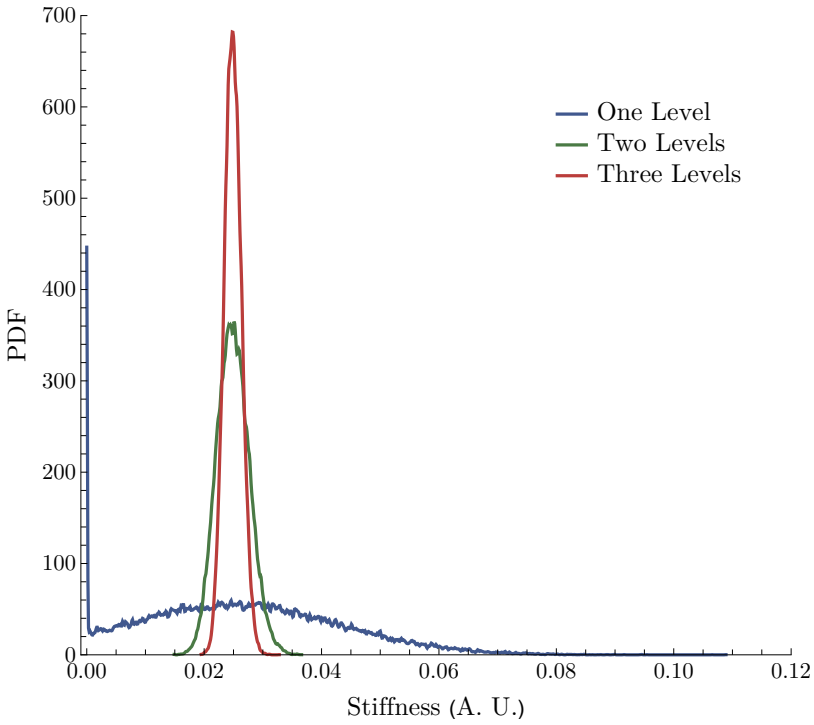

Figure 4.2: We show the probability distribution function of stiffness for one, two and three level networks when a nominal point in bond portion space is selected for each case with the same excess bond portion on each scale and a corresponding stiffness of .025. We add Gaussian random noise with zero mean and standard deviation .005 to each bond portion. We find increasing the number of heirarchical levels increases resilience to errors and leads to narrow distributions of final mechanical properties.

4.2 Analytical Prediction of Relative Error

We now treat a limit in which the target point $\vec{p}^*$ in bond portion space is suitably far from the contour of vanishing stiffness that we can safely assume the distribution of "noisy" points centered about the target has negligibly little statistical weight in regions of bond portion space in which stiffness is zero. For N levels, we define an excess bond portion $p_{e,i}$ for each level, with $1 \leq i \leq N$:

$$p_{e,i} = p_i - p_{c,i} \tag{4.2}$$

and once more assume the distribution of errors, $\mathcal{P}(\vec{\delta})$, has the form of Eq. 4.1.

We then define the reduced stiffness

$$\bar{K} = \frac{K}{k \prod_{i=1}^{N} (1 - p_{c,i})} \tag{4.3}$$

With this definition we now find the expected deviation in the stiffness of a network with N hierarchical levels. The mean of $\bar{K}$ is

$$\left\langle \bar{K} \right\rangle = \int \cdots \int \left(\prod_{i=1}^{N} (p_{e,i} + \delta_i) \right) \mathcal{P}(\delta_1, \ldots, \delta_N)\, d\delta_1 \cdots d\delta_N \tag{4.4}$$

$$= \prod_{i=1}^{N} p_{e,i} \tag{4.5}$$

while the mean square stiffness is

$$\left\langle \bar{K}^2 \right\rangle = \int \cdots \int \left(\prod_{i=1}^{N} \left(\delta_i + p_{e,i} \right)^2 \right) \mathcal{P}(\delta_1, \cdots, \delta_N)\, d\delta_i \cdots d\delta_N \tag{4.6}$$

$$= \prod_{i=1}^{N} \sigma_i^2 + p_{e,i}^2 \tag{4.7}$$

The standard deviation in stiffness is then

$$\Delta\bar{K} = \sqrt{\prod_{i=1}^{N}\left(\sigma_i^2 + p_{e,i}^2\right) - \prod_{i=1}^{N} p_{e,i}^2} \tag{4.8}$$

Here it has been assumed that $p_{e,i} \gg \sigma_i$ for all i, so integration can be carried out with the assumption that Eq. 3.12 holds for all values δ_i that contribute appreciably to the integral. In the special case in which the excess bond portion is the same on each length scale, and each bond portion has the same standard deviation, (4.8) reduces to

$$\sqrt{\left(\sigma^2 + p_e^2\right)^N - p_e^{2N}},$$

with $p_e = \bar{K}^{1/N}$. The relative error in stiffness then scales with N as

$$\frac{\Delta\bar{K}}{\bar{K}} = \frac{\sqrt{\left(\sigma^2 + p_e^2\right)^N - p_e^{2N}}}{p_e^N} \tag{4.9}$$

$$= \sqrt{\left(1 + \frac{\sigma^2}{p_e^2}\right)^N - 1} \tag{4.10}$$

$$\approx \frac{\sqrt{N}\sigma}{p_e} \tag{4.11}$$

or

$$\frac{\Delta\bar{K}}{\bar{K}} \approx \frac{\sqrt{N}\sigma}{\bar{K}^{1/N}}, \tag{4.12}$$

where the last approximation holds when $\sigma \ll p_e$. For a target $\bar{K}$, this functional form predicts the optimal number of levels to be

$$N^* = \lfloor -2\ln\left(\bar{K}\right) \rfloor \tag{4.13}$$

We have run numerical tests to check the above results, using the technique described in the previous section to generate the expected standard deviation of stiffness. We have specifically considered a structure diluted such that is has one one-thousandth of its maxi-

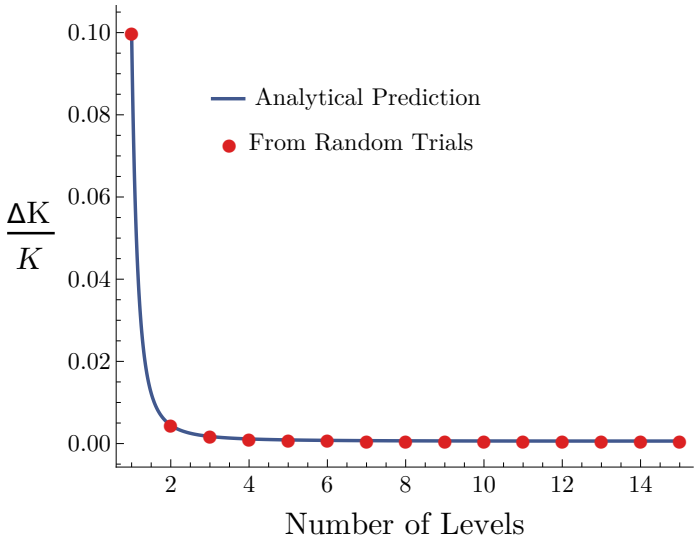

Figure 4.3: We show the relative standard deviation in stiffness for networks with one to fifteen levels of structural hierarchy, when each network has been diluted on each scale such that it has one one-thousandth its maximum possible stiffness.

mum possible stiffness. For networks with one, two and three hierarchical levels, we used models fitted from simulation data, while for networks with more levels of structures, we relied upon the general scaling prediction given by Eq. 3.12. In all, we considered structures with one to fifteen levels of structure. As shown in Fig. 4.3, our formula for $\frac{\Delta K}{K}$ consistently works well suitably far from a contour of vanishing stiffness.

4.3 Alternative Distributions

We recognize that a number of other classes of distributions may be of interest. Here, we treat two additional possibilities: variability in the width of the distribution of the bond portions achieved in practice for a given hierarchical level, and correlations between the distributions of bond portions on different hierarchical levels.

4.3.1 Variable Variances

To address the possibility of non-constant variance of the bond portions of different hierarchical levels, we still presume the errors to be independent on each scale and normally

distributed, but we allow the standard deviation of error in bond portion at the smallest length scale to be different from the standard deviation for all other scales. For an N-level network, suppose $N-1$ levels exhibit random errors with standard deviation σ_a, while the remaining level exhibits random errors in bond portion with standard deviation σ_b. In this case, the probability distribution function for the N-dimensional vector of errors, $\vec{\delta}$, should take the form

$$\mathcal{P}\left(\vec{\delta}\right) = \frac{1}{(2\pi)^{2/N}\,\sigma_a^{N-1}\sigma_b}\exp\left\{-\frac{1}{2\sigma_a^2}\prod_{i\neq 2}\delta_i^2 - \frac{\delta_2^2}{2\sigma_b^2}\right\} \tag{4.14}$$

We consider once more a point in bond portion space with the same excess bond portion on each level, and that this excess bond portion is much greater than either σ_a or σ_b. A straightforward modification to the above derivation for a constant standard deviation yields

$$\frac{\bar{K}}{\Delta\bar{K}} = \sqrt{\frac{\sigma_b^2}{\bar{K}^{2/N}} + (N-1)\frac{\sigma_a^2}{\bar{K}^{2/N}} + (N-1)\frac{\sigma_a^2\sigma_b^2}{\bar{K}^{4/N}}} \tag{4.15}$$

We consider the greatest value for σ_b for an N-level network such that the relative variation in stiffness is no greater than the relative deviation in stiffness for a single-level network with a bond portion distribution of width σ_a. Equating the right-hand sides of (4.12) and (4.15) yields

$$\frac{\sigma_b}{\sigma_a} = \bar{K}^{2/N}\sqrt{\frac{1}{\bar{K}^2} - \frac{N-1}{\bar{K}^{2/n}}}\sqrt{\frac{1}{\bar{K}^{2/N} + (N-1)\sigma_a^2}} \tag{4.16}$$

We show this behavior for the case in which the product of excess bond portions is fixed at 0.1, and at all levels of structure but the second, the standard deviation of the error in bond portion is 0.001 (Fig. 4.4**(a)**). The ratio of the maximum standard deviation on the second level such that the overall relative variation in stiffness remains less than or equal to that for a one-level network is plotted vs. the number of levels of hierarchy.

We can use the foregoing discussion to explore the marginal benefit of adding another level of hierarchy, by first considering a lattice with $N-1$ levels of structure, each of which

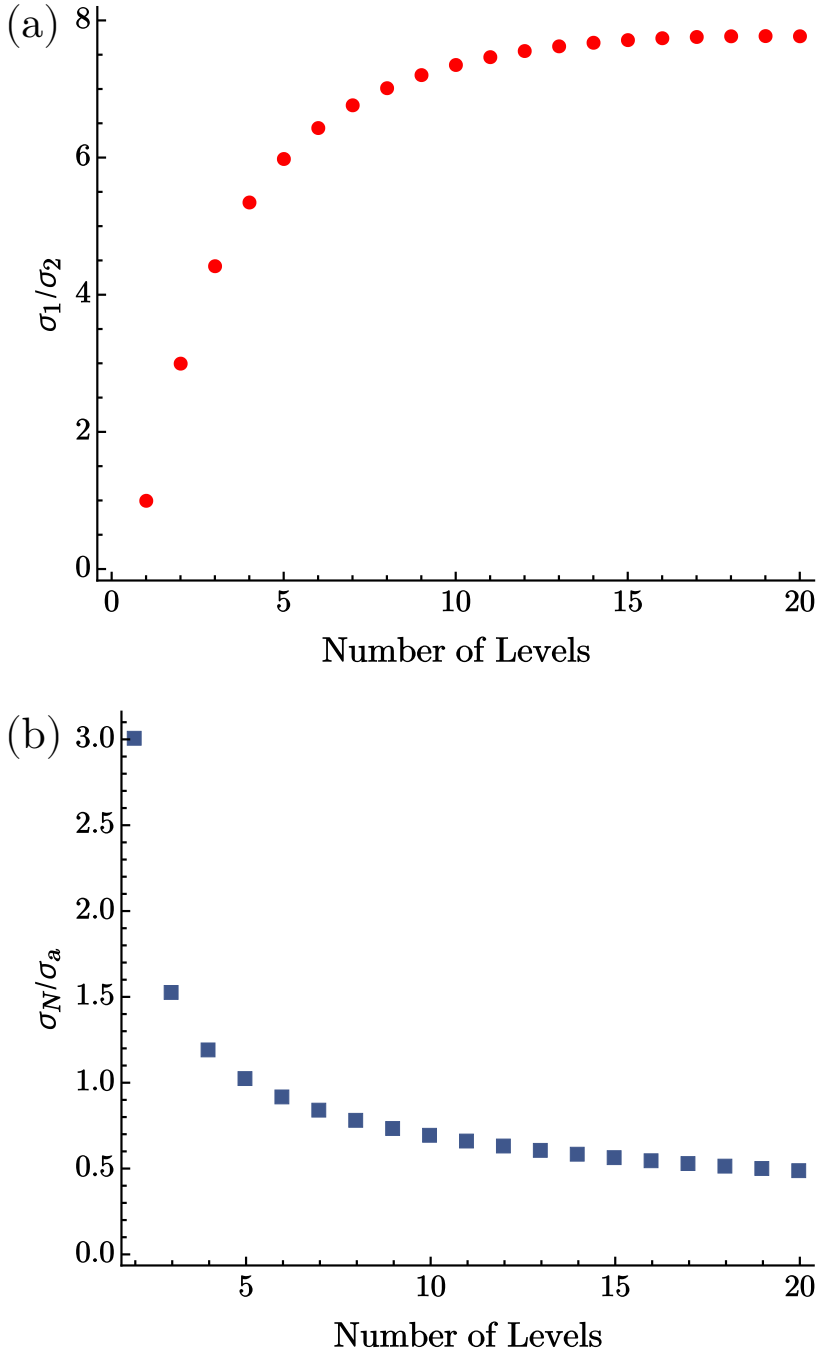

Figure 4.4: **(a)** The ratio of the standard deviation of bond portion on the 'new' level to the standard deviation of bond portion for the 'original' hierarchical levels at which the variation in stiffness of the new structure is equal to the variation in stiffness of the one level structure. The new level can always be assembled with a higher variation in bond portion. The effect saturates at a large number of levels, and allows for a striking amount of imprecision in assembly. **(b)** The ratio of the standard deviation of the Nth level to that of the other $N-1$ levels, such that adding the Nth level does not increase the relative variation in stiffness.

has an identical distribution of bond portions with standard deviation σ_a. If this lattice, in turn, is used to construct each large-scale bond in an N-level lattice, we may identify the largest standard deviation of bond portion, σ_N, on the large scale such that the relative fluctuation in stiffness of the overall structure is not increased by the addition of another level. Note first that (4.15) gives the relative fluctuation for the N-level lattice when σ_b is replaced by σ_N. Equating this result to formula (4.12), applied to an $(N-1)$-level lattice, yields

$$\frac{\sigma_N}{\sigma_a} = \sqrt{\frac{(N-1)\left(\bar{K}^{2/N(N-1)} - 1\right)}{1 + (N-1)\sigma_a^2 \bar{K}^{-2/N}}} \tag{4.17}$$

We show this behavior in Fig. 4.4**(b)** for the case $\bar{K} = 0.1$, $\sigma_a = 0.001$.

4.3.2 Correlated Errors

We also consider the case in which the errors in bond portion on different structural levels are identically distributed, but correlated. For a network with N structural levels, we consider an $N \times N$ covariance matrix $\mathbf{\Sigma}$ which takes the form

$$\Sigma_{i,j} = \begin{cases} \sigma^2, & i = j \\ \rho\sigma^2, & i \neq j \end{cases} \tag{4.18}$$

In this case, the probability distribution function for a vector of bond portion errors $\vec{\delta}$ is given by

$$\mathcal{P}\left(\vec{\delta}\right) = \frac{1}{(2\pi)^{N/2}\left|\mathbf{\Sigma}\right|} \exp\left[-\frac{1}{2}\vec{\delta}^T \mathbf{\Sigma^{-1}} \vec{\delta}\right] \tag{4.19}$$

To illustrate the persistent robustness of hierarchical materials, we show a plot of relative error in stiffness vs. number of levels, with fixed σ and varying coupling strength ρ (Fig. 4.5). While large correlations between errors eventually cause $\frac{\Delta\bar{K}}{\bar{K}}$ to increase, we find that having more than one level of structure always decreases $\frac{\Delta\bar{K}}{\bar{K}}$.

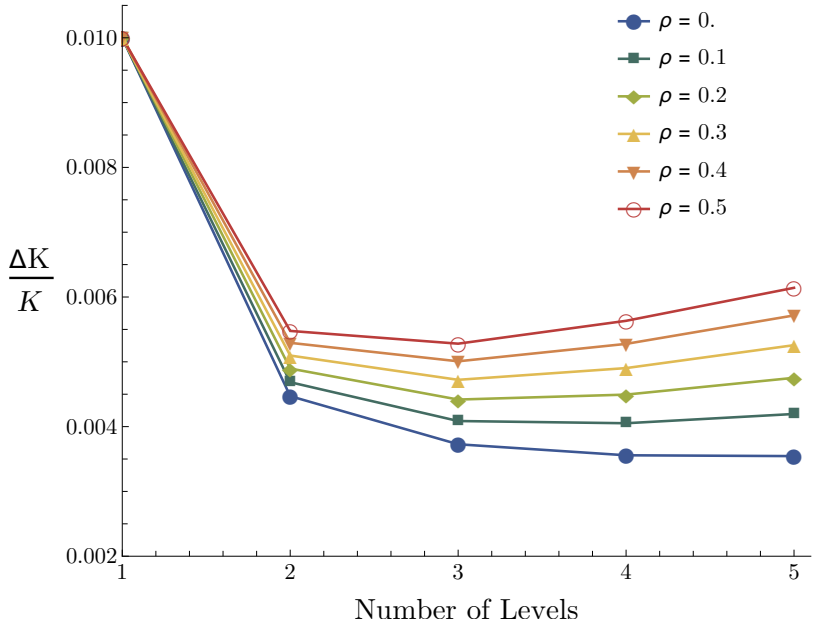

Figure 4.5: The relative error is plotted against the number of hierarchical levels for cases in which the product of excess bond portions is 0.1, and the diagonal elements of the covariance matrix are 10^{-6}, and ρ is varied from 0.0 to 0.5.

In view of the results of these alternative investigations, we anticipate that protection against fluctuation in stiffness is a generic benefit of structural hierarchy, and does not depend sensitively on the precise details of the distribution of errors in assembly.

4.4 Economy of Material

We emphasize that the above results are not a consequence of a greater quantity of material, such that the modification of the number of bonds has less of an effect on material properties. We demonstrate this by computing the number of bonds per unit area for networks with one, two and three levels of structural hierarchy for different stiffness values. As we have only directly computed stiffness values and bond densities for a discrete set of large-scale and small-scale bond portions, and we find no precise stiffness value common to a single-scale, two-scale and three-scale network, we employ interpolation. We choose points in bond portion space for one, two and three-level structures with uniform excess bond portion, with stiffnesses of .02, .03 and .04, in units of fiber stretching modulus over

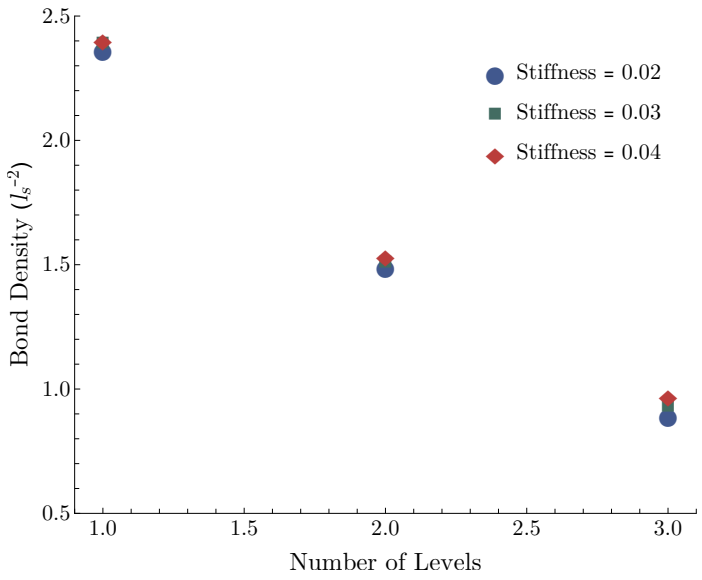

Figure 4.6: We show the scaling of density of small-scale bonds per unit area needed to achieve a target stiffness, vs. the number of hierarchical levels for stiffness values of .02, .03, .04, in units of stretching modulus over small-scale bond length, l_s. Area is measured in units of l_s^2

small-scale bond length. In each case, we find that the target stiffness can be achieved with a lower density of small-scale bonds when the number of hierarchical levels is increased, as shown in 4.6.

4.5 Summary

The results presented in this chapter provide a compelling response to our opening inquiry, regarding what underpins the robustness of hierarchical, filamentous tissues. Our findings suggest that the emergence of hierarchical structures, rather than being encumbered by the variability of the tissues' structure at each level of assembly, may have been aided by an intrinsic geometric benefit to hierarchical arrangement. This affect may then decrease the need for a co-evolved error-correcting mechanism, helping to pave the way for the development of large size. Moreover, as hierarchy can facilitate an improved strength-to-weight ratio, this can all be accomplished while making more frugal use of scarce resources.

CHAPTER 5
INTRODUCING GEOMETRIC AND TOPOLOGICAL DISORDER

Until now, we have considered hierarchical networks derived from crystalline structures, but many biological tissues exhibit no crystalline order [31, 3, 15]. Sites may exhibit no translational or rotational symmetry. Similarly, bonds may have variable length, and lack orientational order. While dilution of bonds removes strict rotational and translational symmetry, we nonetheless expect the stiffness of diluted crystalline networks will be influenced by their initial crystallinity. In this chapter, we present an alternative means of producing a hierarchical, diluted filamentous network. We develop diluted, two-level hierarchical networks in which the large scale, small scale or both scales may possess a structure derived from a random point set. We expect a scaling law of the form Eq. 3.12 to once more capture the dependence of stiffness on coordination number, as coordination number number has been established as a useful control parameter for a variety of disordered solids, such as packings of hard and soft colloids [32, 33, 34]. Nonetheless, we desire direct quantitative confirmation, and anticipate illuminating insights may arise from treating hierarchical networks created from geometrically disordered structures directly.

5.1 Alternative Network Architecture

As the foundation for our alternative network, we choose a Poisson disk packing, which consists of points distributed randomly in the plane as densely as possible while respecting the constraint that no two points be closer than some minimum distance. Such structures have long been of interest in computer graphics, and efficient algorithms are known for constructing them [35].

Once the random point set has been created, we connect points using a Delaunay triangulation. This triangulation consists of a set of line segments, whose end points are points

within the point set, that form a triangular tiling of the region enclosed by the convex hull of the point set. Triangles obey the constraint that no point in the point set is contained within the circumcircle of any triangle. This means of connecting points tends to reject especially acute or obtuse angles. Moreover, a Delaunay triangulation yields a network which, for large numbers of vertices, has a mean coordination number of approximately six. This follows from the fact that a triangulation of N points with k points on its convex hull has $3N - 3 - k$ edges [36]. As each bond is shared by two vertices, the mean coordination number is obtained by multiplying the number of edges by two and dividing by the number of vertices. For a large point set, the number of vertices will scale with the square of the area encompassed by the network, while the perimeter of the convex hull will scale linearly, so that the mean coordination number, z, will scale as

$$z = \frac{2(3N - 3 - k)}{N} \tag{5.1}$$

$$= 6 - \frac{3}{N} - \frac{2k}{N} \tag{5.2}$$

$$\approx 6 \tag{5.3}$$

If the network has width w, then for a given density of points, we expect $N \propto w^2$ and $k \propto w$. The leading error term in the approximation in Eq. 5.3 should be of order $N^{-1/2}$. We show an example triangulation of a random point set below in Fig. 5.1.

As the structure above has no crystalline order in its site positions or bond orientation, and the coordination number of vertices is variable, even without dilution of bonds, we refer to this structure as disordered, to distinguish it from the triangular Bravais lattice with nearest neighbor connections.

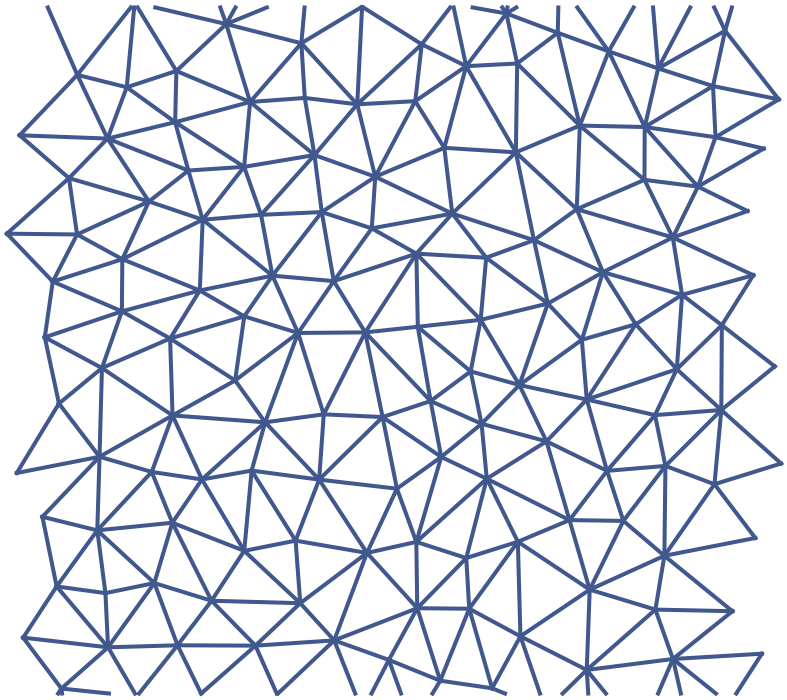

Figure 5.1: We show an example of a Delaunay triangulation of a random Poisson disk packing.

5.2 Adding Hierarchy

We now address the means by which a structure with two hierarchical levels is created, with the possibility that one or both levels is the geometrically and topologically disordered structure described in the previous section. We use one protocol when the small-scale structure is disordered, regardless of the large-scale structure, and a different protocol when the small-scale structure is crystalline, but the large-scale structure is disordered.

5.2.1 Grain-Based Network Assembly

To construct a structure with large-scale disorder and small-scale crystalline order, we form the skeleton of the large-scale lattice by creating a Delaunay triangulation of a random point set, then optionally dilute the bonds in this network in the manner described in Chapter 2. We then endow the large-scale bonds with some non-zero width to construct an envelope. Next, we break this envelope into large-scale tiles, each of which is filled with a crystalline

"grain". As tiles are not derived from a crystal lattice, they will generally be irregularly shaped, and thus cannot be completely tiled by a triangular Bravais lattice. After as much of each large-scale tile as possible has been filled with a lattice of small-scale bonds, we piece the tiles back together, and fill in the remaining voids by drawing polygons that enclose contiguous unfilled segments of large-scale tiles. We then fill these polygons with a triangular tiling using Triangle [37], with the constraint that triangles have no internal angles measuring less than $30°$, and that the area of each triangle be no greater than 1.5 times the area of a facet of the triangular Bravais lattice with nearest neighbor connections. After the small-scale structure has been created, we once more dilute on the small scale, using the technique described in Chapter 2. We illustrate this procedure schematically in Fig. 5.2.

We propose two checks of the reasonableness of our approach for combining large-scale geometric disorder and small-scale crystalline order. First, we check that the small-scale bonds within each large-scale grain tend to exhibit a high degree of orientational order. For structures expected to have approximate six-fold rotational symmetry, a common order parameter is Ψ_6, which, for a network of N vertices, is defined by

$$\Psi_6 = \left| \frac{1}{N} \sum_{j=1}^{N} \frac{1}{z_j} \sum_{k \in nn(j)} e^{6i\theta_{jk}} \right|, \tag{5.4}$$

where z_j denotes the coordination number of the jth vertex, $\theta_{j,k}$ is the angle between the positive x axis and the bond from j to k, and the outer bars denote the complex amplitude. Ψ_6 will be exactly 1 for perfect six-fold orientational order, and 0 in the complete absence of such order. We find that, within, large-scale tiles, the mean value of Ψ_6 is approximately $.83$. The distribution of intra-tile Ψ_6 values is clustered at the high end and slightly skew-left. Apart from confirming a generally high value of Ψ_6, we have also confirmed that the grain-based procedure described above reproduces a fully crystalline lattice when carried out with a crystalline large-scale envelope. We therefore feel confident in our ability to

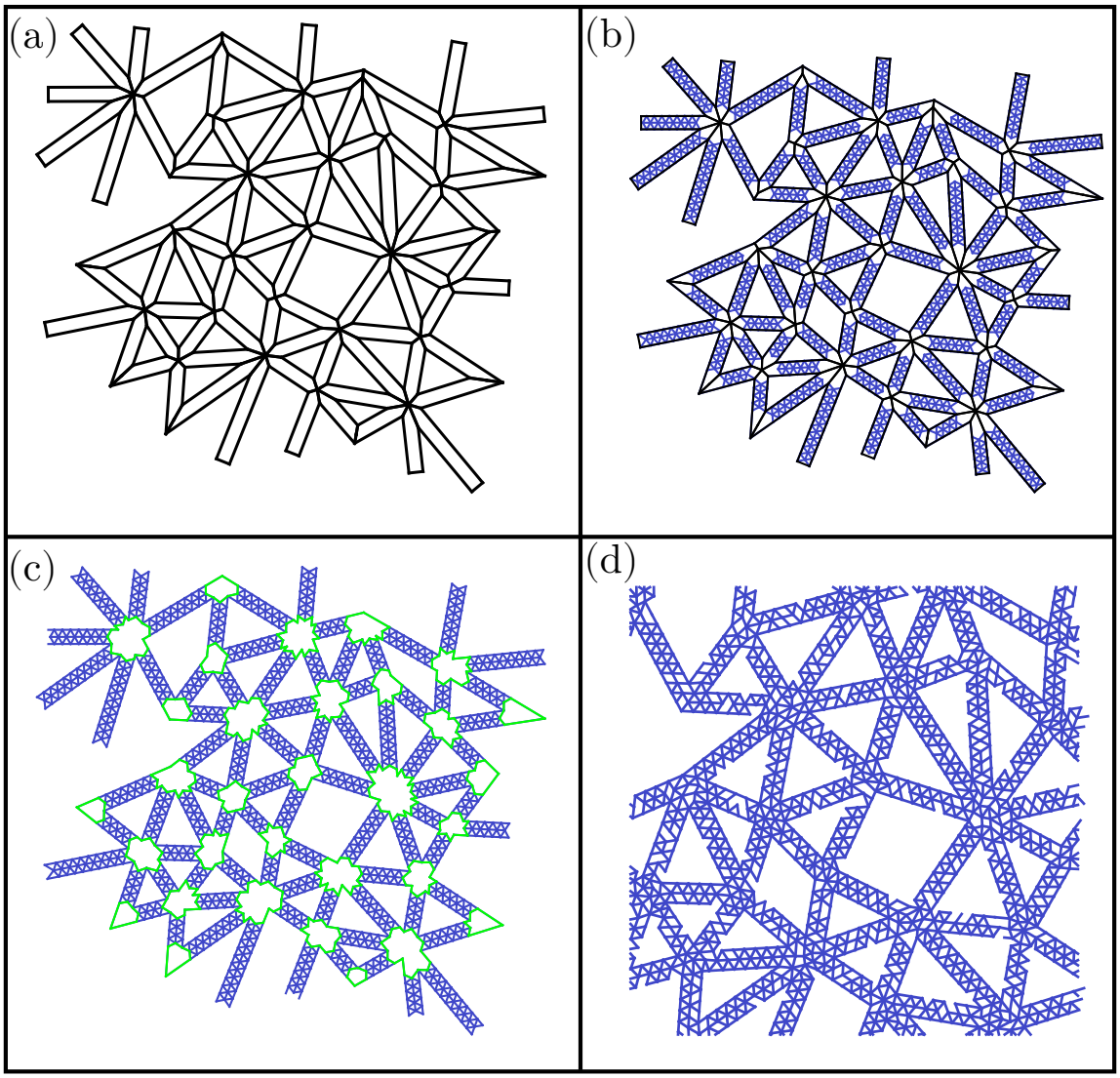

Figure 5.2: We demonstrate the manner in which a network with large-scale geometric disorder and small-scale order is created. We begin by defining the large-scale structure, creating an envelope, and breaking that envelope into tiles, as in **(a)**. We next fill tiles with crystalline grains **(b)**, create polygons formed from the union of adjacent grain boundaries, as shown in **(c)**, and triangulate grain boundaries to form the final network, as in **(d)**. Here, we retain ninety percent of large and small-scale bonds.

selectively preserve small-scale order while introducing large-scale disorder.

5.2.2 Small-Scale Geometric Disorder

If the small-scale network is geometrically disordered, the network creation process is somewhat more straightforward than the process described above. In this case, either a crystalline or disordered large-scale envelope is constructed. Next, we reject all small-scale bonds that do not have at least one vertex inside the large-scale envelope, as well as any small-scale bond that crosses multiple edges of the large-scale envelope. This process is illustrated in Fig. 5.3. We also considered a policy in which small-scale bond were strictly rejected if both vertices were not contained within the large-scale envelope, but found that this process created comparatively spindly large-scale bonds. Both policies yield a final network in which the small-scale vertices along the edges of large-scale bonds have a mean coordination number of approximately 4; however, keeping small-scale bonds that straddle the edges of the large-scale envelope yields edge vertices with a bimodal distribution of coordination numbers, with peaks at 2 and 6, where as keeping only small-scale edges contained entirely within the large-scale envelope yields a distribution of edge vertex coordination numbers with a single peak at 4. More details may be found in Appendix D.

5.3 Outlook

In summary, we are now in a position to simulate networks with one of two structures on the large and small-scale structure with a fixed topology and fixed translational and rotational symmetry, or a structure with variable topology and a lack of translational and rotational symmetry. While the geometrically disordered structure has different bond lengths, we nonetheless seek to control for as many variables as possible by ensuring the *mean* bond length remains the same. We accomplish this by determining the mean bond length resulting from various minimum point separations, and calculating the optimal minimum spacing by interpolation. The mean bond length was found to be a linear function of the minimum

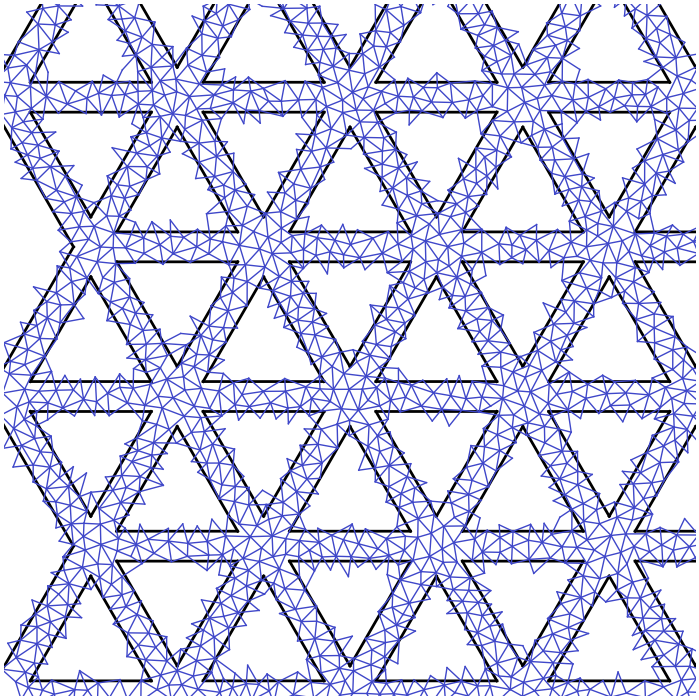

Figure 5.3: We indicate how the small-scale structure is defined for a hierarchical network with small-scale geometrical disorder. The large-scale envelope is indicated with a dark, black stroke, while the small-scale structure is shown in blue. Note that some small-scale bonds straddle the large-scale envelope.

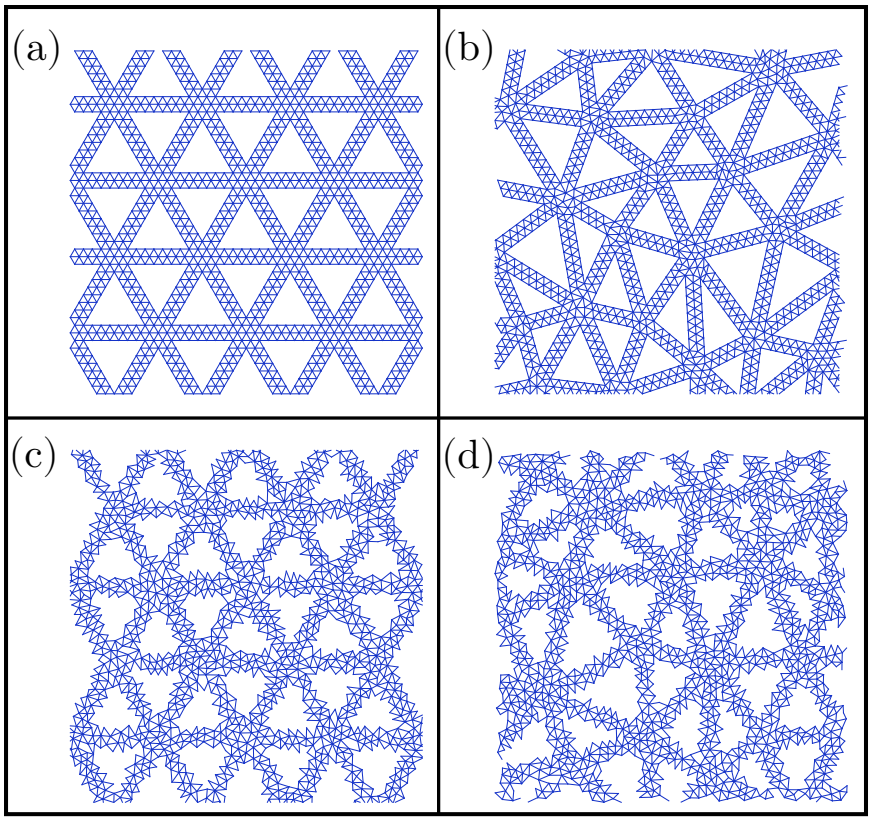

Figure 5.4: We show two-level hierarchical networks with **(a)** crystalline order on both scales, **(b)** large-scale geometric disorder and small-scale crystalline order, **(c)** large-scale crystalline order and small-scale geometrical disorder, and **(d)** geometrical disorder on both scales.

point spacing, and we found that a minimum distance of $.716$ yielded a mean bond length very close to 1. Thus, we suppose that, when we simulate a material whose small-scale structure is created from the triangulation of a random point set, we still simulating a material with more or less the same basic ingredients. We have also considered fixing the mean density of vertices, rather than the mean bond length, when moving from a triangular lattice to a disordered lattice. We studied structures in which mean vertex density was fixed using the analyses described in the coming chapter, and obtained similar results. We offer this alternate analysis in Appendix F. For ease of comparison, we show networks with the four possible combinations of order and disorder in Fig. 5.4. With this extended set of model systems in hand, we are in a position to investigate the mechanical consequences of topological and geometrical disorder.

CHAPTER 6

MECHANICAL CONSEQUENCES OF GEOMETRICAL DISORDER

Now that we have a model system for exploring structures with disorder in their site positions, bond alignment, and topology, in addition to disorder introduced by removal of bonds, we will expand upon the study of hierarchical network mechanics discussed previously in this thesis. We find that the portion of bonds retained at each length scale remains a good control parameter for predicting the stiffness of a network, and that a mathematical model with the form of Eq. 3.12 is still appropriate. The maximum attainable stiffness, however, can diminish significantly with the loss of crystalline order. We find this effect is most pronounced with the loss of small-scale crystalline order. Moreover, loss of crystalline order leads to a requirement of significantly more material to achieve a given stiffness. We attribute these phenomena to boundary effects that occur at the edges of large-scale bonds. Given the presence of multiple, distinct length scales, we find these boundary effects to be an inherent feature of hierarchical, filamentous materials that cannot be avoided by making the system size arbitrarily large.

6.1 Simulation Procedure

We once more subject networks to uniaxial tensile tests, as described in Chapter 3. As before, portions of large and small-scale bonds retained are varied independently from .6 to 1, in steps of .05. We once more obtain curves of energy vs. tensile stretch, and attempt to fit them to a power law of the form

$$E(\Delta y) = a\Delta y^b, \tag{6.1}$$

where a and b are fitting parameters, and Δy is the tensile stretch. We estimate the stiffness at standard strain of $.001$ by evaluating the second derivative of the residual strain energy with respect to stretch:

$$K = \frac{d^2E}{d\Delta y^2}\Big|_{\Delta y = L/1000} \tag{6.2}$$

$$= ab(b-1)\left(\frac{L}{1000}\right)^{b-2} \tag{6.3}$$

where K denotes tensile stiffness, and L is the length of the sample along the direction in which the tensile strain is imposed.

In Fig. 6.1, we compare heat maps showing tensile stiffness accross bond portion space for networks with each combination of large and small-scale structure. Strikingly, removal of only large-scale crystalline order diminishes maximum stiffness by approximately 11 percent, while removing only small-scale crystalline order results in a reduction of maximum stiffness of just over 40 percent. Further, loss of crystalline order on the small scale drastically increases the fraction of small-scale bonds that must be retained to achieve at least marginal rigidity.

6.2 Analysis

6.2.1 Checking the Scaling Model

We begin our analysis by checking the validity of the scaling law expressed in Eq. 3.8. Confirmation of this scaling law in the absence of crystallinity would give general credence to the arguments we present in Chapter 4 regarding the robustness of hierarchical materials against errors in assembly, because the mathematical form of the dependence of stiffness on bond portion directly leads to the observed effect, and the effect does not depend sensitively upon the specific value of any critical bond portion. In each case, we found strong

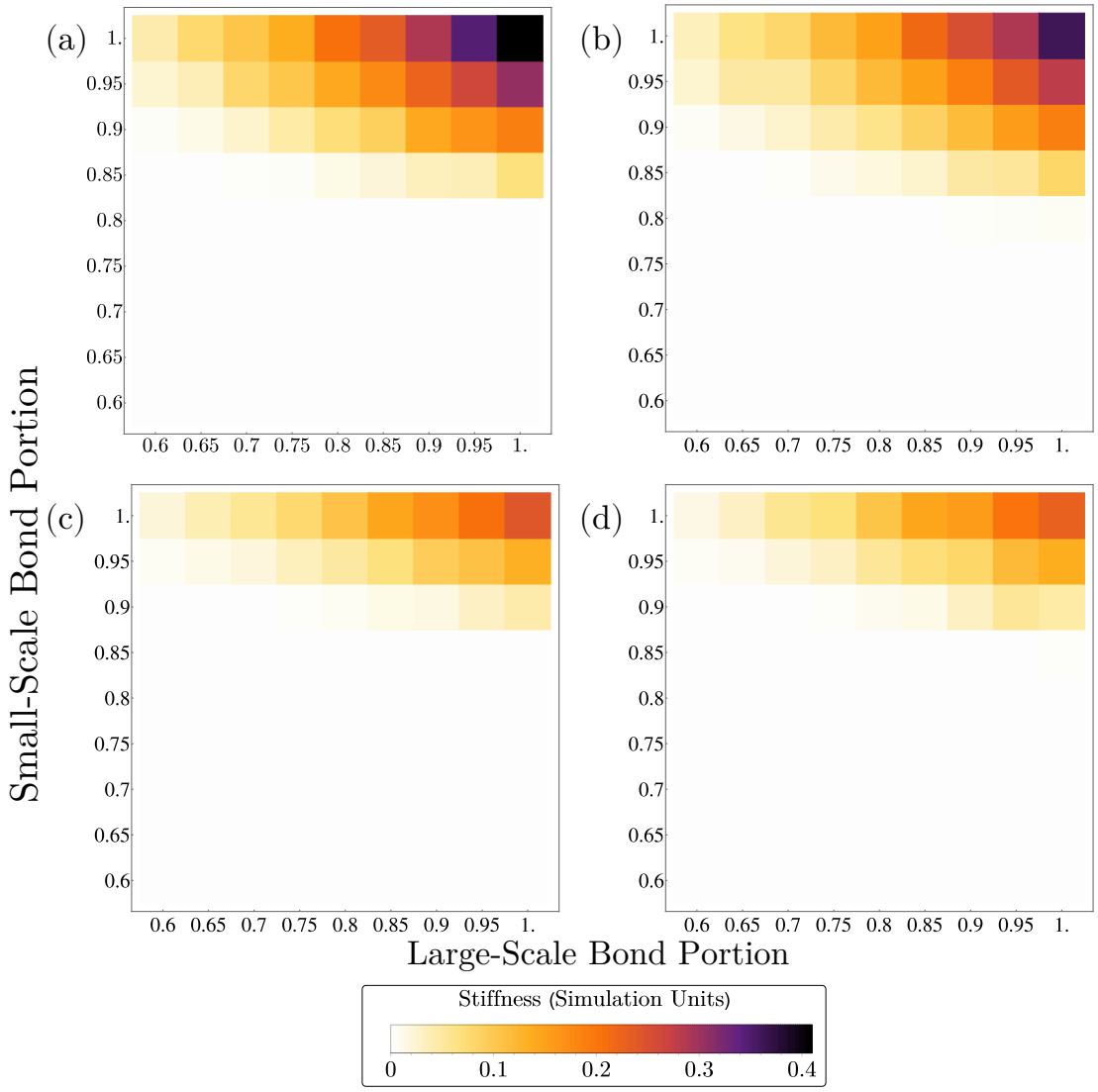

Figure 6.1: We show heat maps displaying tensile stiffness throughout bond portion space for **(a)** crystalline order on the large and small scales, **(b)** large-scale geometrical disorder and small-scale crystalline order, **(c)** large-scale crystalline order and small-scale geometrical disorder, **(d)** geometrical disorder on both scales.

Table 6.1: Maximum attainable stiffness, large and small-scale bond critical portions, and r^2 values for agreement between our scaling ansatz and simulation data are shown for each combination of large and small-scale structure. Crucially, structures that lack small-scale crystalline order require a far higher portion of small-scale bonds to be retained, and are significantly softer than their crystalline counterparts, even when fully connected.

Large / Small Scale	k	p_l	p_s	r^2
Order/Order	.410	.58	.83	.989
Disorder/Order	.364	.62	.82	.988
Order/Disorder	.244	.62	.89	.990
Disorder/Disorder	.230	.63	.89	.989

agreement between our scaling model and the stiffness data (i.e., $r^2 \approx .99$). We show fitting results in Table 6.1.

6.3 Significance of Small-Scale Structure

6.3.1 Alternate Scaling Law

We now seek to account for the markedly greater effect of removing crystalline order on the small scale, as opposed to the large scale. For a hint regarding the origin of this disparity, we turn to connectivity, rather than bond portion. As the fraction of bonds retained should be in direct correspondence with the mean coordination number of a network, we propose to re-write our scaling model for stiffness with coordination number on the large and small scale taking the place of bond portion, so that it takes the form:

$$K = \begin{cases} K_{max} \frac{(z_l - z_{l,c})(z_s - z_{s,c})}{(z_{l,max} - z_{l,c})(z_{s,max} - z_{s,c})}, & z_l > z_{l,max} \quad \& \quad z_s > z_{s,c} \\ 0, & \text{otherwise,} \end{cases} \tag{6.4}$$

where z_l and z_s are the large-scale and small-scale mean coordination number, $z_{l,c}$ and $z_{s,c}$ are the large-scale and small-scale critical coordination number, and $z_{l,max}$ and $z_{s,max}$ are the maximum large-scale and small-scale coordination numbers when no bonds have been removed. For all cases, $z_{l,max}$ is very nearly 6 (the finite size of our networks prevents it from being precisely 6), whereas $z_{s,max}$ varies significantly with the small-scale structure,

Table 6.2: Data are shown for the critical large-scale and small-scale mean coordination numbers for each combination of order and disorder.

Large / Small Scale	z_l	z_s	R^2
Order/Order	3.44	4.09	.994
Disorder/Order	3.52	3.94	.990
Order/Disorder	3.42	4.10	.997
Disorder/Disorder	3.44	4.01	.995

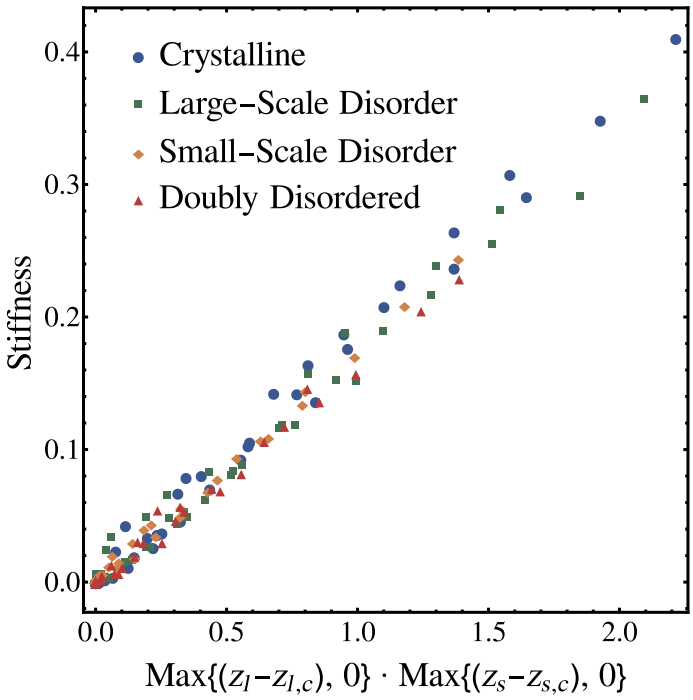

Figure 6.2: We show the scaling of the stiffness vs. the product of excess small-scale and large-scale coordination number for networks with each combination of large-scale and small-scale structure.

as discussed below. We calculated coordination number directly for each combination of bond portion and each combination of large-scale and small-scale structure, by dividing the number of edges on a given length scale by the number of vertices. We find this scaling law still works well, as shown in Table 6.2. Notably, the large-scale and small-scale critical coordination numbers are much more similar among all network types. Moreover, the scaling of tensile stiffness with respect to the product of the product of excess small-scale and large-scale coordination number, where by excess we refer to the actual coordination number minus the critical coordination number. We illustrate this near collapse in Fig. 6.2.

6.3.2 Consequences of Small-Scale Disorder

The results just discussed raise a question: If the threshold large-scale and small-scale coordination numbers are similar for all network architectures, why is the threshold small-scale bond portion so much greater when the small-scale structure is non-crystalline? To trace this effect, we begin with the observation that the coarse edges of large-scale bonds made of a disordered small-scale structure appear to have significantly more perimeter. This suggests that, especially for more slender large-scale bonds, a significantly greater fraction of small-scale vertices may be on the edge of a large-scale bond, rather than in the interior. This larger fraction of nodes on the edge can in turn lead to more vertices near or below the threshold connectivity for marginal stiffness, leading to abrupt softening with dilution of bonds.

We investigate the role of small-scale edge nodes by considering networks that are fully connected on the large and small scale, with each combination of large-scale and small-scale structure. For each network, we identify edges on the perimeter by regarding each network as a planar line graph, and enumerating its faces. A face of a planar line graph is a cycle that does not enclose any edges in its interior. Once faces have been enumerated, we use an area threshold to select those faces made up of edges of large-scale bonds. We show a sample image demonstrating the results of this process in Fig. 6.3. We then found the fraction of small-scale vertices on the edge of a large-scale bond, as opposed to in the interior of a large-scale bond, for networks with crystalline large-scale structure, and either crystalline or geometrically disordered small-scale bonds. We carried out these calculations for large-scale bonds with varying aspect ratios, that is, the quotient of length divided by width. Large aspect ratios result in a marked disparity between the fraction of small-scale vertices on the edge, while the gap narrows considerably for small aspect ratios.

We further study the effect of small-scale structure on the mean coordination number on the small scale. The fact that a greater fraction of small-scale vertices are along the edges of large-scale bonds in the case of small-scale disorder may account for the part of

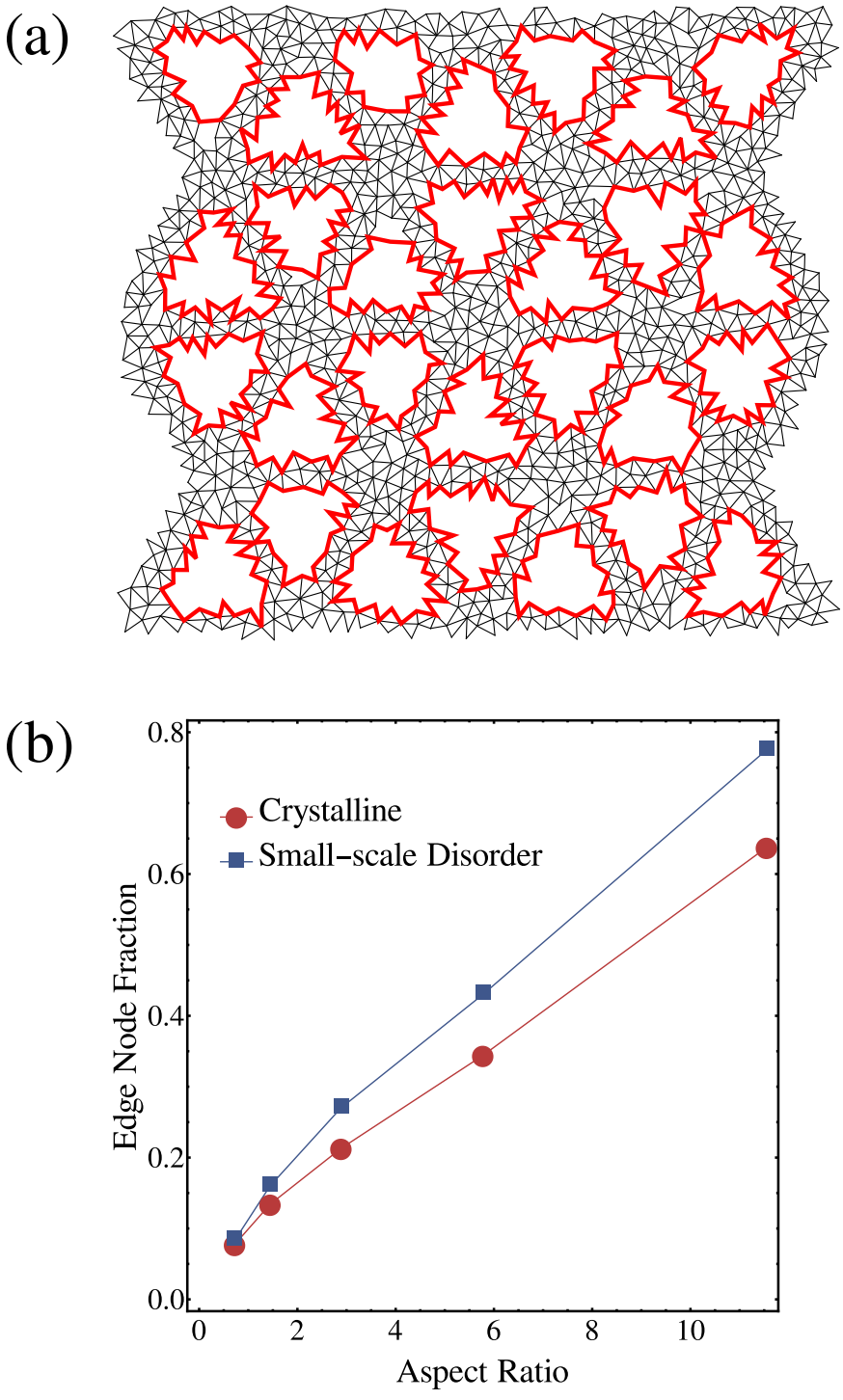

Figure 6.3: In **(a)**, we show edges of large-scale bonds marked in red, laid over a network with large-scale crystalline order and a geometrically disordered small-scale structure. In **(b)**, we show the fraction of vertices on the edge of, rather than in the interior of, large-scale bonds for networks with large-scale crystalline order and either crystalline or geometrically disordered small-scale structure.

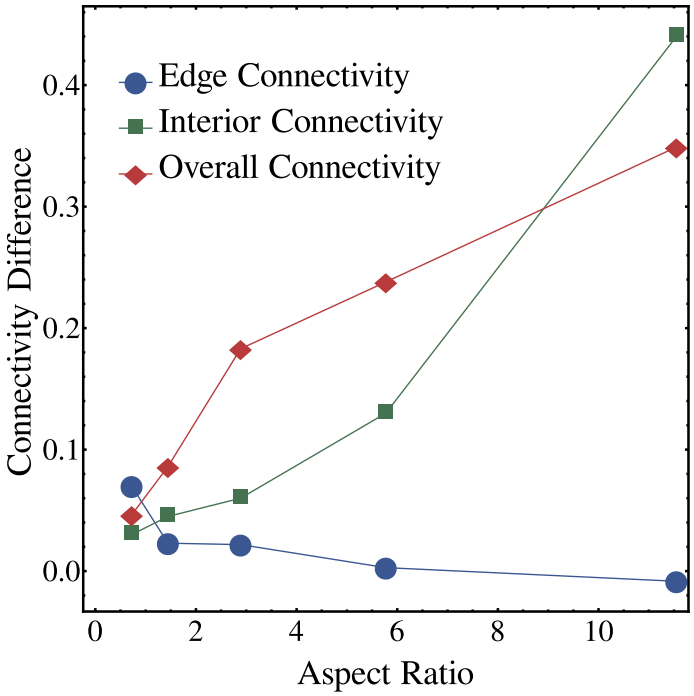

Figure 6.4: Difference in mean small-scale coordination is shown for small-scale vertices on the edges of large-scale bonds, small-scale vertices in the interior, and all small-scale vertices for networks with large-scale crystalline order and either small-scale crystalline order or small-scale geometrical disorder. We note that mean coordination number of edge nodes is similar for all aspect ratios of large-scale bonds, but that interior connectivity, and consequently overall connectivity, are very sensitive to the aspect ratio.

the discrepancy between the threshold small-scale bond portion with and without small-scale crystalline order, as the mean small-scale coordination number is about four along the edge of a large-scale bond in all cases. We suspect another contribution, however. This is borne out by a calculation of the mean coordination number for small-scale vertices on the interior of large-scale bonds. While this quantity is similar when large-scale bonds have a low aspect ratio, a sizeable difference emerges for comparatively slender large-scale bonds. We find that the coarse surface resulting from a disordered small-scale structure has a system-wide effect, that leaves the network much closer to the threshold for marginal stiffness, even before dilution of small-scale bonds.

6.3.3 Economy of Material

Despite the findings just discussed, it still seems puzzling that, if we are generating hierarchical networks with one of two small-scale structures, each with similar mean coordination numbers and mean bond lengths, the small-scale coordination number differ so much when the same fraction of bonds is removed. We resolve this by noting that, for a given large-scale structure, the number of small-scale bonds per unit area is somewhat greater when the small-scale structure is geometrically disordered. We show this disparity in Fig. 6.5, in which we plot stiffness vs. small-scale bonds per unit area for two-level hierarchical networks with each combination of large-scale and small-scale structure. We choose networks with no dilution of large-scale bonds, and small-scale bond portions varied from .6 to 1. We used two separate protocols to compute small-scale bond density. If the large-scale structure was crystalline, we used a parallelogram made of multiple copies of the primitive cell for the triangular lattice, whereas for networks with geometrically disordered large-scale structure, we used a rectangular averaging cell that encompassed all but the edges of the network.

Our plots of stiffness vs. density reveal a striking feature - small-scale crystalline order vastly reduces the amount of material needed to achieve a given stiffness. While a modest penalty is incurred due to loss of large-scale order, the penalty of losing small-scale crystalline order is such that the amount of material needed to construct a fully connected network that is crystalline on both scales would create a network with small-scale geometrical disorder and large-scale crystalline order just at the edge of marginal rigidity. This suggests that, in the evolution of a tissue, reliable construction of a consistent small-scale structure is by far more important, and that more variability can be tolerated at larger length scales. Therefore, after a robust assembly mechanism is established, a modular assembly process to create a larger, more complex tissue can proceed that has a tolerance to "sloppiness" at tertiary levels of assembly.

We have also sought to preemptively address the concern that the increased density

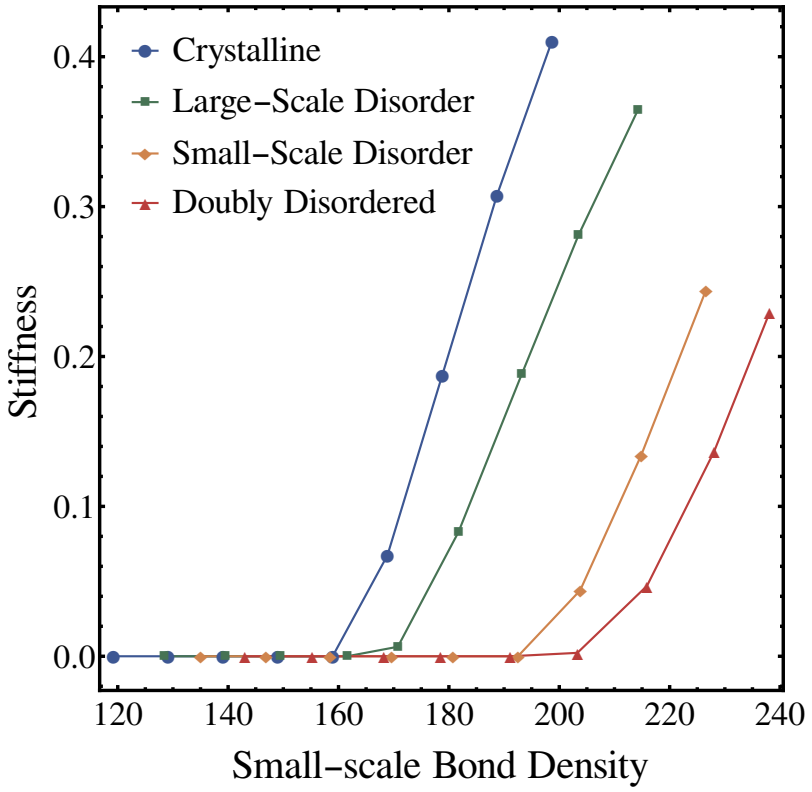

Figure 6.5: We show network stiffness vs. density for two-level hierarchical networks with each combination of small-scale and large-scale structure. In each case, we fixed the large-scale bond portion at 1, while varying the small-scale bond portion from .6 to 1. We note that small-scale structure is the principle factor controlling material efficiency.

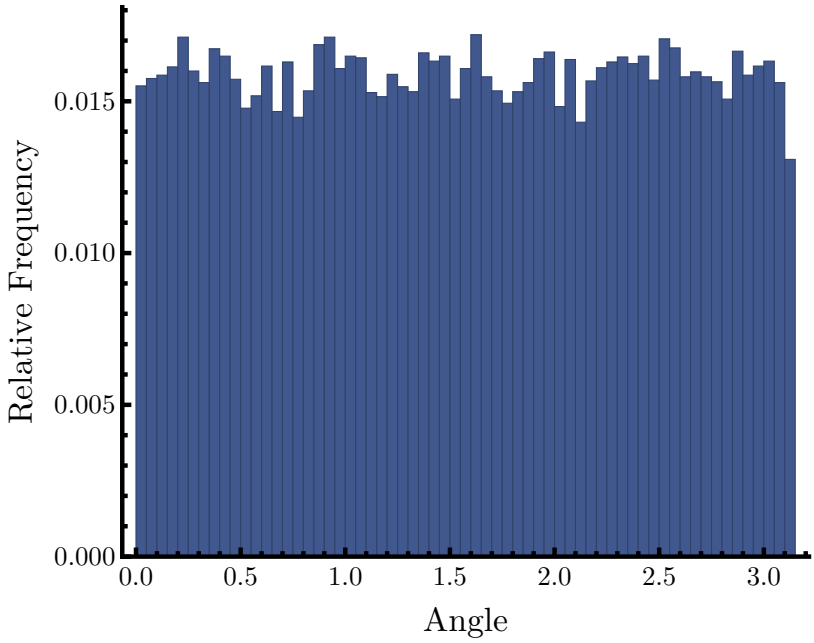

Figure 6.6: We show a histogram of relative frequencies of different angular orientations, on the range $[0, \pi]$, for bonds in a network formed by triangulating a random point set. We find the distribution to be more our less homogeneous, indicating closer packing due to spontaneous alignment does not account for the slightly greater density of small-scale bonds in this case.

of material resulting from loss of geometrical and topological order may be the result of a spontaneous alignment of bonds along some direction. We have confirmed by direct calculation that bonds in geometrically disordered networks exhibit no orientational order, by finding the angle between each bond and the positive x axis. As may be seen in Fig. 6.6, we see a nearly constant distribution.

6.4 Discussion

We have established that our scaling law predicting the dependence of stiffness on bond portion on each scale of a hierarchical elastic network remains useful when the structure one or more scales is not derived from a crystalline lattice. This lends credence to our proposal that structural hierarchy generically guards a material against large fluctuations in its mechanical properties. Nonetheless, sacrificing small-scale crystalline order comes at a cost, and leads to a markedly lower attainable stiffness for a given structural building

block, and a less efficient use of material. We therefore anticipate that, in the context of the evolution of tissues, there would be a far greater pressure to evolve a reliable means of carrying out the first stage of assembly, and that more variability is to be expected at later stages of assembly.

CHAPTER 7
DETAILED STIFFENING MECHANISMS AT THE LARGE AND SMALL SCALES

We have presented results corroborating the usefulness of the notions of bond portion and coordination number for hierarchical, elastic networks, and have provided evidence that these concepts remain relevant even without crystalline structure. We now wish to systematically explore the specific means by which small-scale and large-scale structure contribute to the overall mechanical response of hierarchical, filamentous materials. Through fine-grained studies of displacement fields and vibrational modes, we identify distinct responsibilities for each length scale. We find that the small scale dominates the frequency density of states at high frequency, while also ensuring stiff large-scale bonds, and conferring an emergent bending stiffness to large-scale bonds. On the other hand, the both small and large-scale structure are integral in coordinating system-wide distribution of an applied load. In the following sections, we support this viewpoint with both normal mode analysis for infinitesimal displacements, and statistical characterization of displacement fields resulting from small but non-infinitesimal applied strain.

7.1 Normal Mode Analysis

7.1.1 Computing Normal Modes

To begin, we consider the normal modes of vibration of the network. These describe collective states of low-amplitude oscillation that evolve with simple harmonic motion. Given a general pairwise interaction energy $U(\vec{r}_i, \vec{r}_j)$ between pairs of connected vertices, the leading order expansion of the potential energy about a point of mechanical equilibrium for a network with N vertices in d spatial dimensions is

$$U(\vec{r}+\vec{u}) \approx \frac{1}{2}\sum_{i=1}^{N}\sum_{j\in nn(i)}\sum_{1\leq\alpha,\beta\leq d}\frac{\partial^2 U}{\partial r_{i,\alpha}r_{j,\beta}}u_{i,\alpha}u_{j,\beta} + \frac{1}{2}\sum_{i=1}^{N}\sum_{\alpha=1}^{d}\frac{\partial^2 U}{\partial r_{i,\alpha}^2}u_{i,\alpha}^2, \tag{7.1}$$

where $\vec{r}$ denotes the full set of $d \cdot N$ vertex coordinates, $\vec{u}$ denotes the $d \cdot N$-dimensional displacement vector, i and j are unique indices identifying the vertices, $nn(i)$ denotes nearest neighbors to which vertex i is connected, and α and β denote Cartesian components of vectors the positions of nodes i and j, respectively.

This above expansion invites the definition of a $d \cdot N \times d \cdot N$ stiffness matrix, $\mathbf{K}$, with components

$$K_{lm} = \frac{1}{2}\frac{\partial^2 U}{\partial u_l \partial u_m}, \tag{7.2}$$

where $1 \leq l, m \leq d \cdot N$. Elements $K_{l,m}$ may be read off from the expansion of the potential energy in Eq. 7.1, with the convention that the displacement of the component α of position $\vec{r}_i$ corresponds to component $d \cdot i + \alpha$ of $\vec{u}$. To quadratic order, the energy may then be expanded as

$$U = \vec{u}^T \mathbf{K} \vec{u}. \tag{7.3}$$

Let $\vec{F}$ be the vector of all Cartesian components of all forces on the vertices in the network. The ith component of F is then

$$F_i = -\frac{\partial U}{\partial u_i} \tag{7.4}$$

$$= -\sum_{j=1}^{d\cdot N} K_{ij} u_j, \tag{7.5}$$

that is, the ith component of $\mathbf{K}\vec{u}$. Finally, let $\mathbf{M}$ be the $d \cdot N \times d \cdot N$-dimensional

diagonal matrix in which the entries $d(i-1)+1$ to $d \cdot i$ are the mass m_i of the ith site. For small-amplitude distortions, the equation of motion for the displacement field is then

$$\frac{d^2\vec{u}}{dt^2} = -\mathbf{M}^{-1}\mathbf{K}\vec{u} \tag{7.6}$$

The normal modes of this network are then the $d \cdot N$ eigen vectors of the matrix $\mathbf{M}^{-1}\mathbf{K}$, which we call the dynamical matrix. The ith normal mode evolves in time with simple harmonic motion with frequency ω_i, which is the square root of that normal mode's eigenvalue. A normal mode with an eigen frequency of zero corresponds to a collective displacement of the vertices in the network which, to leading order in the displacement field, costs no energy. As rigid rotations and translations must cost no energy, each network must have at least $d + \binom{d}{2}$ zero-frequency eigenvalues. In this work, normal modes were computed using the package MAGMA, which uses GPU acceleration to enable rapid calculation of the spectra of high-dimensional matrices [38].

7.1.2 Analysis of Zero Frequency Modes

We take particular interest in normal modes of zero frequency. Our numerical procedure for obtaining eigenvalues generally never yields values that are precisely zero, but we identify zero modes by noting that a cluster of very low-frequency modes, on the order of 10^{-6} or less, in simulation units, always appears. This low-frequency cluster is separated from the next cluster by about four orders of magnitude, and so we regard all modes in this cluster as true zero-frequency modes. We illustrate this point with a representative histogram of the log base 10 of normal mode frequencies in Fig 7.1.

We now assess identification of zero modes as a heuristic for anticipating the stiffness of a network. For each combination of large and small-scale bond portion and each combination of network structure, we compute the fraction of vibrational modes that have zero frequency. As may be seen in Fig. 7.2, the fraction of zero-frequency modes is set almost entirely by the small-scale bond portion. This suggests that simply quantifying the fraction

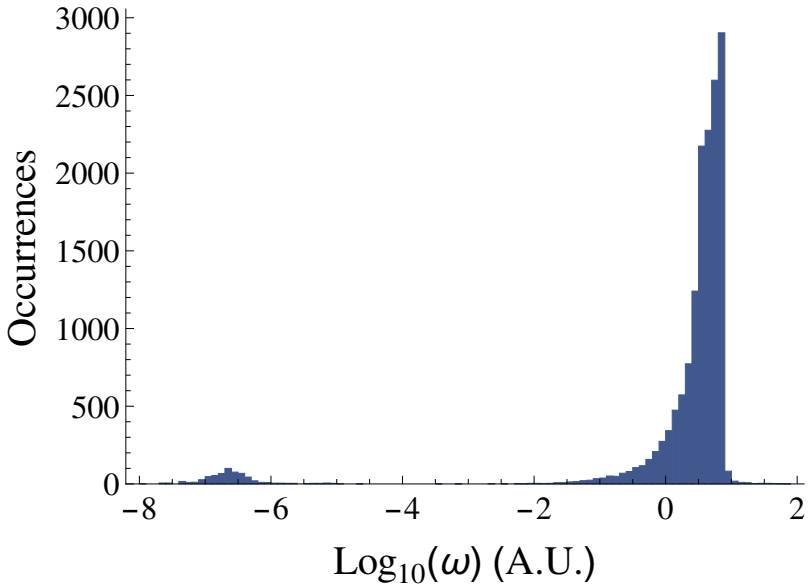

Figure 7.1: We show the histogram of the log base 10 of normal mode frequencies for a hierarchical network. Note the bimodal nature of the distribution, with one cluster centered near -7. We regard this lower cluster as consisting of zero frequency modes.

of zero-frequency modes does not properly predict the transition to marginal rigidity, as it fails to capture the role of the large-scale bond portion.

7.1.3 Soft Modes

While the fraction of zero-frequency modes is evidently not predictive of whether or not a network is stiff, we now turn our attention to the notion of a "soft mode", which we regard as a vibrational mode with small but non-zero frequency. For the purpose of our analysis, we choose as a cutoff one percent of the frequency at which the cumulative distribution function of frequency reaches .99. This is done to account for the presence of a very small number modes of exceptionally high frequency that arise when one level or the other is disordered. We find that the fraction of soft, non-zero modes exhibits a marked dependence on the large-scale, as well as the small-scale bond portion, and that the fraction of such modes is greatest along a belt in bond portion space approximately coinciding with the contour separating floppy networks from rigid networks.

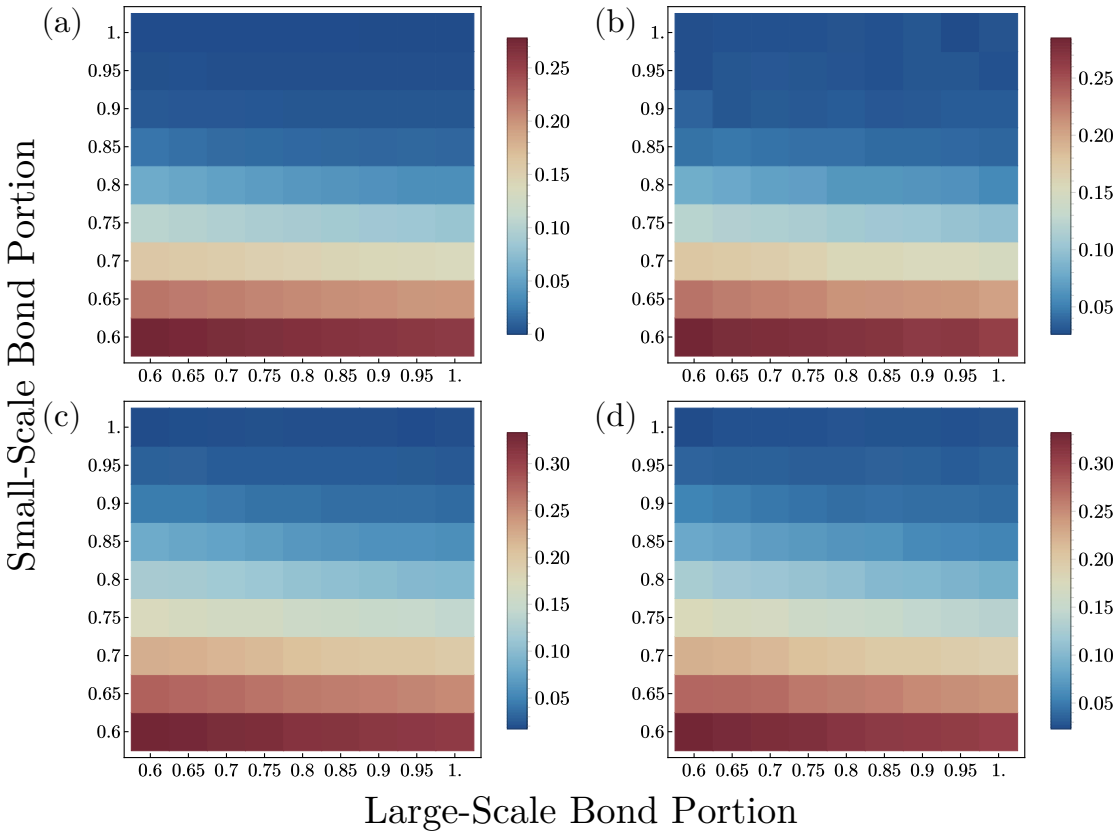

Figure 7.2: We show the fraction of vibrational modes with zero frequency for two-level networks with **(a)** crystalline order on both scales, **(b)** crystalline order on just the small scale, **(c)** crystalline order on just the large scale, and **(d)** crystalline order on both scales.

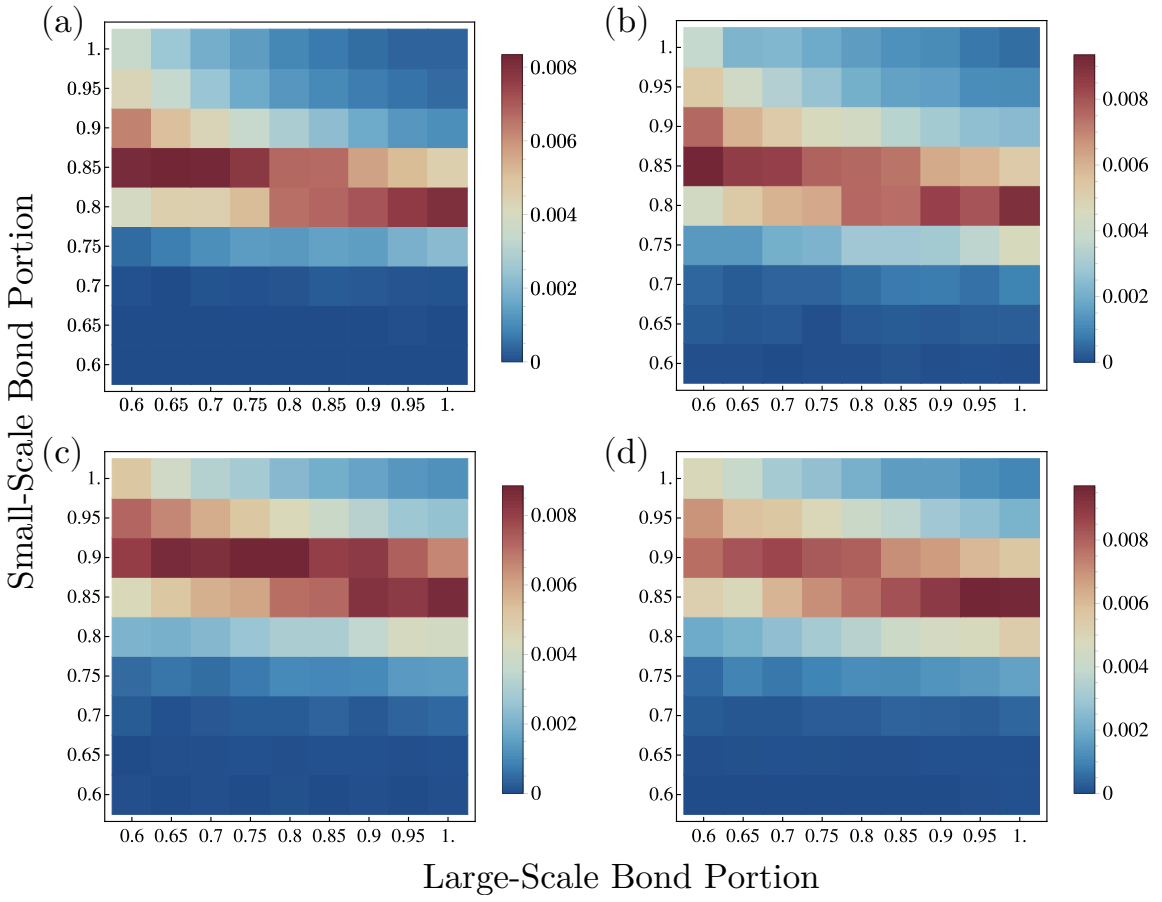

Figure 7.3: We show the fraction of soft modes vs. large-scale and small-scale bond portion for networks with **(a)** crystalline order on both scales, **(b)** crystalline order on just the small scale, **(c)** crystalline order on just the large scale, and **(d)** no crystalline order on either scale.

7.1.4 Density of States

We can gain insight into the mechanics of networks by studying the distribution of normal modes across the frequency spectrum. While this distribution is, in principle, discrete, it is often useful to define a density of states, $D(\omega)$, such that the number of vibrational modes with frequencies between ω and $\omega + d\omega$ is $D(\omega)d\omega$. Given the eigenvalues of the dynamical matrix for a network, we can calculate a density of states by first sorting frequencies into bins of size b. We then find the mean frequency $\bar{\omega}$ within each bin, and obtain a discrete distribution $N(\omega)$ of the number of vibrational modes between the minimum frequency and ω. If $\bar{\omega}_i$ is the mean frequency of the ith bin, we define

$$\Delta_1 = \bar{\omega}_i - \bar{\omega}_{i-1} \tag{7.7}$$

$$\Delta_2 = \bar{\omega}_{i+1} - \bar{\omega}_i \tag{7.8}$$

Treating N as continuous, we approximate the rate of change of N with the Taylor expansions

$$N(\bar{\omega}_i - \Delta_1) \approx N(\bar{\omega}_i) - \Delta_1 \frac{dN}{d\omega}\Big|_{\omega=\bar{\omega}_i} + \frac{\Delta_1^2}{2}\frac{d^2N}{d\omega^2}\Big|_{\omega=\bar{\omega}_i} + \mathcal{O}(\Delta_1^3) \tag{7.9}$$

$$N(\bar{\omega}_i + \Delta_2) \approx N(\bar{\omega}_i) + \Delta_2 \frac{dN}{d\omega}\Big|_{\omega=\bar{\omega}_i} + \frac{\Delta_2^2}{2}\frac{d^2N}{d\omega^2}\Big|_{\omega=\bar{\omega}_i} + \mathcal{O}(\Delta_2^3) \tag{7.10}$$

Rearranging the above terms, we obtain the approximation

$$\frac{dN}{d\omega}\Big|_{\omega=\bar{\omega}_i} \approx \frac{\Delta_1^2 N(\bar{\omega}_{i+1}) + (\Delta_2^2 - \Delta_1^2)N(\bar{\omega}_1) - \Delta_2^2 N(\bar{\omega}_{i-1})}{\Delta_1^2\Delta_2 + \Delta_2^2\Delta_1} \tag{7.11}$$

We carried out these calculations for networks with each type of large-scale and small-scale structure. We consistently found that the small-scale controls the density of states.

We demonstrate this in Fig. 7.4, in which we show the density of states for networks with large-scale geometric disorder and small-scale crystalline structure, with the small scale bond portion fixed at either $.9$ or 1, and the large-scale bond portion varied from $.6$ to 1, in steps of $.05$. Curves for $D(\omega)$ for different large-scale bond portions nearly overlap.

7.2 Non-Affine Parameter

We now seek to account for the distinct role of large-scale and small-scale structure by considering a measure of the departure of a network's displacement field from that which one would naïvely expect, given the external loading conditions. Suppose a vertical strain γ is imposed on a square sample of a simple elastic material, with its lower edge at $y = 0$ and its upper edge at $y = L$, where L is the side length. If the material has a Poisson ratio, σ, characterizing the ratio of lateral contraction to vertical stretch, a general point (x, y) should be transformed to (x', y') according to

$$\begin{pmatrix} x' \\ y' \end{pmatrix} = \begin{pmatrix} 1 - \gamma\sigma & 0 \\ 0 & 1 + \gamma \end{pmatrix} \begin{pmatrix} x \\ y \end{pmatrix} \tag{7.12}$$

That is, the coordinates are acted upon by a simple affine transformation that re-scales the x and y coordinates by independent amounts.

Following previous work [39, 40, 41], we now characterize the departure of the network's behavior from that of a simple elastic continuum by subtracting the affine y displacement. Given a predicted affine displacement $u_{y,a}$ given by Eq. 7.12, and a true y displacement, u_y for each vertex in the network, we define the y non-affine parameter, α, to be

$$\alpha = \frac{|u_y - u_{y,a}|}{\gamma l_s}, \tag{7.13}$$

where γ is the applied strain at the boundary, and l_s is the mean small-scale bond length.

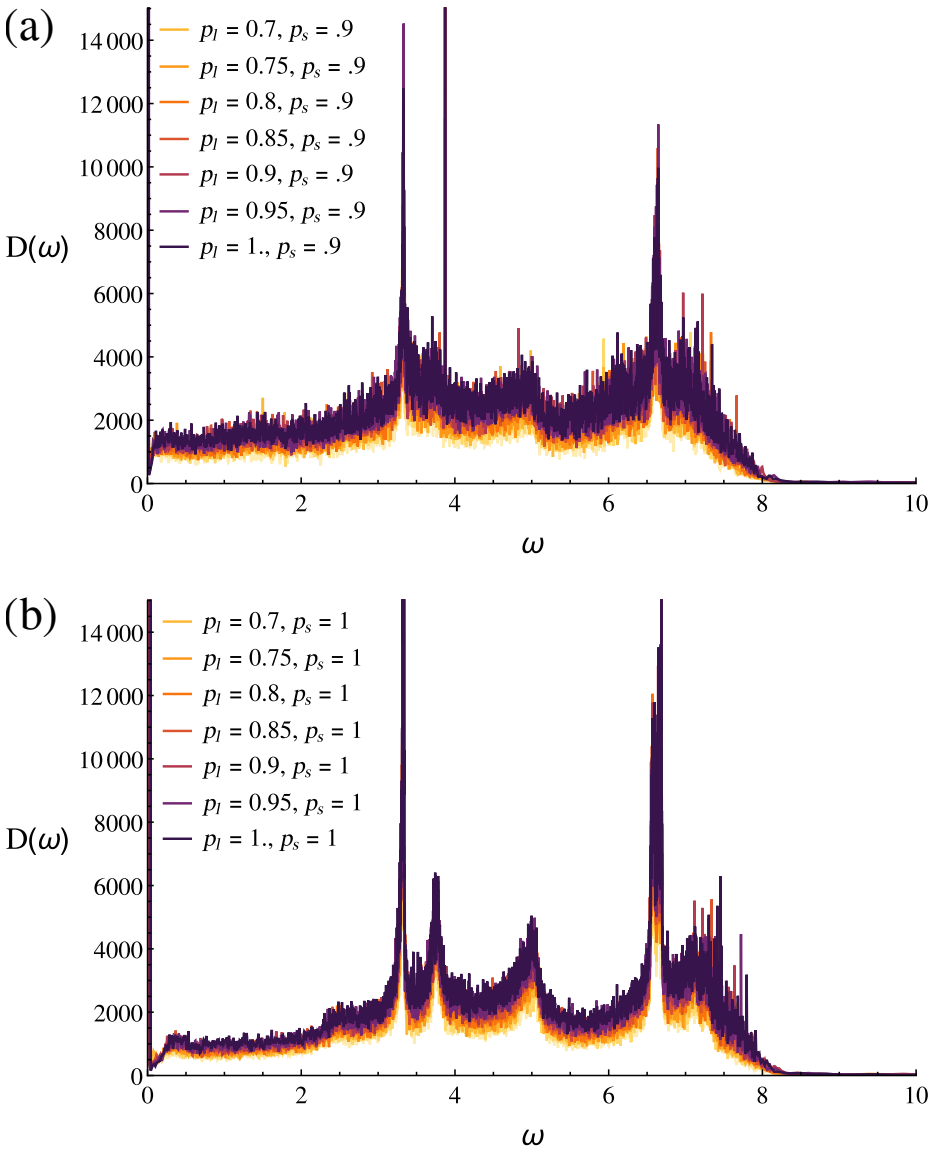

Figure 7.4: We show a comparison of density of states at fixed small-scale bond portion and variable lage-scale portion with the small-scale bond portion fixed at **(a)** .9 and **(b)** 1. We find that the density of states depends mostly upon the small-scale bond portion.

We then consider the mean value of α for two-level networks with each combination of small-scale and large-scale bond portion and each combination of network structure. We have found it illuminating to plot $< \alpha >$ vs. the small-scale bond portion, for varying fixed values of the large-scale bond portion. As seen in Fig. 7.5, curves corresponding to varying large-scale bond portions collapse on a common plateau at low small-scale bond portion, and abruptly decrease beyond the small-scale threshold for rigidity. At large values of small-scale bond portion, however, curves tend to be stratified according to large-scale bond portion. We thus find that, while the small-scale connectivity is important for eliminating soft modes of deformation, the large scale is essential in coordinating system-spanning force networks. To gain further insight into the transition that occurs at rigidity percolation, we turn to further statistical characterization of the displacement field.

7.3 Skewness of Strain

The precipitous drops in the non-affine parameter near the transition to marginal rigidity suggest a stark change in the distribution of strain throughout the network. To gain some practical intuition for this, we introduce a means of visualizing the networks' strain fields after stretching and relaxation. We have found that there is a large dynamic range of residual strain in bonds after relaxation – sometimes strain may vary by over ten orders of magnitude from the least to the most deformed bond. To produce a coherent visualization, we have therefore mapped the absolute value of each strain, γ to the interval $[0, 1]$ using

$$f(\gamma) = \frac{\log_{10}(\gamma) - \log_{10}(\gamma_{min})}{\log_{10}(\gamma_{max}) - \log_{10}(\gamma)}, \tag{7.14}$$

where γ_{min} and γ_{max} are the minimum and maximum magnitudes of strain among all bonds.

In 7.6, we show strain fields for networks with large-scale geometrical disorder and small-scale crystalline order. We fix the large-scale bond portion at one, while varying

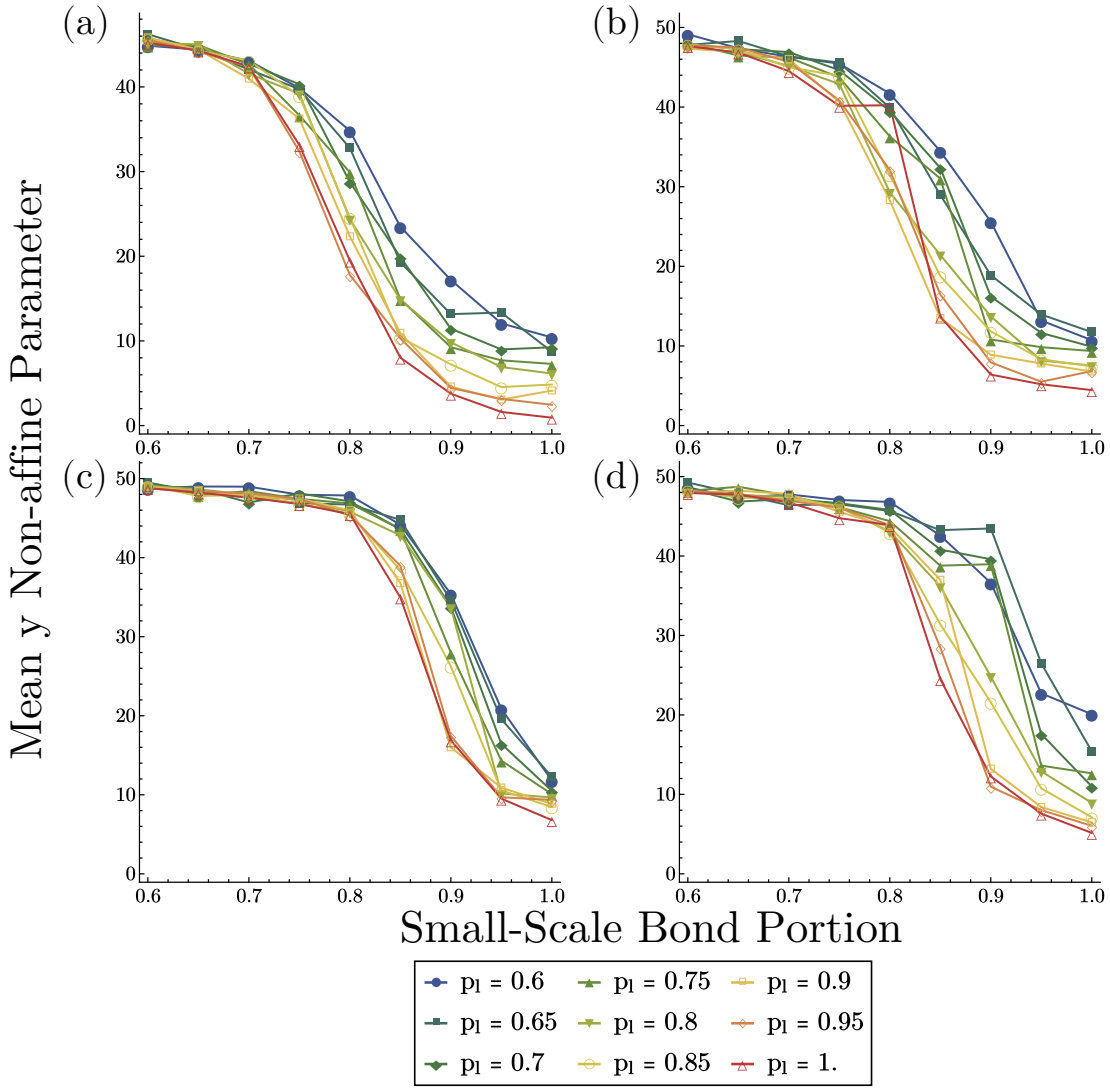

Figure 7.5: We show non-affine parameter vs. small-scale bond portion for large-scale bond portions varying from .6 to 1 in steps of .05, with **(a)** crystalline structure on both scales, **(b)** large-scale geometric disorder, **(c)** small-scale geometric disorder, and **(d)** geometric disorder on both scales. Color and symbol codes for different large-scale bond portions are given in the legend beneath the plots.

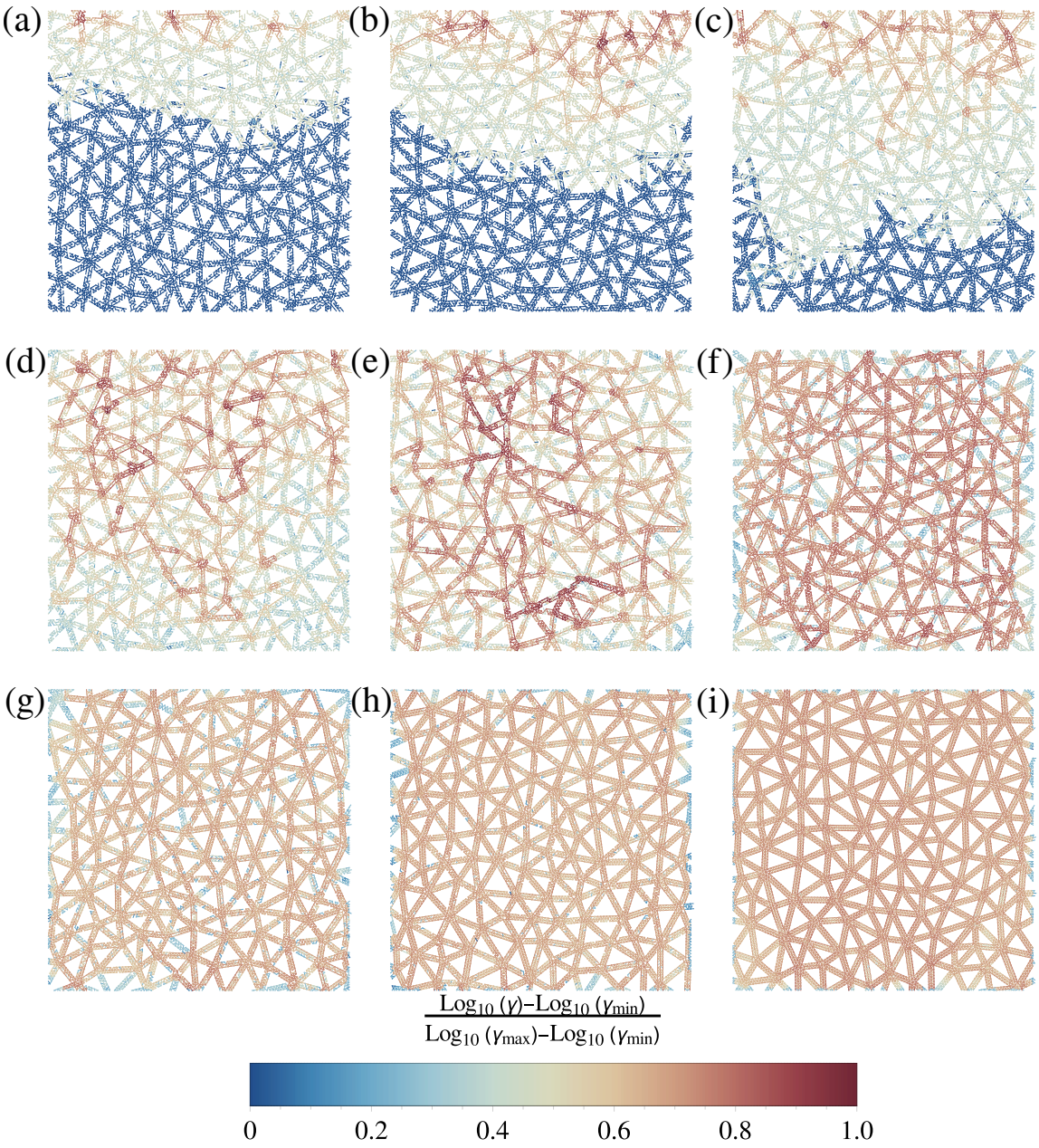

Figure 7.6: In panels **(a)**-**(i)**, we visualize the strain distribution in networks with large-scale geometric disorder and small-scale crystalline order, with a large-scale bond portion of 1 and a small-scale bond portion that ranges from .6 in panel **(a)** to 1 in panel **(i)**, in steps of .05.

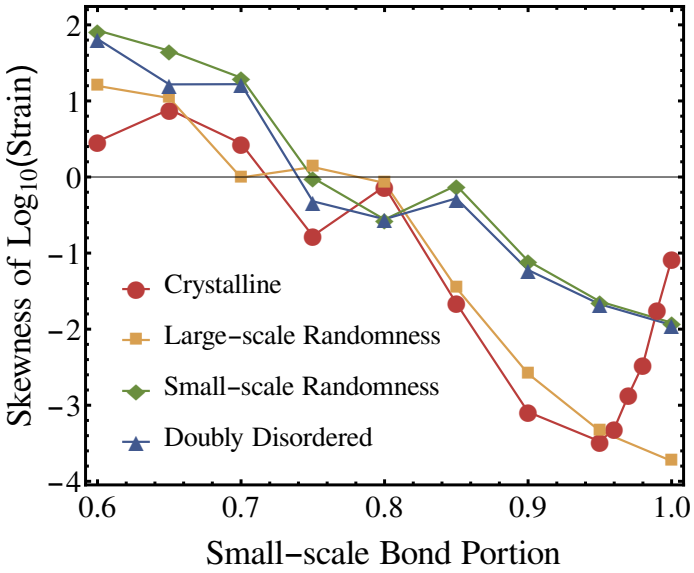

Figure 7.7:

the small-scale bond portion from .6 to 1. For low small-scale connectivity, application of a vertical displacement initially leaves most bonds more or less unstrained, while, at the rigidity threshold, a percolating network of force chains emerges, spanning from top to bottom. Even after the attainment of a non-zero stiffness, pockets of bonds bearing comparatively little strain can be readily discerned, and are only suppressed when the small-scale bond portion exceeds .9. This suggests that there tend to be two sub-populations of bonds, one with relatively large strain and the other exhibiting a much smaller deformation. The unstrained bonds initially make up the majority, while at high small-scale connectivity the load is more evenly distributed, and undeformed bonds are in a small minority.

While a fairly coherent story has emerged from this analysis, we also note that the skewness of the logarithm of the strain in the fully crystalline lattice is unique in that it abruptly increases near full small-scale connectivity. To address this, we find it illuminating to view visualizations of residual strain after relaxation for networks with each combination of small-scale and large-scale structure, which we present in Fig. 7.8. The small-scale bonds in the middle of horizontal large-scale bonds appear to take up comparatively little strain, as they are contained in bonds whose orientation is perpendicular to the direction of

applied strain. This once again stratifies the distribution of strain borne by different bonds.

This comparison is further supported by an exhaustive survey of the distribution of strain for networks of different types. In figures 7.9 and 7.10, we show histograms of strain for networks with small scale crystalline order and either crystalline large-scale order or large-scale disorder. We track the change in strain distribution as the small-scale bond portion is varied from .6 to 1, while the large-scale bond portion is held fixed at 1. In both cases, there is initially a bimodal distribution, with two peaks separated by about 5 orders of magnitude. At large small-scale bond portion, these distributions coalesce into one distribution, centered at the approximate value of the global strain imposed on the network, with a half width of about 1 order of magnitude. We find that this distribution is once more stratified in the case of networks with crystalline order on the large and small scales.

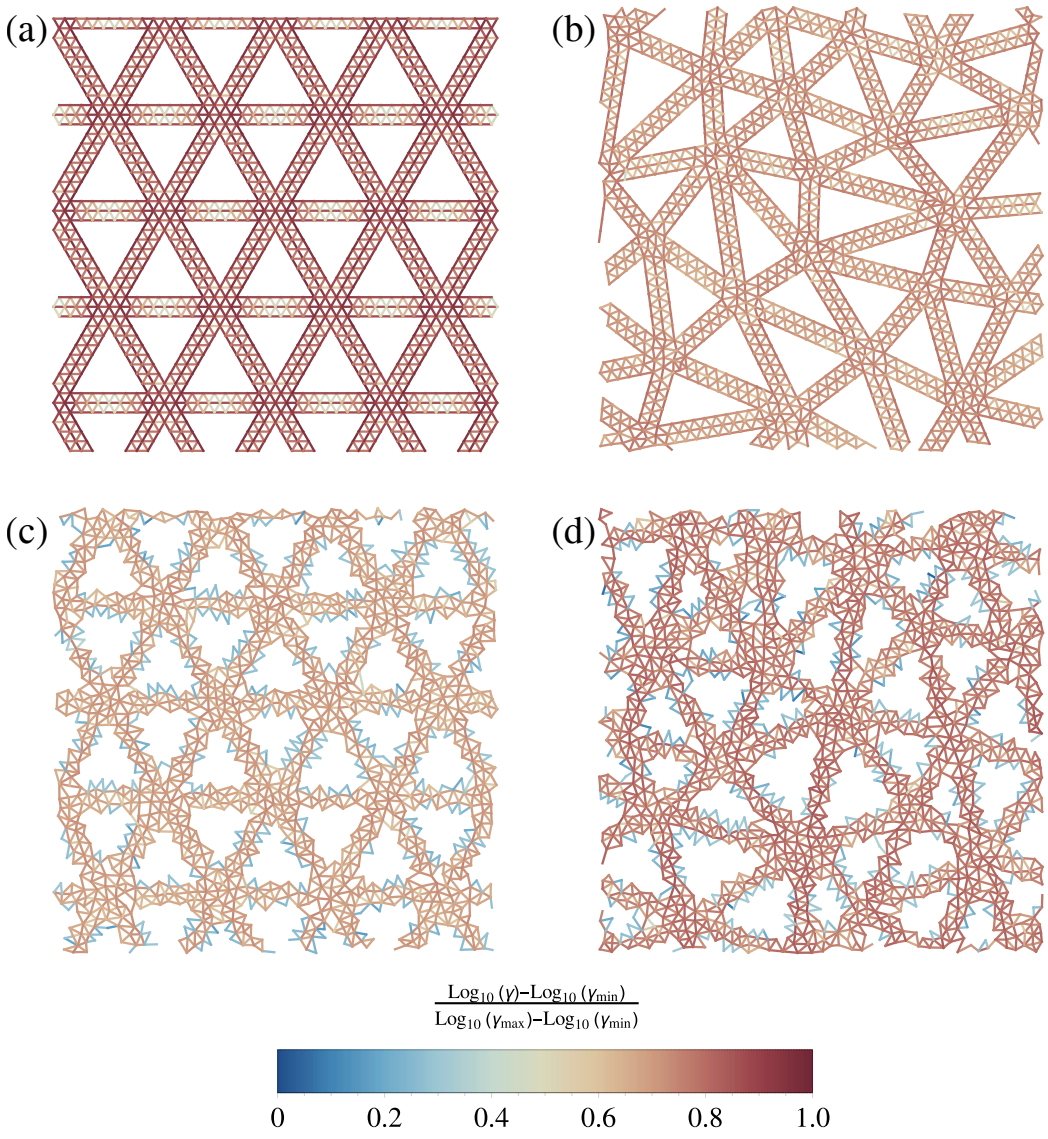

Figure 7.8: We show the relative distribution of strain for close-up samples of networks with full large-scale and small-scale connectivity, with **(a)** crystalline structure on both scales, **(b)** large-scale geometric disorder, **(c)** small-scale geometric disorder, and **(d)** geometric disorder on both scales.

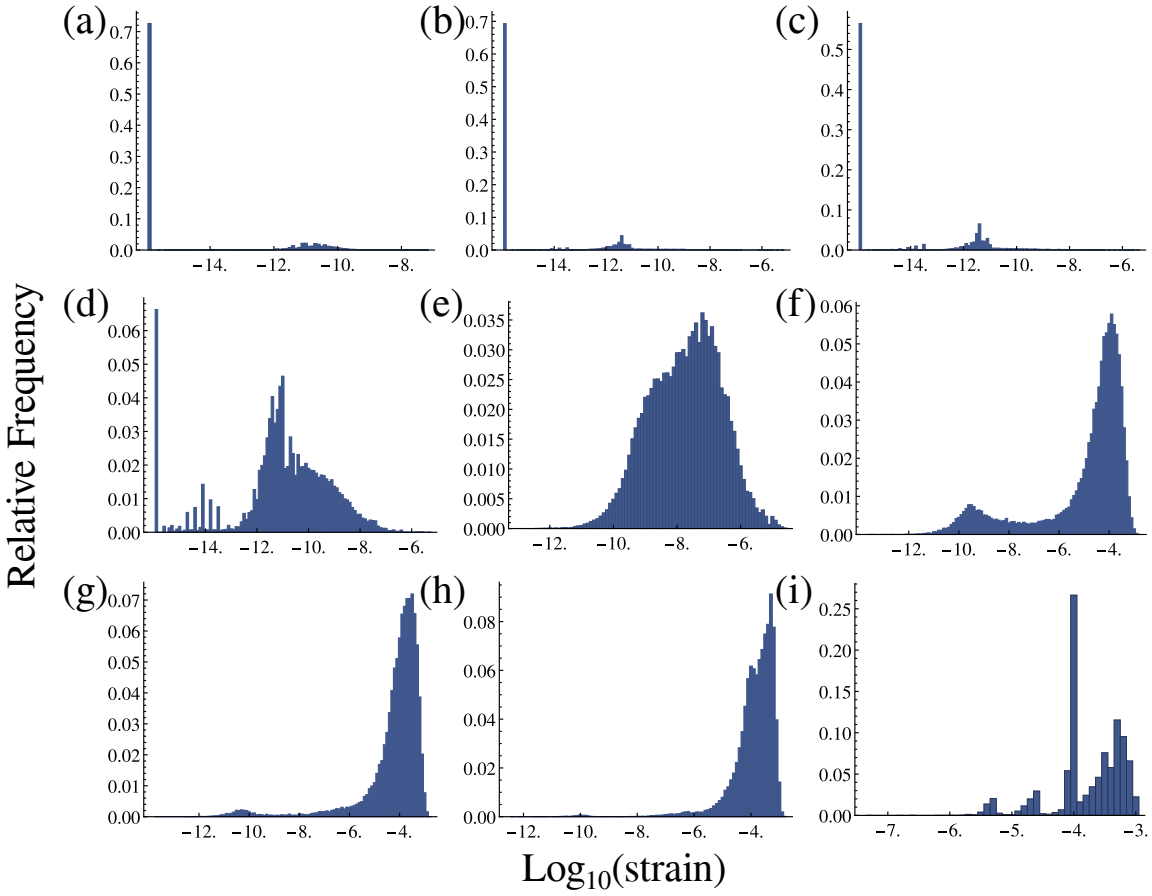

Figure 7.9: We show the distribution of the $\log_{10}$ of strain for networks with crystalline small-scale and large-scale structure and with full large-scale connectivity, with the small-scale bond portion varying from .6 to 1.

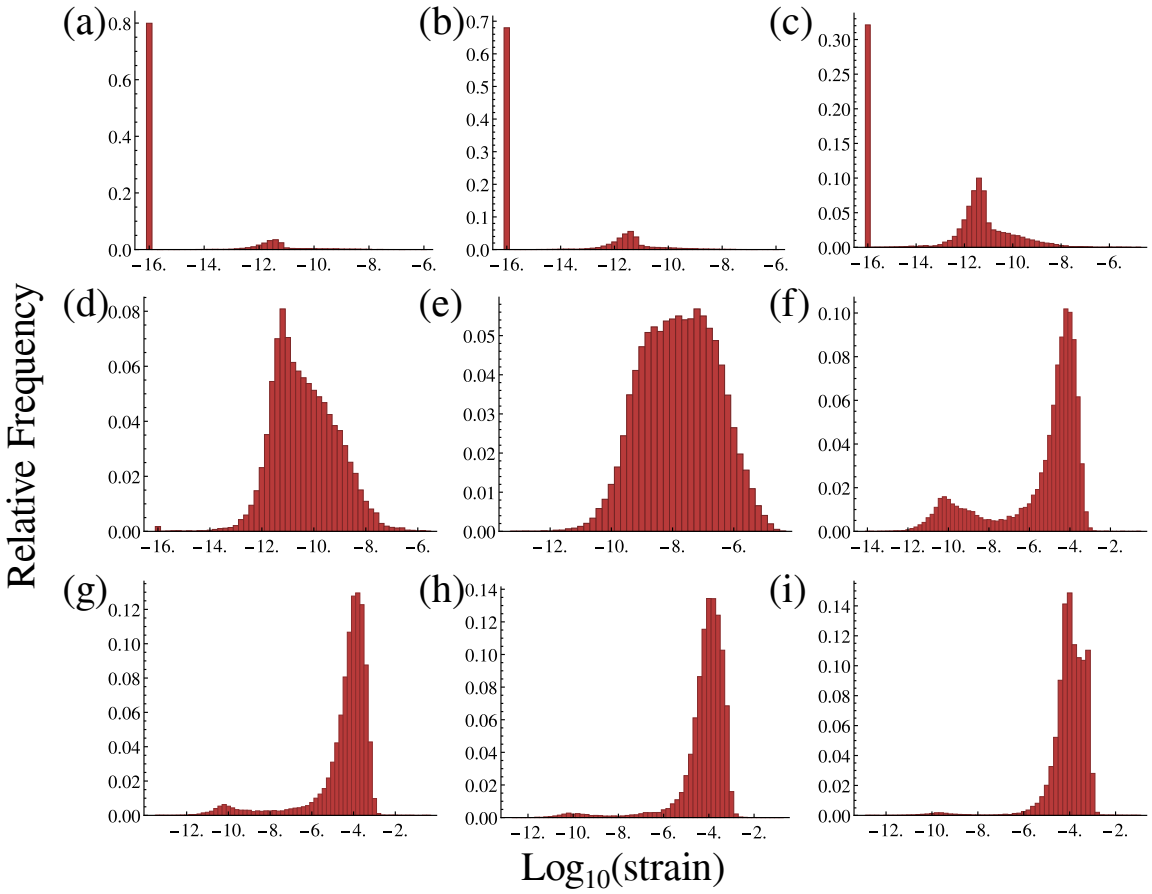

Figure 7.10: We show the distribution of the $\log_{10}$ of strain for networks with crystalline small-scale structure and no large-scale crystalline order, with full large-scale connectivity and small-scale bond portion varying from .6 to 1.

CHAPTER 8
CONCLUSION

We proposed at the outset to shed light on the reliability of hierarchical materials in nature, despite the seemingly daunting task of creating the intricate structures that have been reported in the literature. We developed a novel extension to the dilute lattice model, and provided evidence for the continued usefulness of the notion of coordination number in controlling the mechanics of hierarchical elastic networks. This result builds upon the brilliant seminal work of Maxwell, while offering a useful tool for gaining insight into modular assembly processes. That hierarchy has been found to confer resilience against variability at each stage of construction suggests that the emergence of complex body plans may have been a launching pad, rather than a stumbling block.

While large and small-scale structure contribute to the elastic moduli of hierarchical materials in mathematically analogous ways, there are important mechanistic differences in the roles of small-scale and large-scale structure. We have found that the small scale sets the vibrational density of states of hierarchical networks, and is consequential in determining whether or not there are soft modes of deformation along the periphery of large-scale bonds. Large-scale connectivity, on the other hand, enables coordinated, long-range force chains to emerge. Our results suggest that precise control of small-scale structure is much more significant in ensuring a stiff finished product.

Of course, the variety of tissues in nature is vast, and many additional matters remain to be addressed. We regard material heterogeneity to be of particular importance. A first at accounting for this might consist in assigning bonds two or more different stiffnesses, with bonds of different stiffness either interspersed, or organized into domains of locally uniform stiffness. We also envision incorporating a non-zero bending stiffness for small-scale bonds into our model, and exhaustively exploring the behavior of our networks as

the ratio of bending to stiffness is varied. Finally, we contemplate the prospect of building upon previous modeling efforts to incorporate active stresses [42, 43, 44], to bring our model system to life.

Appendices

APPENDIX A

EMERGENT BENDING STIFFNESS OF LARGE-SCALE BONDS

We anticipate that varying the angles between large-scale bonds cannot be done without a cost in energy, even if no bending energy is been explicitly prescribed, because changing the angle between two large-scale bonds will generally demand a change in the lengths of the small-scale bonds of which they are composed. We have quantified this effect, and found that large-scale bonds have a non-negligible bending stiffness if the small-scale bond portion is above the critical threshold for marginal stiffness. We consider two adjacent large-scale bonds which, in their rest state, subtend an angle θ_0. We then anticipate that, two first order, changing their angle of separation to some other angle, θ, will cost an energy

$$E_{Bend} = \frac{k_B}{2} \left(\theta - \theta_0\right)^2 , \tag{A.1}$$

where k_b is a bending stiffness.

We seek to determine the bending stiffness for pairs of large-scale bonds subtending an angle $\frac{\pi}{3}$ radians, both for crystalline and geometrically disordered small-scale structure, with varying fractions of small-scale bonds retained. We do this by orienting the large-scale bonds such that the line bisecting them is parallel to the horizontal, then displacing the top of the upper large-scale bond by an amount Δh, while fixing the bottom of the lower large-scale bond. We show a schematic in Fig. A.1. If the large-scale bonds both have a length l, then the height of the pair of bonds will be

$$h = 2l \sin\left(\frac{\theta}{2}\right) , \tag{A.2}$$

where we assume that, for suitably small values of Δh, the length of each large-scale bond will change negligibly, and the principal mode of deformation will be bending. Inverting

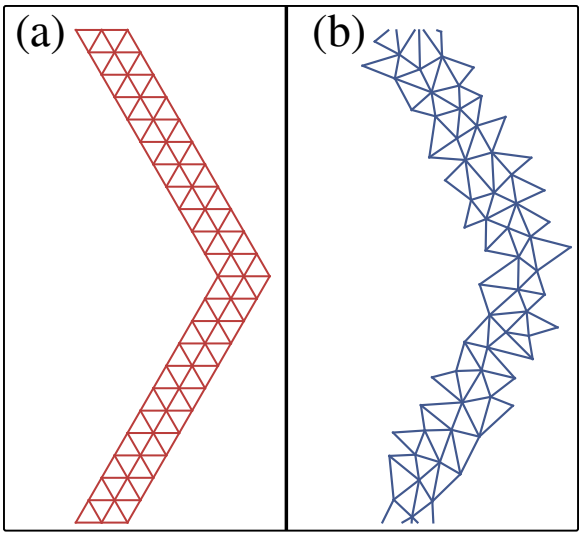

Figure A.1: We show representative examples of large-scale bonds subtending an example of $\frac{\pi}{3}$ radians, with the bisector of the angle between them aligned with the horizontal. In **(a)**, we show large-scale bonds with crystalline small-scale structure, and in **(b)**, we show large-scale bonds with geometrically ordered small-scale structure.

equation Eq. A.2 to solve for θ as a function of h, and inserting the result into Eq. A.1, we find

$$E_{bend} = \frac{k_B}{2}\left[2\sin^{-1}\left(\frac{h}{2l}\right) - \theta_0\right]^2 \tag{A.3}$$

To explore the dependence of large-scale bending stiffness on small-scale bond portion, we prepared pairs of large-scale bonds as described above, with 50 realizations for each combination of small-scale structure and bond portion. The small-scale bond portion was varied from $.6$ to 1, in increments of $.05$. We varied the height of the top of each large-scale bond from 10^{-4} to 10^{-3}, in units of large-scale bond portion. We considered six displacements in all, chosen to be evenly distributed on a $\log_{10}$ scale. For networks with an appreciable residual strain energy after relaxation, we found good agreement with Eq. A.3. We show a characteristic fit in Fig. A.2. As for full hierarchical networks, we consider the bending stiffness to be zero if the fit to Eq. A.3 yields a correlation coefficient r less than $.9$. This was found to consistently correspond to a large decrease in residual strain energy, of about 10 orders of magnitude.

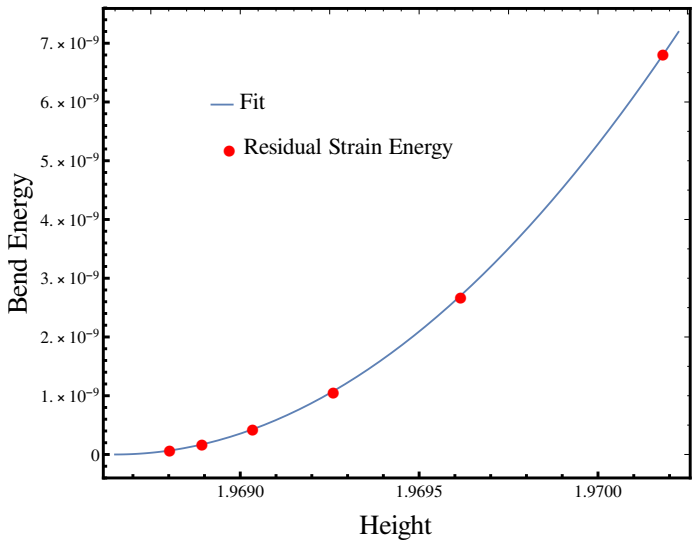

Figure A.2: We show a fit of residual strain energy vs. height of displacement of the top of the large-scale bond to equation A.3 for a pair of large-scale bonds.

We found bending stiffness to decrease much more abruptly than stretching stiffness. Nonetheless, the mean bending stiffness for a given small-scale bond portion still remained non-zero until approximately the same small-scale bond portion at which stretching stiffness vanishes, for a given small-scale structure. Thus, for all regions of bond portion space for which a network has non-zero stiffness, we expect bending stiffness to play a minor role. We further noted that large-scale bonds made up of a crystalline array of small-scale bonds have a markedly higher bending stiffness than those made of geometrically disordered small-scale bonds. Our results also suggest that bending stiffness can vary considerably from one large-scale junction to the next, so that the elastic properties of a hierarchical network can be somewhat variable from one large-scale junction to the next. We show our findings, with error bars attesting to the large variability of bending stiffness, in Fig. A.3. In this plot upper (lower) error bars indicate the mean deviation from the mean of bending stiffness from the mean value for stiffness values greater than (lower than) the mean stiffness value.

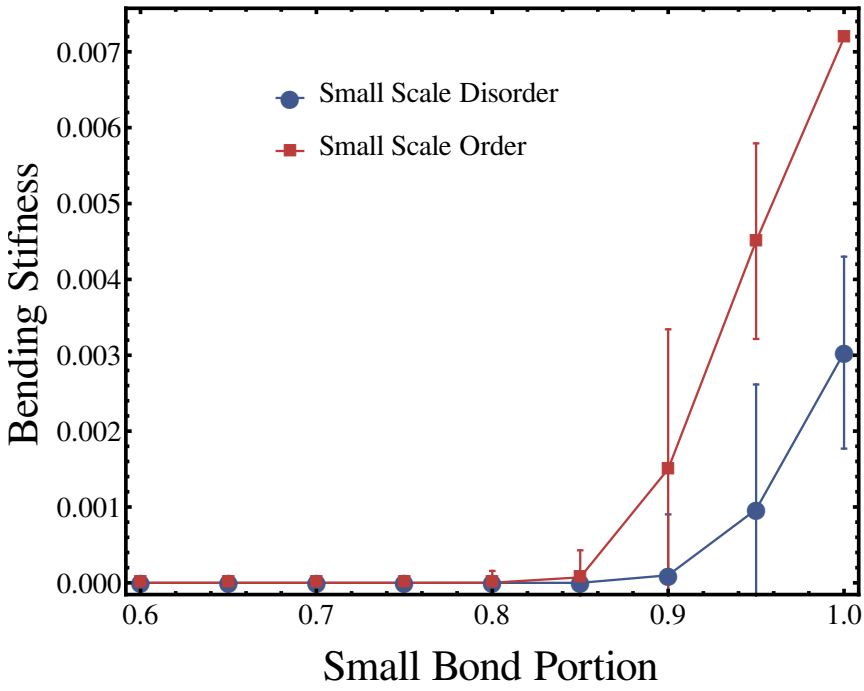

Figure A.3: We show mean bending stiffness vs. small-scale bond portion for large scale bonds made of either crystalline or geometrically disordered small-scale bonds. While a clear trend is discernable, bending stiffness can vary considerably from one specimen to the next.

APPENDIX B

OBTAINING CRITICAL BOND PORTIONS

We discuss in further detail the process by which the critical bond portions were obtained for networks with varying levels of structural hierarchy. We begin by briefly confirming our results for a one-level dilute triangular lattice are in agreement with published values. As seen in B.1, we obtain the expected dependence of stiffness upon bond portion, with the rigidity threshold in the vicinity of the value anticipated from Maxwell counting.

We next isolated the paths in bond portion space for two-level networks along which either the large or small-scale bond portion was fixed at 1, while the other bond portion was varied from .6 to 1. We fit linear trend lines to each set of points, and identified the critical bond portion as the x intercept. There is a slight discrepancy for the fit of stiffness vs. large-scale bond portion, as the small bending stiffness between pairs of large-scale bonds leads to an avoidance of a perfect first-order critical point. Results are shown in Fig. B.2.

We obtained three level bond portions in a similar procedure to that used for two-level bond portions, with two bond portions fixed at 1, and the third varied from $.8$ to 1. As shown in Fig. B.3, we added an extra point when fitting for the small-scale critical bond portion, at which the large-scale and intermediate-scale bond portions, p_l and p_{im} were held at 1, and p_s was set to $.85$. This was done to provide three points for which the stiffness was non-zero. Fits for the critical values of p_l and p_{im}, illustrated in Fig. B.4 were more straightforward, as both $p_{l,c}$ and $p_{im,c}$ appear to be less than $.8$.

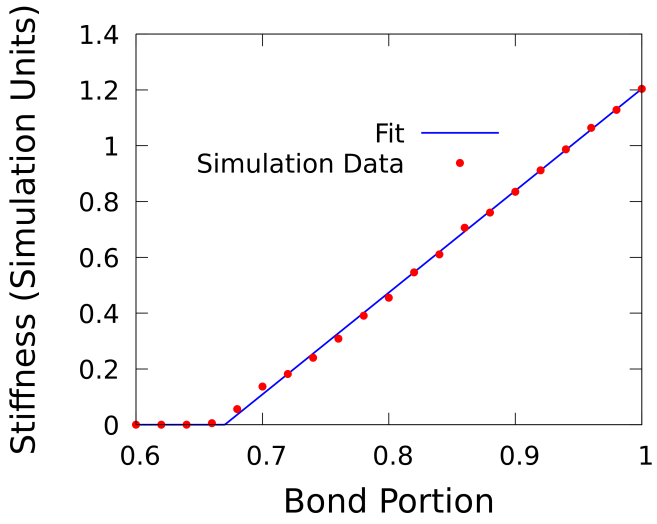

Figure B.1: We confirm that our results are in agreement with conventional expectations for a single-level dilute triangular lattice.

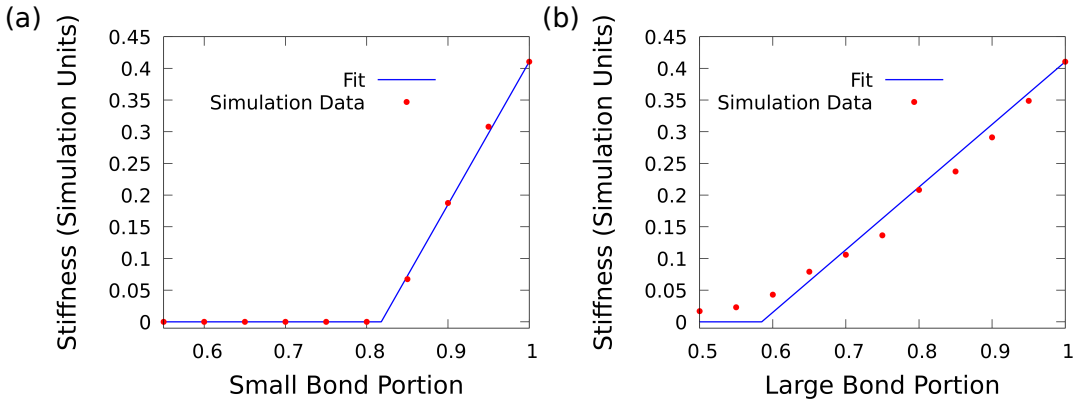

Figure B.2: We find the critical bond portions for **(a)** the small scale and **(b)** the large scale for a hierarchical lattice with two levels of spatial organization. The scaling of stiffness with the large-scale bond portion indicates a small bending stiffness for large-scale bonds.

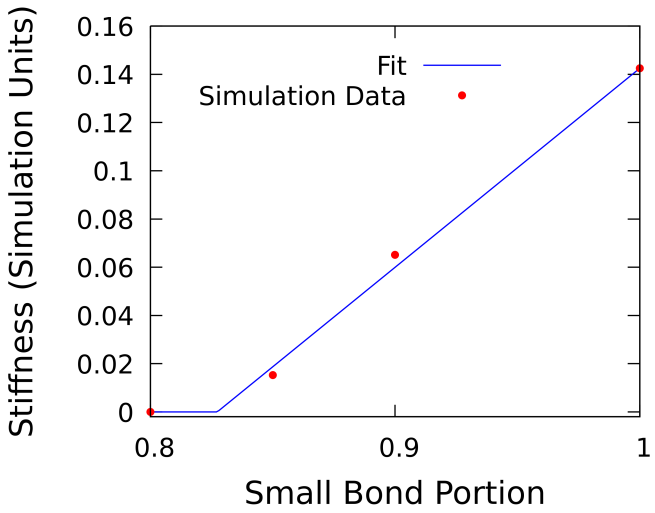

Figure B.3: We find the critical small-scale bond portion for a three-level lattice, with an extra point at $p_s = .85$, $p_{im} = 1$ and $p_l = 1$, to provide at least three points for fitting a line for extrapolation to the x intercept.

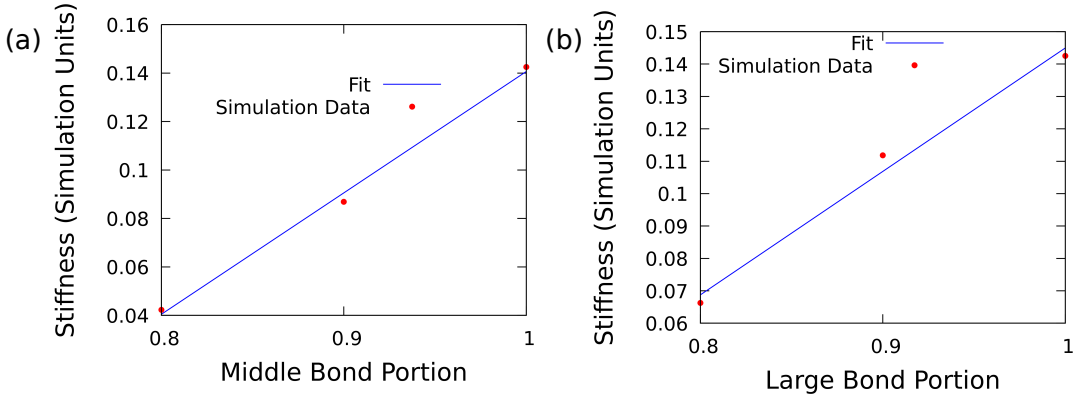

Figure B.4: We find the critical bond portions for **(a)** the intermediate-scale bond portion and **(b)** the large-scale bond portion, by fitting a line to the points at which the other two bond portions are fixed at one, and extrapolating to find the x intercept.

APPENDIX C

CONSTRAINTS ON LARGE-SCALE BOND ASPECT RATIOS

Our model is liable to fail if the width of a large-scale bond is either too great or too small in comparison with the length of the bond. We first consider the case in which bonds are too wide; here, the network ceases to behave as a structure with two, disparate length scales, and appears more like a sheet with small perforations. This is because our hierarchical networks may be viewed as single-scale triangular lattices with holes removed from them. It may be shown that, for large bonds of length l and width w, each of these holes is an equilateral triangle with side length s given by

$$s = l - w\sqrt{3} \tag{C.1}$$

If each small bond has a length a, large bonds are n_l small bonds long, and large bonds have r rows of small-scale bonds, (C.1) is equivalent to

$$s = a\left[n_l - \frac{3\,(r-1)}{2}\right] \tag{C.2}$$

We now seek the region over which the addition of a hole to an otherwise unbroken sheet has an appreciable affect upon the displacement field of a sheet under tensile strain, with the top and bottom pinned in the y direction, but free to relax in the x direction. We begin with a reference network, with overall dimensions of 200 by 200, in units of small-scale bond length, with no hole, and apply a strain of 0.05% in the vertical direction. We then apply this same strain to networks with holes in their centers, with hole side lengths varying from 2 to 15, in units of small-scale bond length. In each case, we subtract the displacement field at each point in the reference network from the displacement field in a network with a hole, omitting those points removed by the formation of the hole.

In seeking the region within which a hole has appreciably altered the mechanics of the network, we apply the following criterion: if the magnitude of the discrepancy between the displacement field in the presence of a hole and the displacement field in the absence of the hole is at least the applied strain times the small-scale bond length, the point lies within the "region of influence" of the hole. Mathematically, if $\vec{u}_{ref}$ is the reference displacement field, $\vec{u}_{hole}$ is the displacement field with the hole, and ε is the applied strain, then, for a discrepancy field $\vec{d} = \vec{u}_{hole} - \vec{u}_{ref}$, the magnitude d should satisfy

$$d \geq \varepsilon a \tag{C.3}$$

where εa is the approximate elongation of a small-scale bond in a perfectly affinely deformed network with overall strain ϵ. In Fig. C.1, we show two cases: a deformed network with a hole of length 5, and a deformed network with a hole of length 10. Networks are colored to show the magnitude of the discrepancy between the displacement fields in the networks with and without the hole, and the boundary of the holes region of influence is shown with a bold, red stroke.

While the region of influence is modest for small hole size, the region of influence for large hole size is considerable. To set a standard for widest acceptable width, given a certain length, we calculate the maximum difference from the center of the hole to a point on the perimeter of the center of influence. We denote this distance by r_{max}. For the lattices we consider, the center-to-center separation of holes of length l, separated by a single large-scale bond, is $\frac{l}{\sqrt{3}}$. Therefore, the size of the region of influence of a hole should be comparable to or greater than this length. We find that, for holes with side length s of 3 or greater, in units of small-scale bond length, r_{max} is roughly linear with hole size:

$$r_{max} \approx 5.6s - 15 \tag{C.4}$$

with $r^2 = 0.99$. This demands

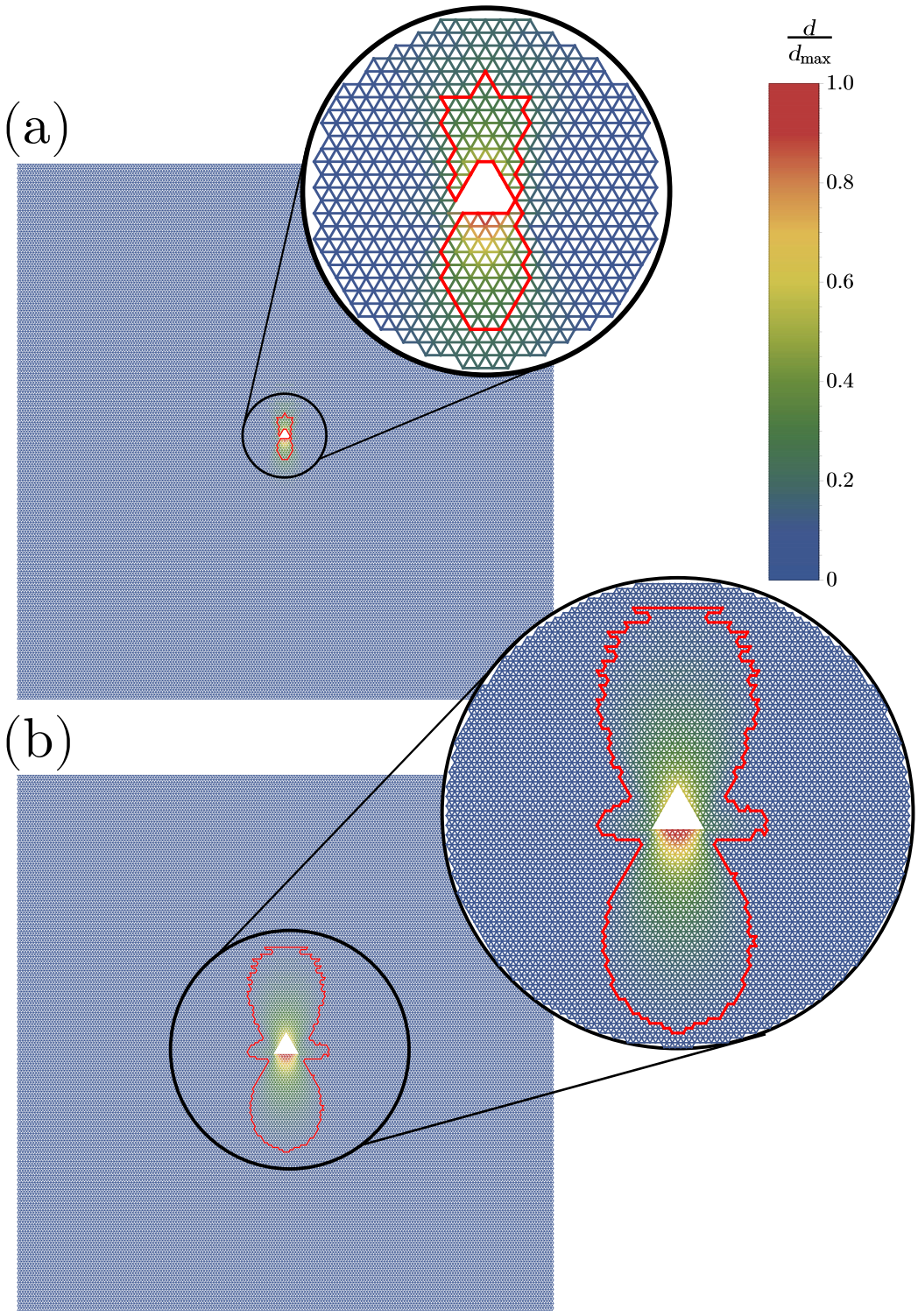

Figure C.1: We show networks with triangular apertures **(a)** 5 small-scale bonds wide and **(b)** 10 small-scale bond widths wide, with bonds color-coded to show the discrepancy field, $\vec{d} = \vec{u}_{hole} - \vec{u}_{ref}$. Insets show a close-up view of the regions of influence, whose borders are marked with a bold, red stroke.

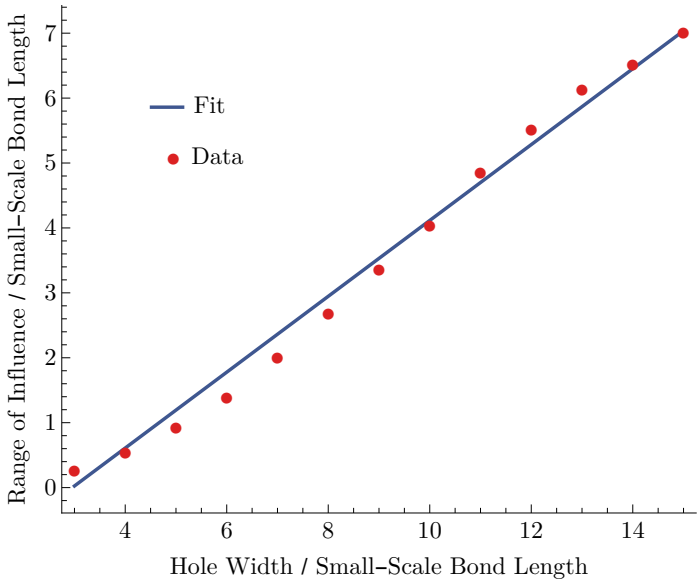

Figure C.2: We show data for the range of influence size of a triangular aperture in a triangular lattice, vs. the width of the triangular aperture. The range of influence size appears to scale very nearly linearly with hole size.

$$\frac{l}{\sqrt{3}} \leq 5.6s - 15 \tag{C.5}$$

$$\frac{l}{\sqrt{3}} \leq 5.6\left(l - w\sqrt{3}\right) - 15 \tag{C.6}$$

or

$$l - 2w \gtrsim 3 \tag{C.7}$$

We show data in Fig. C.2. While we have chosen to study networks in which springs have a stiffness of one, in units of one-dimensional stretching modulus over small-scale bond length, the equilibrium configurations of networks in their strained states would remain equilibrium configurations for the same loading conditions if the stiffness of each spring were re-scaled by the same multiplicative factor. We therefore find that the foregoing considerations should be of general applicability.

On the other hand, a bond may also be too narrow. Our analysis is sure to fail if large-scale bonds are only one or two bonds wide. In this case, the connectivity at the small scale is less than or equal to 4, and so the removal of even a small fraction of small-scale bonds will immediately destabilize the network. Further, overly narrow large-scale bonds will be highly susceptible to bending, which invalidates our picture of a primarily stretching-stabilized structure. In general, a thin rod of length l, with Young's modulus E, becomes unstable to buckling along direction $\hat{x}$ under a load

$$F_{cr} \propto \frac{EI}{l^2} \tag{C.8}$$

with

$$I = \int x^2 dA \tag{C.9}$$

where the integral is over the cross section of the rod [45]. In two dimensions, for a rod of width w,

$$I = \frac{w^3}{12} \tag{C.10}$$

The prefactor in (C.8) depends upon the precise boundary conditions at the ends of the rod, and is of order unity. On the other hand, we note that the network will generically contract in the direction transverse to applied tensile strain. Given a Young's modulus E for a large scale bond, a strain ε will lead to a force

$$F = wE\varepsilon \tag{C.11}$$

In all, (C.8), (C.10), and (C.11) suggest bending will become a concern when

$$\frac{Ew^3}{l^2} \sim wE\varepsilon \tag{C.12}$$

or

$$\frac{l}{w} \sim \varepsilon^{-1/2} \tag{C.13}$$

We briefly confirm that, for the cases treated in the main text, in which $l = 10$ and $w = \sqrt{3}$, in units of small-scale bond length, our networks abide by the bounds prescribed by Eqs. C.7 and C.13. First, we note that

$$l - 2w = 10 - 2\sqrt{3} \tag{C.14}$$

$$\approx 6.536 \tag{C.15}$$

$$> 3 \tag{C.16}$$

On the other hand, we evaluate stiffness strains of less than 1%, so that $\epsilon^{-1/2} \geq 10$. On the other hand,

$$\frac{l}{w} = \frac{10}{\sqrt{3}} \tag{C.17}$$

$$\approx 5.773 \tag{C.18}$$

and so we are comfortably within both bounds on the length-to-width ratio of large-scale bonds.

APPENDIX D

PROCEDURE FOR CREATING HIERARCHICAL NETWORKS WITH SMALL-SCALE DISORDER

In the main text, we noted that, in creating hierarchical networks with small-scale disorder, we have chosen to retain small-scale bonds when they are either entirely inside the large-scale envelope, or if they straddle an edge of the large-scale envelope. We here address an alternative possibility, in which bonds are retained only if they are entirely inside a large-scale envelope. This latter procedure will result in slightly different edges along large-scale bonds. We contrast these two edge types visually in Fig. D.1.

Both policies for determining which small-scale bonds to retain result in a mean connectivity along the edges of large-scale bonds of approximately 4. In particular, we obtain 4.08 when keeping straddling bonds, and 4.06 when rejecting straddling bonds. In Fig. D.2, we contrast the distributions yielded by these two policies.

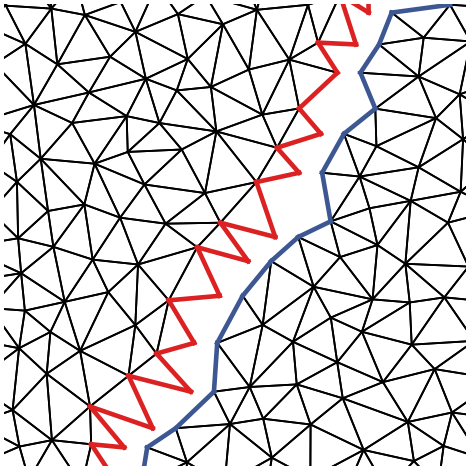

Figure D.1: We illustrate the difference between a procedure in which small-scale bonds are retained if they straddle a large-scale boundary, and a procedure in which small-scale bonds are only retained if they are entirely inside a large-scale envelope. We show the former case in the upper-left half, and the latter case in the lower-right half.

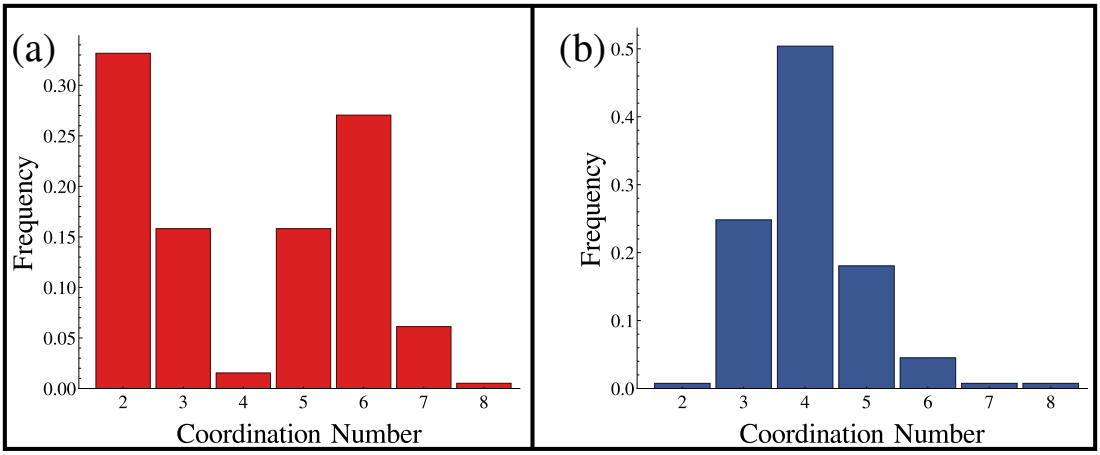

Figure D.2: We show the distribution of coordination number for small-scale vertices along large-scale edges in hierarchical networks with small-scale disorder when **(a)** small-scale bonds straddling large-scale boundaries are kept, and **(b)** small-scale bonds are only accepted when they are within the large-scale envelope. While one distribution is bimodal, and the other has a single peak at 4, both yield very similar means.

APPENDIX E

FURTHER CHECKS OF THE SCALING MODEL

We we are hopeful, given the considerations in Appendix C, that the networks considered in the main text are appropriate for testing our scaling law relating bond portion to stiffness, and for elucidating the role of structure on different length scales, we here confirm by direct calculation that our considerations hold good for networks with large-scale length and width. We consider two-level hierarchical networks, with length and a length 10 times the small-scale bond length l_s, and a width $2\sqrt{3}l_s$. We repeated calculations for networks with each type of large-scale and small-scale structure - either crystalline or a Delaunay triangulation of a random point set. A representative sample of each case is shown in Fig E.1.

We applied the tensile simulation procedure described in the main text to three relaizations of each class of network, once again with the small and large-scale bond portions independently varied from .6 to 1.. As may be seen in Fig. E.2 and Table E.1, Eq. 3.8 remains a reliable way to capture the stiffness of the network. While our search of parameter space is not exhaustive, we nonetheless regard these additional results as valuable corroboration of the claims put forth in the main text.

Table E.1: Data are shown for the critical large-scale and small-scale connectivities for each combination of order and disorder, with large-scale bonds twenty times the length of small-scale bonds and the same aspect ratio as before.

Large / Small Scale	k	p_l	p_s	r^2
Order/Order	.343	.59	.77	.992
Disorder/Order	.345	.63	.82	.994
Order/Disorder	.218	.62	.81	.994
Disorder/Disorder	.241	.64	.79	.988

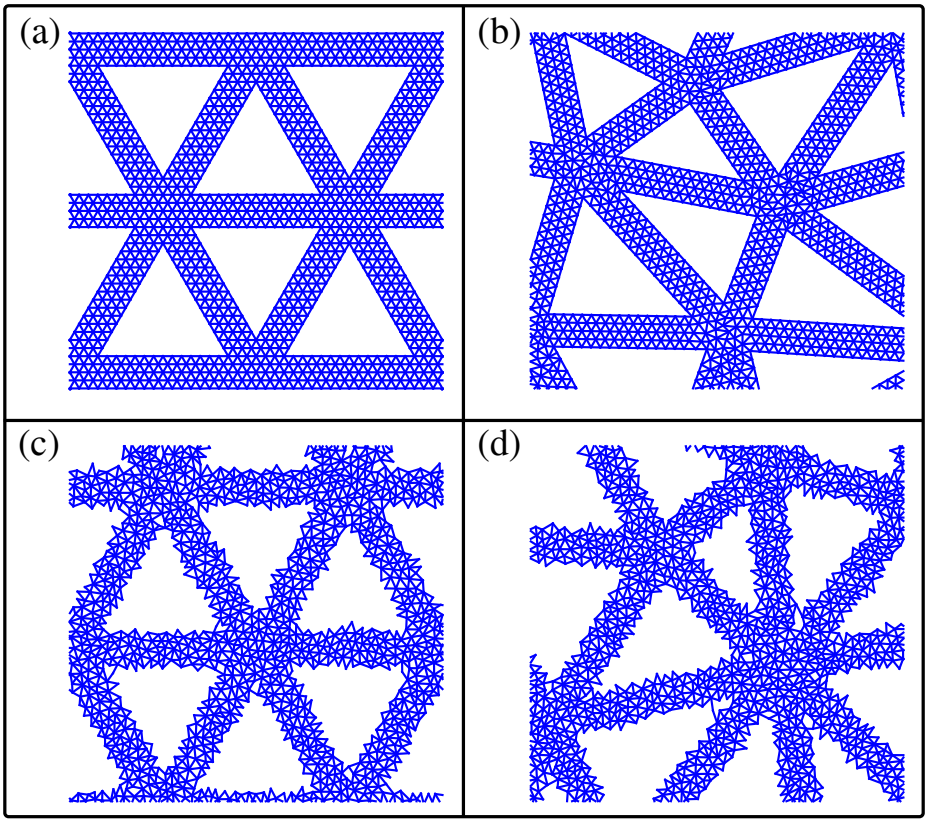

Figure E.1: We show two-level networks with a length of 10 times the mean small-scale bond length, and a width $2\sqrt{3}$ times the mean small-scale bond length with **(a)** crystalline order on both scales, **(b)** crystalline order on just the small scale, **(c)** crystalline order on just the large scale, and **(d)** geometric disorder on both scales.

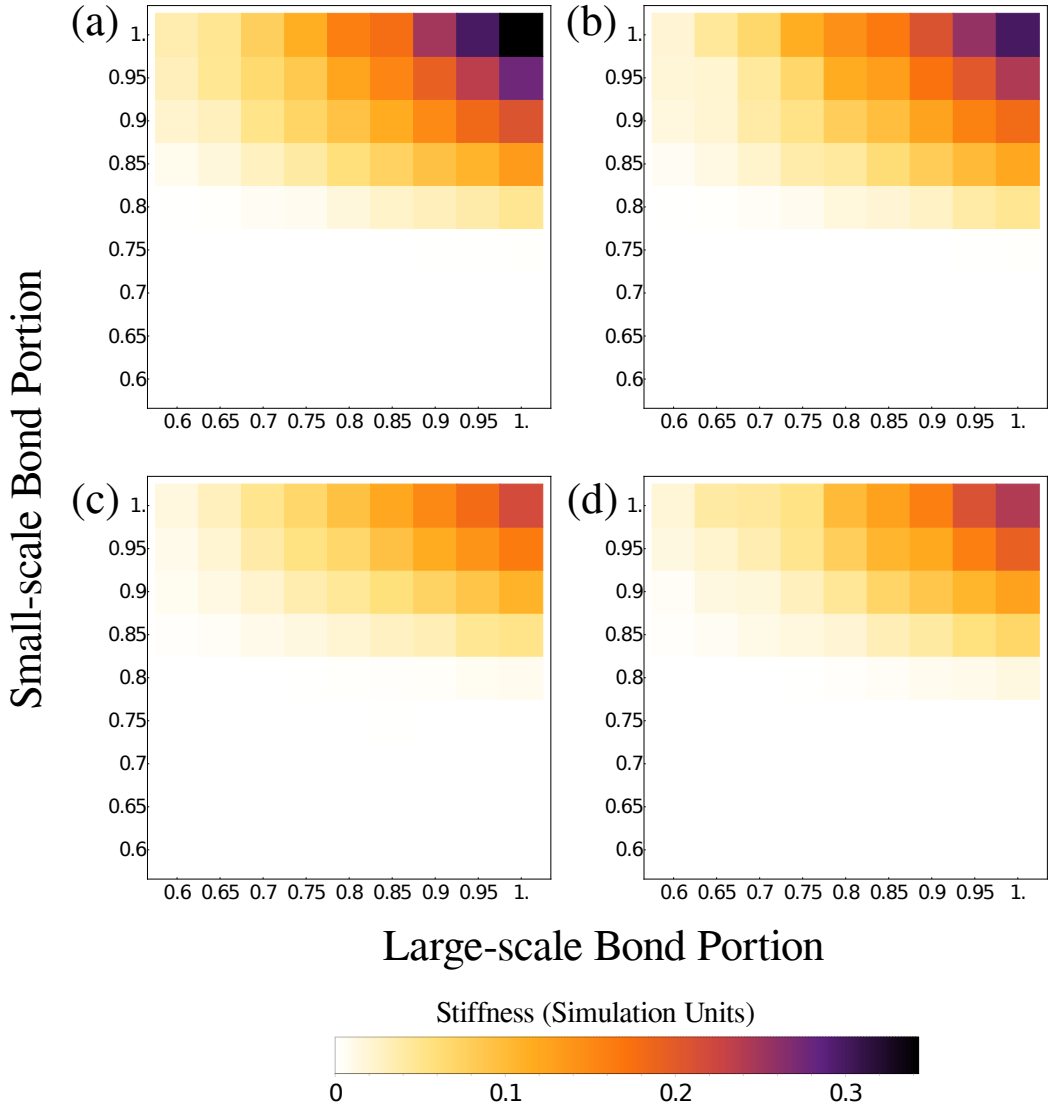

Figure E.2: Data are shown for networks with large-scale bonds that are, on average, twenty times the length of small-scale bonds, but with aspect ratios that are once again $\frac{10}{\sqrt{3}}$. As before, data are shown for **(a)** crystalline order on both scales, **(b)** large-scale disorder and small-scale order, **(c)** large-scale crystalline order and small-scale disorder, and **(d)** geometric order on both scales.

APPENDIX F

DISORDERED NETWORKS WITH FIXED NODE DENSITY

As mentioned in the main text, when we created networks without crystalline order, we chose to keep the mean bond portion the same as it is for crystalline networks. We also considered the possibility of fixing the density of vertices, as this afford a comparison between two polymer networks in which cross-linker density is held fixed. This choice led to a slightly larger mean separation between neighboring points than that of the crystalline network, and yielded a slightly lower density of material per unit volume. While this change resulted in results that were slightly quantitatively different from those obtained when mean bond length was fixed, the same qualitative story emerged. We once more found sound agreement between the scaling model given by Eq. 3.8 in the main text, as seen in Table F.1 and Fig. F.1. Moreover, we still found the scaling of stiffness with respect to the product of excess large-scale and small-scale connectivity to be similar, and concluded that the presence of a small-scale crystalline structure significantly improves the economy of material acheived by an elastic network, as shown in Fig. F.2

Table F.1: Data are shown for the critical large-scale and small-scale connectivities for each combination of order and disorder, with the constraint that mean vertex density, rather than mean bond length, be held fixed.

Large / Small Scale	k	p_l	p_s	r^2
Order/Order	.410	.58	.83	.989
Disorder/Order	.345	.63	.82	.991
Order/Disorder	.242	.63	.88	.987
Disorder/Disorder	.228	.64	.89	.991

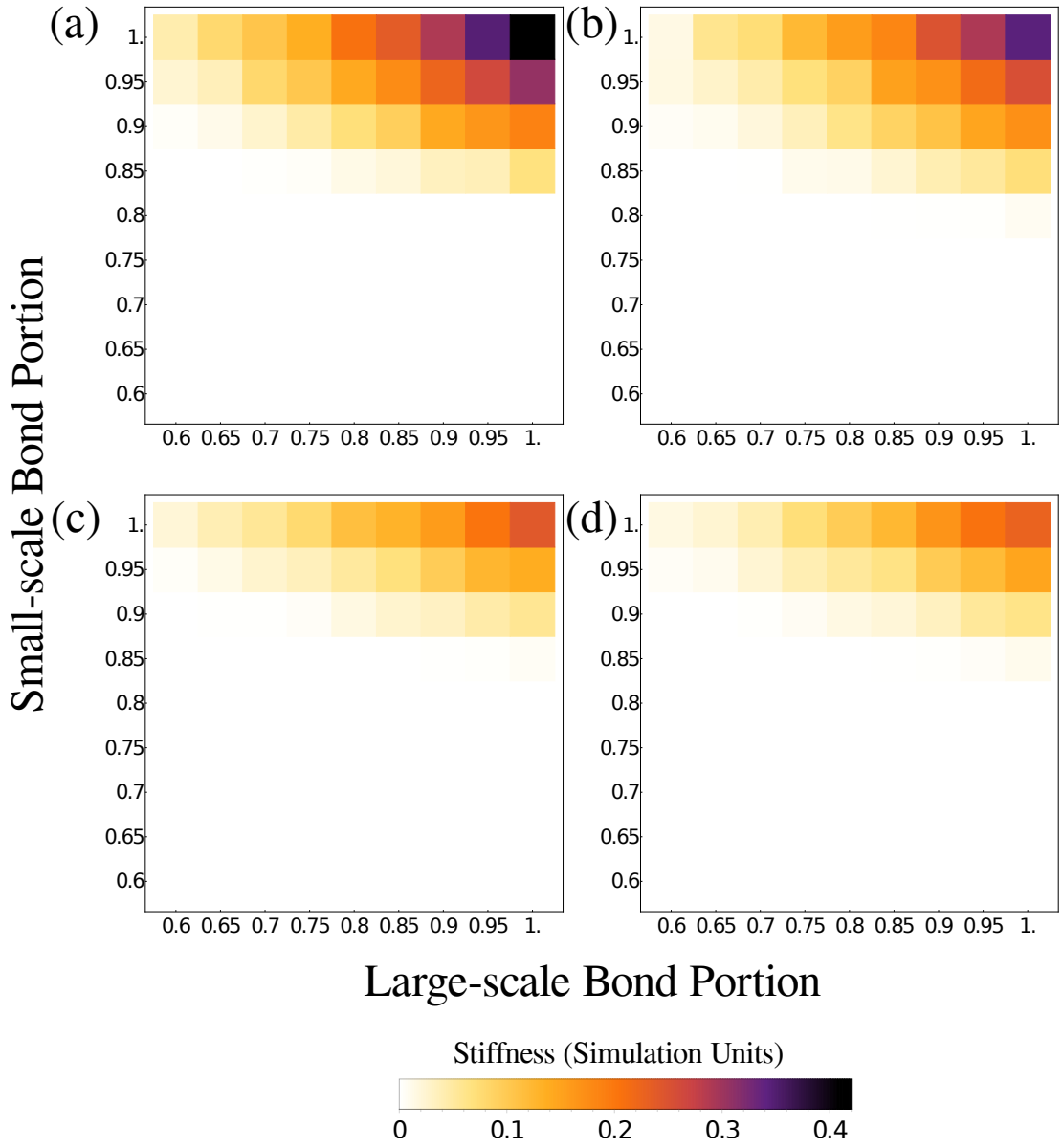

Figure F.1: Data are shown for networks with the same ratio of large length scale to small length scale, but with the constraint that mean vertex density remain the same for geometrically disorded structures as it is for geometrically ordered structures. Shown are stiffness heat maps for **(a)** crystalline order on both scales, **(b)** large-scale disorder and small-scale order, **(c)** large-scale crystalline order and small-scale disorder, and **(d)** geometric order on both scales.

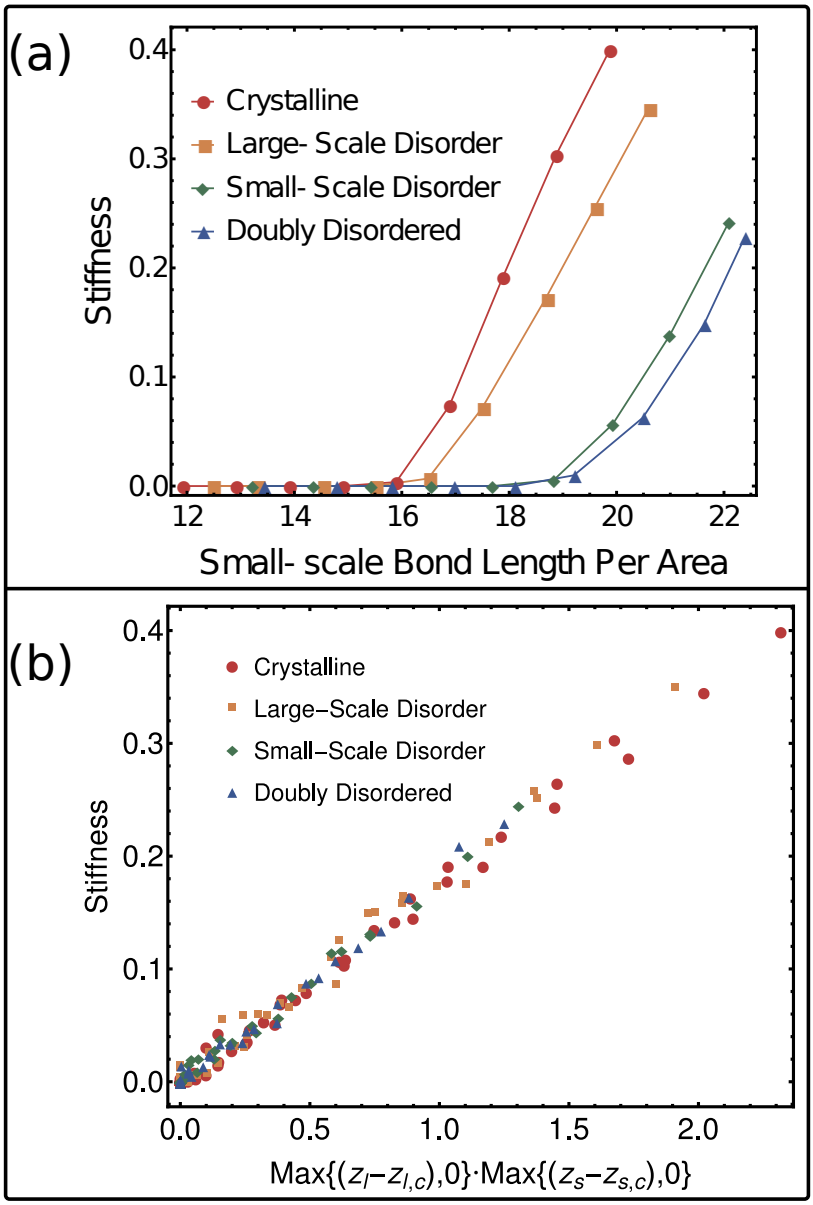

Figure F.2: As in the main text, we show the scaling of stiffness vs. **(a)** the small-scale bond density and **(b)** the product of excess small-scale and large-scale connectivities.

REFERENCES

[1] P. Fratzl and R. Weinkamer, "Nature's hierarchical materials," *Progress in Materials Science*, vol. 52, pp. 1263–1334, 2007.

[2] M. A. Meyers, J. McKittrick, and P. Chen, "Structural biological materials: Critical mechanics-materials connections," *Science*, vol. 339, pp. 773–780, 2013.

[3] U. G. K Wegst and M. F. Ashby, "The mechanical efficiency of natural materials," *Philosophical Magazine*, vol. 84, pp. 2167–2186, 2004.

[4] J. Harris, C. Böhm, and S. Wolf, "Universal structure motifs in biominerals: A lesson from nature for the efficient design of bioinspired functional materials.," *Interface Focus*, vol. 7, 2017.

[5] R. Lakes, "Materials with structural hierarchy," *Nature*, vol. 361, pp. 511–515, 1993.

[6] U. Wegst, H. Bai, E. Saiz, A. Tomsia, and R. Ritchie, "Bioinspired structural materials," *Nature Materials*, vol. 14, pp. 23–26, 2015.

[7] D. Rayneau-Kirkhope, "Stiff auxetics: Hierarchy as a route to stiff, strong lattice based auxetic meta-materials," *Scientific Reports*, vol. 8, 12437, 2018.

[8] J. Lehman and R. S. Lakes, "Stiff, strong, zero thermal expansion lattices via material hierarchy," *Composite Structures*, vol. 107, pp. 654–664, 2014.

[9] R. Oftadeh, B. Haghpanah, D. Vella, A. Boudaoud, and A. Vaziri, "Optimal fractal-like hierarchical honeycombs," *Phys. Rev. Lett.*, vol. 113, 104301, 2014.

[10] D. Rayneau-Kirkhope, Y. Mao, and R. Farr, "Ultralight fractal structures from hollow tubes," *Phys. Rev. Let.*, vol. 109, 2012.

[11] D. Sen and M. J. Buehler, "Structural hierarchies define toughness and defect-tolerance despite simple and mechanically inferior brittle building blocks," *Scientific Reports*, vol. 1, 35, 2011.

[12] M. E. Launey, M. Buehler, and R. O. Ritchie, "On the mechanistic origins of toughness in bone," *Annual Review of Materials Research*, vol. 40, pp. 25–53, 2010.

[13] C. P. Broedersz and F. C. MacKintosh, "Modeling semiflexible polymer networks," *Rev. Mod. Phys.*, vol. 86, pp. 995–1036, 2014.

[14] J. L Silverberg, A. R. Barett, M. Das, P. B. Petersen, L. J. Bonassar, and I. Cohen, "Structure-function relations and rigidity percolation in the shear properties of articular cartilage," *Biophysical Journal*, vol. 107, 7 2014.

[15] J. Feng, H. Levine, X. Mao, and L. M. Sander, "Nonlinear elasticity of disordered fiber networks," *Soft Matter*, vol. 12, 5 2016.

[16] H. E. Amuasi, C. Heussinger, and R. Vink, "Nonlinear and heterogeneous elasticity of multiply crosslinked biopolymer networks," *New Journal of Physics*, vol. 17, 083035, 2015.

[17] J. C. Maxwell, "On the calculation of the equilibrium and stiffness of frames," *Philosophical Magazine*, vol. 27, pp. 294–299,

[18] X. Mao and T. C. Lubensky, "Maxwell lattices and topological mechanics," *Annual Review of Condensed Matter Physics*, vol. 9, pp. 413–433, 2018.

[19] C. R. Calladine, "Buckminster fuller's "tensegrity structures" and clerk maxwell's rules for the construction of stiff frames," *Int. J. Solids Structures*, vol. 14, pp. 161–172, 1978.

[20] R. B. Fuller, "Tensile-integrity structures.," *U.S. Pat*, 3,063,521, 1962.

[21] G. Laman, "On graphs and rigidity of plane skeletal structures," *Journal of Engineering Mathematics*, vol. 4, pp. 331–340, 4 1970.

[22] B. Hendrickson, "Conditions for unique graph realizations," *SIAM J. Comput.*, vol. 21, pp. 65–84, 1 1992.

[23] M. F. Thrope and D. J. Jacobs, "Generic rigidity percolation: The pebble game," *Phys. Rev. Lett.*, vol. 75, pp. 4051–4054, 22 1995.

[24] S. Feng, M. F. Thorpe, and E. Garboczi, "Effective-medium theory of percolation on central-froce elastic networks," *Phys. Rev. B*, vol. 31, pp. 276–280, 1985.

[25] M. Das, F. C. MacKintosh, and A. J. Levine, "Effective medium theory of semiflexible filamentous networks," *Phys. Rev. Let.*, vol. 99, 2007.

[26] X. Mao, O. Stenull, and T. C. Lubensky, "Effective-medium theory of a filamentous triangular lattice," *Phys. Rev. E*, vol. 87, 2013.

[27] Y. Du, N. Pugno, B. Gong, D. Wang, Y. Sun, and Q. Ding, *European Physics Letters*, vol. 111, 56007, 2015.

[28] Y. Chen, T. Li, Z. Ji, F. Scarpa, C. Yao, and L. Wang, "3d printed hierarchical honeycombs with shape integrity under large compressive deformations," *Materials & Design*, vol. 137, pp. 226–234, 5 2018.

[29] E. Bitzek, P. Koskinen, F. Gaehler, M. Moseler, and P. Gumbsch, "Structural relaxation made simple," *Phys. Rev. Let.*, vol. 97, 2006.

[30] J. A. Michel and P. J. Yunker, "Structural hierarchy confers error tolerance in biological materials," *PNAS*, vol. 116, pp. 2875–2880, 8 2019.

[31] S. B. Lindström, D. A. Vader, A. Kulachenko, and D. A. Weitz, "Biopolymer network geometries: Characterization, regeneration, and elastic properties," *Phys. Rev. E*, vol. 82, 2010.

[32] A. Liue and S. Nagel, "The jamming transition and the marginally jammed solid," *Annu. Rev. Condens. Matter*, vol. 1, pp. 347–369, 2010.

[33] C. O'Hern, L. E. Silbert, A. Liu, and S. R. Nagel, "Jamming at zero temperature and zero applied stress: The epitome of disorder," *Phys. Rev. E*, vol. 68, 011306, 2003.

[34] M. van Hecke, "Jamming of soft particles: Geometry, mechanics, scaling and isostaticity," *J. Phys. Condens. Matter*, vol. 22, 033101, 2010.

[35] D. Dunbar and G. Humphreys, "A spatial data structure for fast poisson-disk sample generation," *ACM Trans. Graph.*, vol. 25, 503508, 3 2006.

[36] M. de. Berg, O. Cheong, M. van Kreveld, and M. Overmars, "Computational geometry," in. Berlin: Springer-Verlag, 2008, ch. 9, pp. 193–194.

[37] J. R. Shewchuk, "Triangle: Engineering a 2d quality mesh generator and delaunay triangulator," in *Applied Computational Geometry: Towards Geometric Engineering*, M. C. Lin and D. Manocha, Eds., Berlin: Springer-Verlag, 1996, pp. 203–222.

[38] S. Tomov, J. Dongarra, and M. Baboulin, "Towards dense linear algebra for hybrid gpu accelerated manycore systems," *Parallel Computing*, vol. 36, pp. 232–240, 5-6 2010.

[39] D. A. Head, A. J. Levine, and F. C. MacKintosh, "Distinct regimes of elastic response and deformation modes of cross-linked cytoskeletal and semiflexible polymer networks," *Phys. Rev. E*, vol. 68, 2003.

[40] B. A. DiDonna and T. C. Lubensky, "Nonaffine correlations in random elastic media," *Phys. Rev. E.*, vol. 72, 066619, 2005.

[41] C. P. Broedersz, X. Mao, T. C. Lubensky, and F. C. MacKintosh, "Criticality and isostaticity in fibre networks," *Nature Physics*, vol. 7, pp. 983–988, 2011.

[42] M. Sheinman, C. P. Broedersz, and F. C. MacKintosh, "Actively stressed marginal networks," *Phys. Rev. Let*, vol. 109, 238101, 2012.

[43] P. Roncery and M Lenz, "Connecting local active forces to macroscopic stress in elastic media," *Soft Matter*, vol. 11, pp. 1597–1605, 2015.

[44] P. Roncery, C. Broedersz, and M Lenz, "Fiber networks amplify active stress," *PNAS*, vol. 113, pp. 2827–2832, 11.

[45] L. D. Landau and E. M. Lifshitz, *Theory of Elasticity, Second Edition*. Oxford: Pergamon Press, pp. 97–98.